BRNO UNIVERSITY OF TECHNOLOGY
VYSOKÉ UČENÍ TECHNICKÉ V BRNĚ

FACULTY OF CHEMISTRY
FAKULTA CHEMICKÁ

INSTITUTE OF PHYSICAL AND APPLIED CHEMISTRY
ÚSTAV FYZIKÁLNÍ A SPOTŘEBNÍ CHEMIE

ORGANIC MATERIALS FOR ORGANIC FIELD-EFFECT TRANSISTORS AND ELECTROCHEMICAL TRANSISTORS

ORGANICKÉ MATERIÁLY PRO ORGANICKÉ POLEM ŘÍZENÉ TRANZISTORY A ELEKTROCHEMICKÉ TRANSISTORY

DOCTORAL THESIS
DIZERTAČNÍ PRÁCE

AUTHOR
AUTOR PRÁCE

Ing. Stanislav Stříteský

SUPERVISOR
ŠKOLITEL

prof. Ing. Martin Weiter, Ph.D.

BRNO 2020

BRNO UNIVERSITY OF TECHNOLOGY
FACULTY OF CHEMISTRY

Specification Doctoral Thesis

Department:	Institute of Physical and Applied Chemistry	Academic year:	2019/20
Student:	**Ing. Stanislav Stříteský**		
Study programme:	Chemistry, Technology and Properties of Materials		
Study branch:	Chemistry, Technology and Properties of Materials		
Head of thesis:	**prof. Ing. Martin Weiter, Ph.D.**		

Title of Doctoral Thesis:

Organic materials for organic field–effect transistors and electrochemical transistors

Doctoral Thesis:

The work is focused on the study of the properties of materials suitable for the construction of organic field –effect transistors (OFET) and electrochemical transistors (OECT). The aim is to characterize electrical and optical properties of the studied materials and to optimize the structure and properties of transistors, also with respect to their possible application in bioelectronics. In the field of preparation and study of materials for OFET transistors, special attention will be paid to the relationship between the molecular structure of organic semiconductors used to form the active layer and the resulting properties of the transistor. In the field of OECT preparation, the aim of the work will be to optimize the materials and structure of the transistor so that it is suitable for applications in the field of bioelectronics.

Deadline for Doctoral Thesis delivery: 10.8.2020:

Ing. Stanislav Stříteský Student	prof. Ing. Martin Weiter, Ph.D. Head of thesis	prof. Ing. Miloslav Pekař, CSc. Head of department

In Brno dated 2.9.2019

prof. Ing. Martin Weiter, Ph.D.
Dean

ABSTRACT

This work is aimed to the study of the properties of organic semiconducting materials with a focus on their conductivity and mobility of charge carriers. The main goal of this thesis is to elucidate the relationship between the chemical structure of organic semiconductors and their properties.

The theoretical part of this work is focused on the basics of organic semiconductors, charge transport and a review of the properties of organic semiconducting materials which have led to their application in field-effect and electrochemical transistors. The experimental part presents the overview of the materials used, the methods for their preparation and characterisation methods.

Within the result part, several methods for thin-film preparation were developed or optimize and subsequently their effect on the performance of OFETs were studied. The relevant properties of novel organic semiconducting materials were characterized and discussed with focus on the charge carrier mobility. The biocompatibility of several organic semiconductors were characterized and discussed. Electrical properties, stability and biocompatibility of electroactive polymer inks based on PEDOT:PSS was characterized and discussed with respect to their possible application in bioelectronics. Finally, the organic bioelectronic sensor for detection of the physiological response based on studied materials were constructed.

KEYWORDS

Organic semiconductors, DPP, PEDOT:PSS, OFET, OECT, charge carrier mobility, biocompatibility

ABSTRAKT

Tato práce je zaměřena na studium vlastností organických polovodivých materiálů se zaměřením na jejich vodivost a pohyblivost nosičů náboje. Hlavním cílem této práce je objasnit vztah mezi chemickou strukturou organických polovodičů a jejich vlastnostmi.

Teoretická část práce je zaměřena na základy organických polovodičů, transport náboje a přehled vlastností organických polovodivých materiálů, které vedly k jejich aplikaci v polních a elektrochemických tranzistorech. Experimentální část představuje přehled použitých materiálů, způsoby jejich přípravy a charakterizační metody.

V rámci výsledkové části bylo vyvinuto nebo optimalizováno několik metod pro přípravu tenkých vrstev a následně byl studován jejich vliv na výkon organických polem řízených tranzistorů. Byly charakterizovány a diskutovány relevantní vlastnosti nových organických polovodivých materiálů se zaměřením na pohyblivost nosičů náboje. Byla charakterizována a diskutována biokompatibilita několika organických polovodičů. Elektrické vlastnosti, stabilita a biokompatibilita elektroaktivních polymerních inkoustů na bázi PEDOT:PSS byla charakterizována a diskutována s ohledem na jejich možné použití v bioelektronice. Nakonec byl zkonstruován organický bioelektronický senzor pro detekci fyziologické odpovědi kardiomyocytů na základě studovaných materiálů.

KLÍČOVÁ SLOVA

Organické polovodiče, DPP, PEDOT:PSS, OFET, OECT, pohyblivost nosičů náboje, biokompatibilita

STŘÍTESKÝ, S. *Organic materials for organic field-effect transistors and electrochemical transistors*. Brno, 2020. Dizertační práce. Vysoké učení technické v Brně, Fakulta chemická, Ústav fyzikální a spotřební chemie. Vedoucí práce Martin Weiter.

PROHLÁŠENÍ:

Prohlašuji, že jsem dizertační práci vypracoval samostatně a že všechny použité literární zdroje jsem správně a úplně citoval. Dizertační práci je z hlediska obsahu majetkem Fakulty chemické VUT v Brně a může být využita ke komerčním účelům jen se souhlasem vedoucího práce a děkana FCH VUT.

DECLARATION:

I declare that the dissertation thesis has been worked out by myself and that all the quotations from the used literary sources are accurate and complete. The content of the dissertation thesis is the property of the Faculty of Chemistry of Brno University of Technology and all commercial uses are allowed only if approved by both the supervisor and the dean of the Faculty of Chemistry, BUT.

Ing. Stanislav Stříteský

.....

PODĚKOVÁNÍ:

*Tímto způsobem bych chtěl poděkovat vedoucímu dizertační práce **prof. Ing. Martin Weiter, Ph.D.** za odborné vedení, konzultace a rady, které mi během psaní dizertační práce poskytl. Dále bych chtěl poděkovat všem, kteří mi dali cenné rady a podporovali mě v tomto studiu, především mým rodičům a přítelkyni.*

CONTENT

1 INTRODUCTION 6
2 ORGANIC FIELD-EFFECT TRANSISTORS (OFETS) 7
2.1 Carbon as a basic building block of organic semiconductors 8
2.2 Energy Levels in Organic Semiconductors 10
2.3 Charge transport 12
2.3.1 Transport of charge carriers in organic semiconductors 12
2.4 Materials for OFETs 16
2.4.1 Acenes 16
2.4.2 Diketo-pyrrolo-pyrrole derivatives 18
2.5 Architecture and basic operation principles of OFETs 25
2.5.1 Charge injection 28
2.6 Parameters of OFETs 29
2.6.1 Evaluation of charge carrier mobility 29
2.6.2 Threshold voltage 29
2.6.3 On/Off ratio 30
2.6.4 Contact resistance 30
3 ORGANIC ELECTROCHEMICAL TRANSISTORS (OECTS) 31
3.1 PEDOT:PSS material for OECTs 31
3.2 Architecture and basic operation of organic electrochemical transistors 33
3.3 Parameters of organic electrochemical transistors 34
3.4 Biocompatibility of organic semiconductors 35
4 GOALS OF THE DOCTORAL THESIS 37
5 EXPERIMENTAL 38
5.1 Studied materials 38
5.1.1 Thiophene-benzo-furan DPP derivative 38
5.1.2 Diphenyl-amino-stilbene DPP derivatives 38
5.1.3 Alkyl substituted DPP derivatives 39
5.1.4 Naphthalene derivatives with ethynylene linker 41
5.1.5 PEDOT:PSS inks 41
5.1.6 Organic semiconductors used as reference 42
5.1.7 Supporting materials 43
5.2 Thin film preparation 44
5.2.1 OFET substrates 44
5.2.2 OECT substrates 45
5.2.3 Cleaning routine 45
5.2.4 Spin-coating and physical vapour Deposition 46
5.2.5 Printing techniques 47
5.3 Materials characterisation 50
5.3.1 OFET characterisation 50

5.3.2 OECT characterisations *52*
5.3.3 Optical spectroscopy *53*
5.3.4 Supplementary characterisations *54*
6 RESULTS AND DISCUSSIONS 55
6.1 Organic Field-Effect Transistors 55
6.1.1 Development and optimisation of OFETs based on DPP(TBFu)$_2$ *56*
6.1.2 Diphenyl-amino-stilbene DPPs *61*
6.1.3 Ethyladamantane derivatives of the DPPs *63*
6.1.4 The charge carrier mobility in N,N Ethyladamantyl DPP *66*
6.1.5 Naphtalane derivatives with ethynylene building block *69*
6.2 Organic Electro-Chemical Transistors 73
6.2.1 Biocompatibility of reference materials *73*
6.2.2 PEDOT:PSS The study of biocompatibility, stability and electrical properties *76*
6.2.3 The printed prototype of OECT arrays for real-time cell culture monitoring *81*
6.2.4 Gold printed electrodes for OECT sensors of beating cardiomyocytes *82*
7 CONCLUSIONS 87
8 OVERVIEW AND CONTRIBUTION OF PAPERS 89
9 ABBREVIATIONS 95
10 REFERENCES 97
11 CURRICULUM VITAE 110
12 LIST OF PUBLICATIONS 112
12.1 Impacted publications 112
12.2 Other publications and conference contributions 113
13 APPENDIX 113

1 INTRODUCTION

Organic semiconductors are studied for decades. Although organic semiconductors were firstly classified and used as insulating materials in 1970, by today they found many real applications in semiconducting devices. Most organic semiconductors are based on π-conjugated oligomers or polymers. Organic semiconductors with their lack of strongly bonded atoms in comparison to inorganic semiconductors exhibit many properties determined by intermolecular interaction such as Van der Waals, hydrogen or coulomb bonding interactions. Although the intermolecular interactions of organic semiconductors are weak, which limits their application potential, they have many benefits such as easy molecular tailoring, preparation of final devices by low-temperature and solution deposition methods, mechanical elasticity and compatibility with plastic substrates resulting in low-cost, large area and flexible integrated circuits, namely light-emitting diodes, thin-film transistors, photovoltaic cells, electronic paper or roll-up displays.

The chemical structures of organic semiconductors can be modified with respect to their electronic applications. However, the understanding of relationship between the structure and properties of these materials is still challenging. Therefore, the aim of this thesis is to characterise and optimise novel materials with respect to their possible applications in organic field-effect transistors (OFETs) and organic electrochemical transistors (OECTs). The second aim of this thesis is to bring new knowledge which enable and enhance the utilization of novel organic semiconductors in bioelectronics applications.

The theoretical part of this thesis describes the basics and the state of the art the of organic semiconductors used in organic field-effect transistors and organic electrochemical transistors. The experimental chapter describes the studied materials and methods for their preparation as thin films, and also it provides an overview of methods used for characterisation of transistor devices. The charge carrier mobility was studied by means of organic field-effect transistors. The main research was focused on the study of similar derivatives of diketo-pyrrolo-pyrroles used in OFETs and Poly(3,4-ethylenedioxythiophene): Poly(styrene sulfonate) (PEDOT:PSS) inks used in the OECTs.

The results related to the studies based on OFETs are described with respect to the correlation between the chemical structure of organic semiconductors, their properties and resulting charge carrier mobility. The OECT chapter discuss the results of characterization of biocompatibility and environmental stability of studied materials as well as results related to the proposal of useful transistor architectures for interaction with living cells.

All results discussed within this thesis were published in recognised peer-reviewed journals (8 papers) and presented at international conferences (3 conferences). A detailed description of the contribution of the author to each published paper is also provided in this chapter 8 .

2 ORGANIC FIELD-EFFECT TRANSISTORS (OFETs)

Organic field-effect transistors (OFETs) have been attracting ever more attention due to their potential use in cheap, large-scale and flexible electronic products. The central pillars of OFETs are organic semiconductors, which have shown considerable progress from the amorphous polythiophenes to the present acene crystal. Over recent years, the development of organic semiconductors (OS) has made significant improvement which can be demonstrated by enhancement of charge carrier mobility up to 10 cm^2/Vs or higher. This progress is presented in Figure 1, which illustrates the increase in the charge carrier mobility in OFETs during the last 30 years. The advancement of charge carrier mobility of OS gives these OFETs real potential for applications such as chemical sensors, OLED, CMOS or RFID. In addition, low-temperature deposition methods together with the mechanical elasticity of organic materials provide for OFETs compatibility with plastic substrates, resulting in their application in flexible integrated circuits, electronic paper or roll-up displays [1].

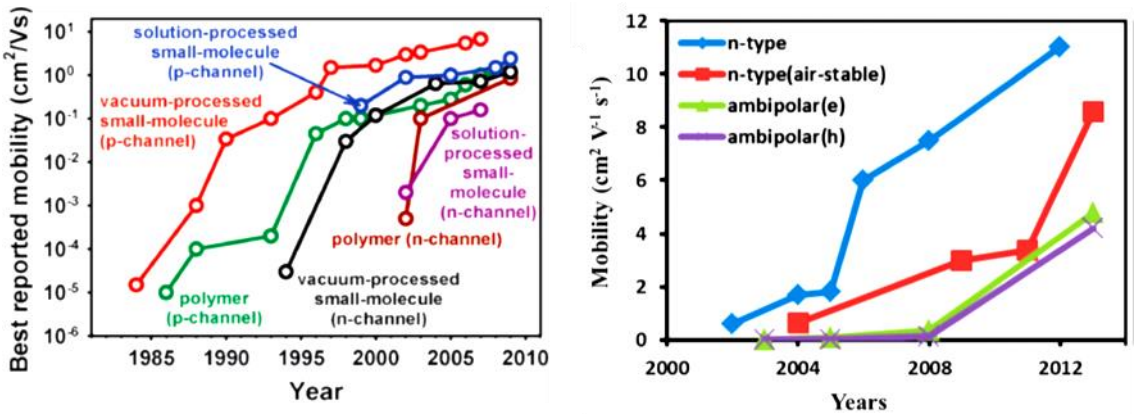

Figure 1 *Time evolution of charge carrier mobility [2; 3].*

2.1 CARBON AS A BASIC BUILDING BLOCK OF ORGANIC SEMICONDUCTORS

The basic building block of organic semiconductors is the carbon atom. The carbon atom has a relatively small size and moderate electronegativity that allows the formation of covalent bonds with the majority of other atoms. Carbon belongs to the IV group of the periodic table, and it enables the formation of four bonds. Carbons can hybridize in several forms that vary at single, double and triple bonds as well as long polymer chains.

Figure 2 shows the chemical structure of ethylene-like fundamental particles of organic semiconductors (oligomers and polymers) with a double bond and sp^2 hybridisation. Ethylene consists of two C-C bonds (sp^2 orbital – σ bond), and the remaining orbital shares p_z electrons. Electrons at a valence orbital and valence orbitals themselves create σ bonds and π bonds. Whenever a σ and π bond are formed, anti-bonding orbitals σ* and π* are also created. The molecular orbitals which create π-bonds and anti-bond orbitals are named the highest occupied molecular orbital (HOMO) and lowest unoccupied molecular orbital (LUMO), respectively. Π-bonds have weaker bonding power than σ bonds, and electrons can move at π-bonds. The electrons which are closer to the nucleus are firmly bonded. These electrons do not participate in charge transport [4].

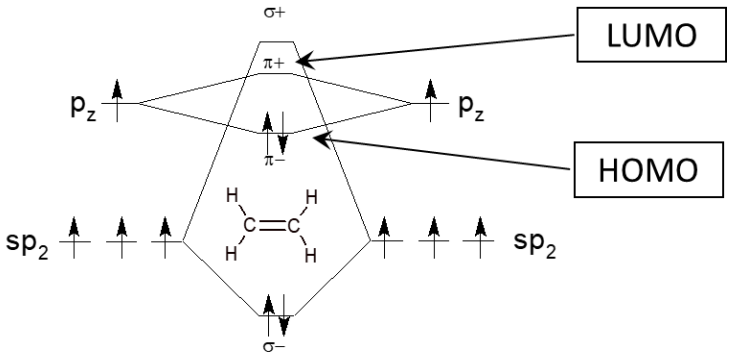

Figure 2 *Schema of an ethylene molecule, LUMO denotes the lowest unoccupied molecular orbital and HOMO denotes the highest occupied molecular orbital by electrons [4].*

The larger the size of molecules, the more sophisticated the electron density in the molecule. For example, benzene (Figure 3) has two resonance forms that create a delocalized π-bond between atoms in the molecule. This delocalisation is called a cloud of π electrons or π-conjugation [4].

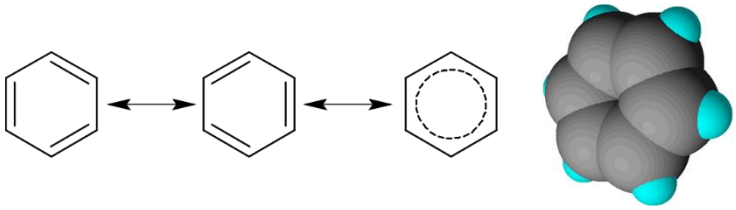

Figure 3 *Benzene structure [4]*

In π-conjugated systems there is a clear trend of band gap dependence (energy gap between HOMO and LUMO level) on their conjugation length. With a higher number of C atoms participating in conjugation, the gap between HOMO and LUMO decreases as shown in Table 1 [4]. One can expect that long conjugated systems will have zero bandgaps. Indeed, conjugated polymers still have finite bandgap due to two unequal bond strengths (single and double bonds) manifested as dimerisation in conjugated organic materials. This phenomenon is known as Pierels instability. However, for a higher dimensional π-electronic system, such as nanotubes and graphenes, Peierls instability does not apply, and these materials can reach semi-metallic or metallic conductivity [4].

Table 1 *The band gap of different materials [5; 6].*

Conjugated molecules	**Bandgap (eV)**
Butadiene	10.5
Hexatriene	8.6
Octatetraene	6.0
Decapentaene	4.9
Benzene	4.8
Naphthalene	4.0
Anthracene	3.4
Tetracene	2.6
Rubrene	2.4
Pentacene	2.1
Hexacene	1.8

2.2 ENERGY LEVELS IN ORGANIC SEMICONDUCTORS

A simplified energy model of an organic semiconductor is presented in Figure 4. On the left side of Figure 4, an energetic scheme of the "gas phase" of an isolated molecule is depicted. The HOMO level is there represented as singlet state $S_{0,}$ and the LUMO level is presented as excited singlet state S_1. These two molecular orbitals predetermine the energetic properties of the OS. The electrons in the HOMO orbital are considered to be the most distant from the nuclei, and therefore they are weakly bonded to the nuclei. Consequently, they are the most likely to be expelled from their orbital and move to the next higher orbital, which is the LUMO. The transfer of one electron from the HOMO to the LUMO orbital necessarily requires energy, which is given by the energy difference of these two orbitals [7].

The position of ground state level is determined by the ionisation energy I_G, which is defined by the amount of energy required to remove the electron from singlet state S_0 (the valence electron) to vacuum level. Similarly, the amount of energy released or spent when an electron is added to a neutral molecule is defined as the electron affinity A_G.

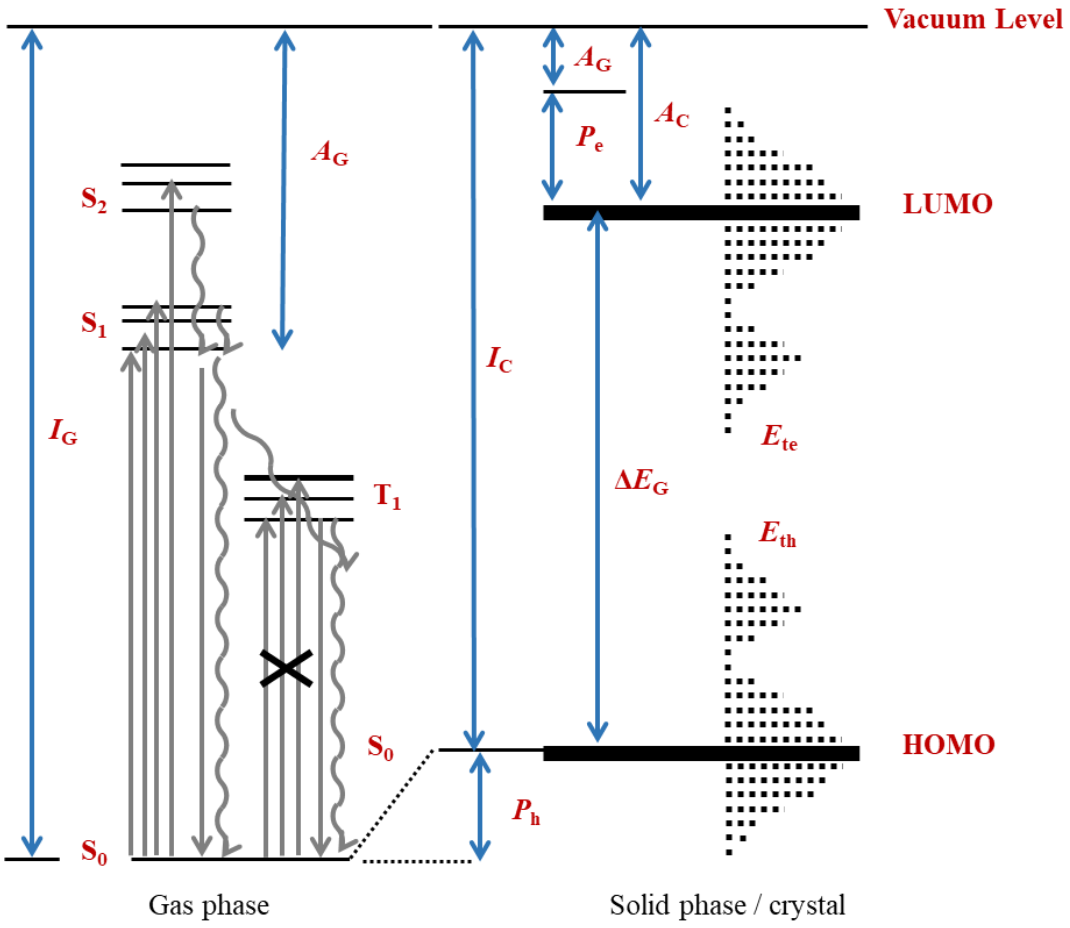

Figure 4 *Scheme of energy levels in organic semiconductors. A denotes electron affinity; I ionisation potential, $P_{h,e}$ polarisation energy of holes and electrons and ΔE_G the band gap associated with "G" gas or "C" crystals [8].*

In many organic materials, the other energetic states like higher singlet states (S_2) or triplet states (T_1) may be detected as illustrated in Figure 4. The triplet states can be occupied by two unpaired electrons. Therefore, the direct excitation of an electron to triplet states T_1 is forbidden. The process of excitation and de-excitation is illustrated in Figure 4 "gas phase." The loss of energy of electron from excitation state S_1 to ground state S_0 (de-excitation) can occur by different processes such as fluorescence, thermal irradiation, transfer energy to triplet states T_1, phosphorescence and others [9].

The energy levels of a solid organic semiconductor are depicted on the right side of Figure 4. If two atoms are close to each other, each energy level will be split into two due to the Pauli exclusion principle, which states that each quantum state can be occupied by no more than one electron. In the solid phase, the energy levels are shifted relatively to the gas phase, since the ionisation potential I_C of the solid differs from I_G by the electronic polarisation energy of holes P_h.

In disordered non-crystalline organic semiconductors, the energy levels are located on molecules and are denoted as LUMO and HOMO orbitals, respectively. The distribution of energy states can be described by the Gaussian distribution of the density of states (DOS). These states play the role of traps for holes and electrons together with deep traps (E_{th} and E_{te}). A useful estimation of the width of the band gap ΔE_G can be provided by the approximate relation $\Delta E_G = I_G - A_G - (P_h + P_e)$, where I_G is the ionisation energy, A_G is the electron affinity in the gas phase, and the P_e and P_h are the electronic polarisation energies of a negative and a positive charge carrier in the solid. Most organic semiconducting materials have bandgap widths at about 2–3 eV, i.e., three times higher than the bandgap of inorganic semiconductors [4; 8].

2.3 CHARGE TRANSPORT

The density of states in disordered systems is often asymmetrical and presents a barrier to the formation of one or another type of carrier. Disordered organic semiconductors support or strongly favour one type of charge carrier. The literature commonly refers to transport of holes and electrons in OS materials as p-type and n-type materials respectively. This designation of materials describes their major carrier transport and semiconducting properties.

Organic semiconducting molecules can be described as electron-rich or electron-poor materials. For example, in pentacene the hydrogen atoms which surround the carbon-conjugated backbone are less electronegative than the backbone itself and this tends to increase the electron density in the delocalized π-electron cloud. The electron-rich conjugated molecule of pentacene has difficulty accepting another electron, but the molecule can lose an electron relatively easily. As a consequence, the transport of positive charge carriers dominates in pentacene films [10]. A similar rule can be applied in the presence of an electron withdrawing group. The strong electron withdrawing group such as –CN, –Cl, –F, $–CF_3$ can then be considered as acceptors of electrons. As a result, it is possible to significantly shift the distribution of the density of the electrons in conjugated molecules [11].

2.3.1 Transport of charge carriers in organic semiconductors

The theory of charge carrier transport in organic semiconductors stems from the theory developed for amorphous inorganic semiconductors, since these materials can be described as disordered systems. The complex description of the transport involves the transport rate, scattering and trapping processes, recombination, tunnelling, hopping and other processes as well as the influence of the distribution of states in the OS [12]. The transport mechanism in organic semiconductors may vary depending on the crystallinity of the OS, which can be tuned from an amorphous to fully crystalline state. Dominantly, organic semiconductors are considered to be semi-crystalline semiconductors. The link between crystallinity and a suitable model of transport mechanism can be seen in Figure 5. Figure 5a illustrates a hopping transport model, where charge jumps from one localised state to another, and this is typical for the amorphous OS. The Poole–Frenkel multi-trap-and-release conduction model (MTR) depicted in Figure 5b is based on charge transport limited by the distribution of energy levels. The band transport model (case c) is useful for description of highly crystalline materials such as pure organic semiconducting crystals, e.g. some acenes [4; 13].

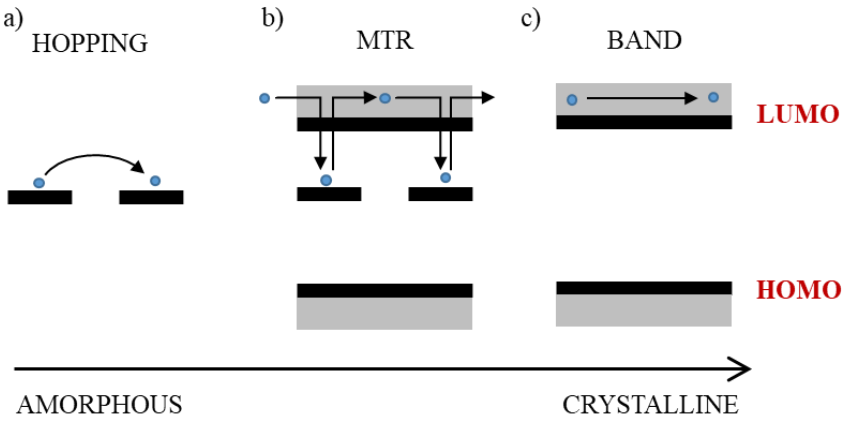

Figure 5 *Illustration of n-type conduction models, a) hopping conduction consists of charge jumps from one localised state to another. b) Poole – Frenkel multi-trap-and-release conduction (MTR) c) band transport theory [4; 13].*

The most important parameter used for description of charge carrier transport in semiconductors is charge carrier mobility (μ), which can be defined as average drift velocity (v_d) per applied electric field (E) determined by the equation [14]

$$\mu = \frac{v_d}{E}. \qquad (1)$$

The charge carrier mobility is the most important parameter of the various transport models.

Band transport model

The band transport mechanism based on transport of charge through valence or conductive band is mostly observed in inorganic materials. In organic semiconductors, band transport can be observed in high crystalline materials. According to band transport theory, the charge carrier mobility μ can be expressed as follows:

$$\mu = \frac{q\lambda}{m\, v_{th}}, \qquad (2)$$

where q is an elementary charge, λ is a free electron path (distance between two collisions), m is an effective mass of the charge carrier, and v_{th} is its thermal velocity [15]. The band transport was observed in highly crystalline rubrene, which is described in detail in Chapter 2.4.1 [16].

Multi-trap and release transport model

The multi-trap and release transport (MTR) model is used for description of charge transport in semi-crystalline organic semiconductors, for example where crystalline domains are separated by an amorphous region. From an energy point of view, the trap-limited band transport is based on the movement of free carriers in delocalized states. Free carriers interact with the localized states (traps), they can be trapped and immobilized in the localized state. After some time, the trapped carriers are thermally excited back to delocalized states. The processes of trapping and release occurs many times during the time when the carrier is crossing through the specimen, until the carrier reaches the opposite electrode. In a simplified MTR model a single energy level of trap E_T in the vicinity of the transport path can be considered. The effective mobility μ_{eff} for MTR model is given by the equation: [17]

$$\mu_{eff} = \mu_0 \alpha e^{-(E_C - E_T)/kT}, \tag{3}$$

where μ_0 is the mobility in the band and α is the ratio of the density of traps to the effective density of state at the transport band edge. In the case of a single trap level of energy E_T with a density of state N_t, the total concentration n_{TOT} of the charge carrier can be split into the concentration of free carriers n_f and trapped carriers n_t. The concentration Θ of trapped carriers is given by

$$\Theta = \frac{n_t}{n_t + n_f} = \frac{N_t}{N_c} e^{-(E_C - E_T)/kT}, \tag{4}$$

where N_C is the effective density of states at the transport band edge, k is Boltzmann's constant and T is the absolute temperature.

Hopping transport model

The low-energy coupling between the molecules in the solid state ensures that the electrons in these materials are strongly localised. From a simplified point of view, the hopping model assumes that charge transport occurs via a sequence of charge transfer steps from one localised state to another [18].

The hopping model is useful for qualitative description of charge transport in disordered materials such as organic semiconducting polymers. The carrier mobility in disordered materials is thermally activated with a temperature dependence of the mobility given by the Pool-Frenkel equation [19]:

$$\mu = \mu_0 e^{-(\Delta_0 - \beta\sqrt{F})/kT}. \tag{5}$$

In equation 5, μ_0 is the mobility at zero electric fields, β is the Pool–Frenkel factor, Δ_0 is the activation energy, F is the electric field, k is Boltzmann's constant and T is the absolute temperature.

A more complex theory of hopping transport was described by Bässler in 1993 [20]. Bässler's disorder model rests in the assumption that the polarisation energy of the charge carrier is located on the molecule. The model describes the dependence of charge carrier mobility, temperature and electric field:

$$\mu = \mu_0 \exp\left[-\left(\frac{2}{3}\frac{\sigma}{kT}\right)^2\right]\exp\left\{C\left[\left(\frac{\sigma}{kT}\right)^2 - \Sigma^2\right]\sqrt{F}\right\}, \quad (6)$$

where μ_0 is the mobility at zero electric field, σ is the distribution of localized transport states, C is an empirical constant, T is temperature, F is an electric field and in addition to the energetic disorder, there exists a position disorder with a Gaussian distribution of variance called off-diagonal disordering Σ [20].

Polaron transport model

The models described above fail to account for the presence of polarons in OS. If the charge carrier is localised on a molecular site, it tends to polarise its neighbouring surroundings. As a result, a polarisation cloud occurs around the charge, and it moves with the charge. The travelling species are called polarons. The stability of a polaron can be defined by two characteristic time constants. The first of these constants is the average time when the charge stays on the molecule and the second is the polarisation time that forms the polarisation cloud around the charge. In inorganic semiconductors, the localisation time is shorter than the polarisation time, and a cloud does not form. However, in organic semiconductors, the localisation time is two magnitudes lower and a polaron has enough time to form [21].

A characteristic of polaron transport is a temperature dependence of the effective mass expressed by the following equation:

$$m_{eff}(T) = m_{eff}(0)e^{T/T_0}, \quad (7)$$

where m_{eff} (0) is the polaron effective mass at zero temperature (T_0), and T is the characteristic temperature. The charge carrier mobility can be described as:

$$\mu = \frac{qa^2}{kT}k_{ET}, \quad (8)$$

where a is the lattice parameter of the molecular crystal, q is an elementary charge, k is Boltzmann's constant, T is the temperature and k_{ET} is the electron transfer rate [17; 21].

2.4 MATERIALS FOR OFETs

This thesis is focused on the study of the relationship between the chemical structure of organic semiconductors and their properties. Organic semiconductors can be divided into two main groups: small conjugated molecules and conjugated polymers. Small conjugated molecules have a better-defined chemical structure and their properties can be easily linked to their chemical structure in comparison to conjugated polymers. Therefore, in this thesis the main attention is focused on small molecules.

2.4.1 Acenes

Acenes and heteroacenes are the most-studied small molecules with semiconducting properties. In most cases small molecular OS are applied in OFETs in the form of well-ordered polycrystalline layers. The OS used in OFETs such as pentacene, rubrene and fullerene (C60) exhibit a mobility of holes and electrons up to 40 cm^2/Vs [1; 2; 22].

Fused rings of acene structures can form a large number of organic semiconductors. Several well-known structures are depicted in Figure 6. The conjugation length of π-delocalized orbitals sway the characteristic properties of acenes. The fused rings are flat and rigid, which lead to excellent stacking properties. Thus the acenes can form large crystals and polycrystalline films with good transport properties [6].

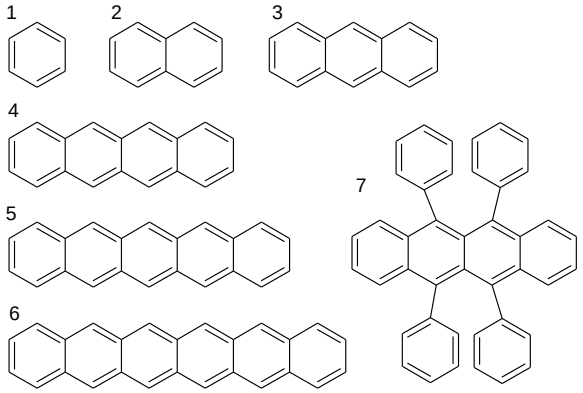

Figure 6 *Structures of acenes: 1 – benzene, 2 – naphthalene, 3 – anthracene, 4 – tetracene, 5 – pentacene, 6 – hexacene, 7 – rubrene*

Anthracene is the smallest representative of the acenes which exhibit transistor characteristics. OFETs based on a single crystal of anthracene showed a hole mobility of 0.02 cm^2/Vs under a low temperature of 170–180 K [23].

Tetracene is another significant derivative of the anthracene analogue, which has a slightly higher degree of conjugation. OFETs prepared from single tetracene crystals exhibit hole mobility up to 1.3 cm^2/Vs [24].

Pentacene and rubrene are popular small molecular OS exhibiting hole transport which have been widely used in OFETs over the past ten years. Organic field-effect transistors based on crystals of pentacene and rubrene showed optimised hole mobility

up to 15–40 cm^2/Vs [1; 2; 22]. Their efficient charge transport is attributed to a widespread π-system with strong intermolecular overlaps, as well as the suitable energy level of the highest occupied molecular orbital (HOMO: −5.1 eV) for efficient injection of holes from contacts. Despite the popularity of pentacenes in organic electronics, they are not ideal for commercial use. The poor solubility of pentacene in conventional organic solvents, as well as its low environmental stability in air, significantly impedes its practical use. Pentacene is relatively easily oxidizable, which disrupts transport and crystallisation. Therefore, pentacene may condense into two crystalline phases that often leads to the growth of the polymorphic crystal, which reduces the performance of OFETs [1; 2; 22].

Rubrene is a tetracene derivative. Like tetracene or pentacene, rubrene molecules have a herringbone motif, but its phenyl substituents could lead to steric interactions upon a long-axis displacement. The highest hole mobility (20–40 cm^2/Vs) was achieved with a rubrene single crystal [25]. A typical property of single organic crystals is anisotropy of the mobility at different crystal axes [8]. This is due to the orientation of the molecules in the crystal and the different lattice distance. The charge motion along the stack is facilitated in comparison with that in the perpendicular direction (Figure 7).

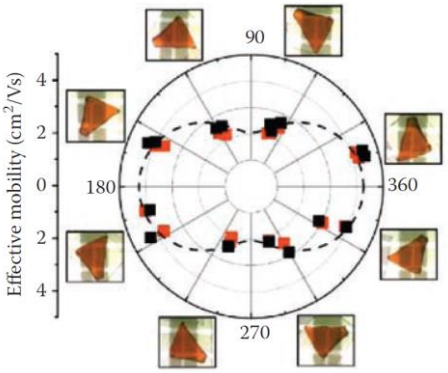

Figure 7 *Polar plot of the mobility at rubrene a-b surface [8; 16].*

Thin films or single crystals based on hexacene are difficult to prepare. However, hexacene films from a monoacetone precursor have been prepared and characterised in OFETs. The low degree of molecular packing of hexacene caused by thin film preparation from the precursor showed a hole mobility up to 4.28 cm^2/Vs and long-term stability in air [26].

As follows from these studies, the molecular packaging is the key factor influencing the charge carrier mobility. In molecular organic semiconductors, intramolecular charge transport is predominantly based on their transport along molecular π-orbitals. In the solid state, the intermolecular charge transport is influenced by the degree of overlap between the adjacent molecules, which significantly determines the mobility of the carriers.

More recently, extensive work has been carried out on the design of acene derivatives to enhance the intermolecular overlaps and thus improve the charge carrier

transport. The acene molecules were purposefully synthesised to achieve herringbone packing, lamellar stacking, brick-wall, and brick stone molecular arrangements with promoted π–π stacking [22]. The differences between the structures can be seen in Figure 8. It was found that plane-to-plane (face-to-face) and brickwall packing with strong π–π intermolecular interactions are favourable for high charge carrier mobility.

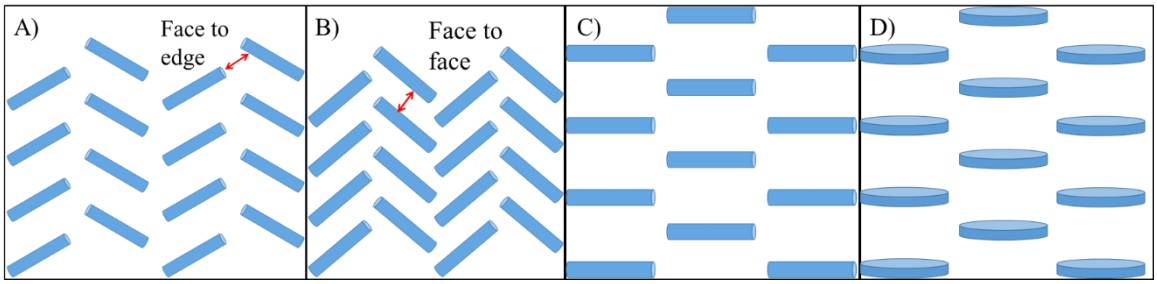

Figure 8 *A) Herringbone packing (face-to-edge) without π–π overlap between adjacent molecules; B) herringbone packing with π–π (face-to-face) overlap between adjacent molecules; C) lamellar motif, 1D π-stacking; D) lamellar motif, 2D π-stacking (brickwall) [3; 22].*

2.4.2 Diketo-pyrrolo-pyrrole derivatives

The basic bicyclic dilactam core of DPP derivatives is shown in Figure 9. The conjugated functional segments such as phenyl, thiophenyl or others, are very often attached to the dilactam core at position R_1 and R_2. These conjugated segments R_1 and R_2 significantly influence the electronic structure of the whole molecule. The torsion angle (α, β) between R_1 and R_2 substituents and the plane of the dilactam core influence their mutual electronic coupling. In planar molecules, in which the $R_{1,2}$ groups are in the same plane as the DPP core, a significant electronic coupling between $R_{1,2}$ and dilactam core was observed [27]. The substituents at position R_3 and R_4 mostly do not contain conjugated chains (such as alkyls) and thus they do not influence the electronic structure of DPP derivatives. The R_1, R_2, R_3 and R_4 may vary with large number of substituents which produce large portfolio of derivatives with different properties. The following paragraphs will focus on two main representative derivatives, namely phenyl and thiophenyl derivatives, which are depicted in Figure 9.

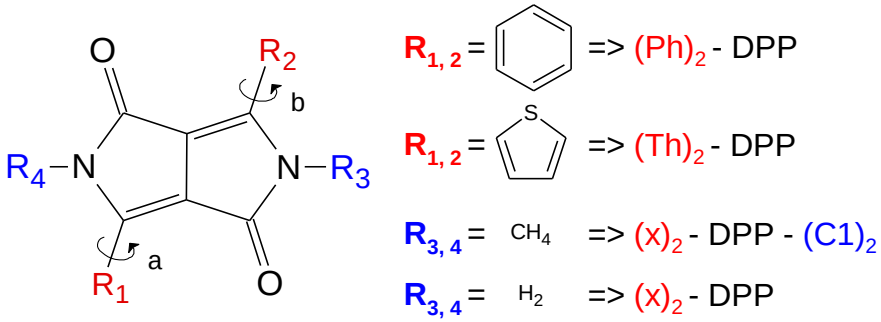

Figure 9 *Scheme of DPP unit; In the text the following will be used: ($R_{1,2}$)-DPP-($R_{3,4}$), $R_{1,2}$ for the conjugated group and $R_{3,4}$ for the alkyl substitution on N-position*

The 3,6-diphenyl-2,5-dihydropyrrolo[3,4-c]pyrrole-1,4-dione was first reported by Farnum et al. forty years ago (illustrated as $(Ph)_2$-DPP in Figure 9). Since the beginning of the first synthesis routes, other synthetic techniques have been developed [28; 29].

The NH group of the dilactam core of the DPP molecules was found to be sensitive to proton acceptors. Deprotonation of NH caused by a proton acceptor leads to increased electron density in the dilactam core, which can be observed as a significant redshift (bathochromic) of DPP. The analogous increase in electron density in the dilactam core can be caused by intermolecular hydrogen bonding between the NH moiety of one molecule and the oxygen atom of another molecule according to Mizuguchi et al [30].

In the presence of an alkyl chain $R_{3,4}$, i.e. without hydrogen bonding interactions, repulsive interaction between $R_{1,2}$ and $R_{3,4}$ can be observed [29]. The repulsive interaction rotates $R_{1,2}$ substituents out of the plane of the dilactam core. The torsion angle of $R_{1,2}$ groups significantly reduces the charge transfer integral between the $R_{1,2}$ group and the central dilactam core. Examples of torsion angles for phenyl DPP derivatives have been reported by Vala et al. and can be found in Table 2 [31; 32].

Table 2 *The torsion angle of phenyl rings of DPP derivatives in the case of mono and di substituents, C1-methyl, C4-butyl, C7-heptyl. T_D denotes the onset of the temperature of degradation, T_M the temperature of the melting point [31; 33].*

DPP Scheme	DPP derivatives	R_3 [α °]	R_4 [β °]	T_D (°C)	T_M (°C)
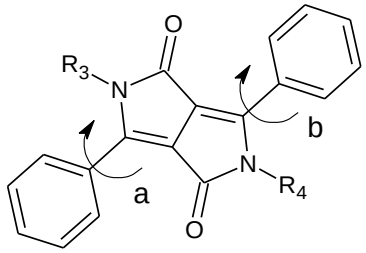	**$(Ph)_2$-DPP-$(H)_2$**	H [7°]	H [7°]	396	-
	$(Ph)_2$-DPP-$(C1)_2$	CH_3 [31°]	CH_3 [31°]	262	234
	$(Ph)_2$-DPP-$(C4)_1$	C_4H_9 [36.0°]	H [6.7°]	281	245
	$(Ph)_2$-DPP-$(C4)_2$	C_4H_9 [36.5°]	C_4H_9 [36.5°]	246	120
	$(Ph)_2$-DPP-$(C7)_1$	C_7H_{15} [36.7°]	H [7.7°]	-	212
	$(Ph)_2$-DPP-$(C7)_2$	C_7H_{15} [35.9°]	C_7H_{15} [35.9°]	290	115

As can be seen from Table 2, the length of the linear alkyl chain has a small or negligible impact on the rotation of $R_{1,2}$ groups. It was observed that the mono N-substitution induces rotation of the R_1 or R_2 substituent next to the substituted nitrogen atom [34].

The size of $R_{1,2}$ also has an impact on the torsion angle. This effect was studied by Dhar et al. in the case of phenyl, thiophenyl and selenophene DPP derivatives with a hexyl side chain ($R_{3,4}$) [29]. The large phenyl DPP showed an torsional angle of 32° with weak intramolecular interaction between the phenyl and dilactam core. However, smaller thiophenyl and selenophene showed lower torsional angles of 9° and 12° with strong intramolecular interaction between the donor and acceptor units as can be seen in Table 3. The smaller $R_{1,2}$ group increases the distance between $R_{1,2}$ and $R_{3,4}$, which

leads to lesser repulsive interactions and consequently a lower torsion angle of $R_{1,2}$ groups [34; 35].

Table 3 *Properties of DPP derivatives [29].*

Derivate	ε_{max} ($M^{-1}cm^{-1}$)	HOMO (eV)	LUMO (eV)	Gap (eV)	Torsion angle (°)	Melting Point (°C)
$(Ph)_2$-DPP-$(C6)_2$	12 600	-5.71	-3.08	2.85	32	134
$(Th)_2$-DPP-$(C6)_2$	27 600	-5.56	-3.10	2.44	9	174
$(Se)_2$-DPP-$(C6)_2$	33 600	-5.49	-3.20	2.40	12	140

An influence of the donor group on the electronic properties of DPP derivatives was observed in selenophene and thiophene DPP derivatives. The lesser electronegativity of selenium (compared to sulphur) and the lower aromaticity of the selenophene ring lead to stronger donor properties of these groups, resulting in higher stabilisation of the excited states. Consequently, higher molar absorption coefficient (ε_{max}) was observed.

The substituted alkyl chain $R_{3,4}$, as well as the size of the $R_{1,2}$ influence the torsion angle and consequently they can change the effective conjugation length. For this reason, the torsion angles α and β of the R_1 or R_2 substituents are the most important conformation parameters.

Physical properties

In organic field effect transistors, the small DPP molecules are used as solid-state thin layers. The properties of DPP molecules in thin layers are influenced by intermolecular interaction such as hydrogen bonding, van der Waal's or π-π stacking interactions. Due to structural features, N- alkyl substituents $R_{3,4}$ at DPP molecules significantly change the physical properties such as thermal stability, melting point or molecular ordering [36].

David et al. studied the thermal properties of $(Ph)_2$-DPP derivatives with different alkyl chains $R_{3,4}$ [33]. They found that the length of the alkyl chain has a large impact on the thermal stability as is illustrated in Table 2. The temperatures of degradation of $(Ph)_2$-DPP derivatives with these alkyl chains are in the order: $(H)_2 > (C7)_2 > (C4)_1 > (C1)_2 > (C4)_2$. The temperatures according to sublimation and evaporation can be observed in the ordering: $(H)_2 > (C7)_1 > (C7)_2 > (C4)_1 > (C4)_2 > (C1)_2$. In contrast, the melting points were observed in the reverse order, i.e., $(C1)_2 > (C4)_2 > (C7)_2 > (H)_2$. The higher stability of $(Ph)_2$-DPP derivatives can be explained by their compact and rigid structure, which are stabilised by intermolecular hydrogen bonds between the −NH group of one molecule and the oxygen atom of the neighbouring one [33; 37].

The similar influence of the alkyl chain on thermal stability was observed by Naik et al. for $(Th)_2$-DPP derivatives as depicted in Table 4 [34].

Table 4 *Thiophenyl DPP derivatives in the publication of Naik et al [34].*

DPP Scheme	Alkyl substituents	Melting point (°C)
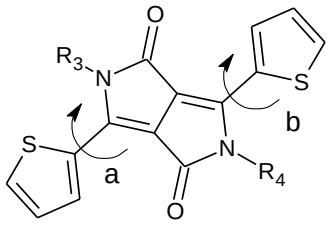	$R_3 = R_4$ = n-hexyl	174
	$R_3 = R_4$ = 2-EthylHexyl	127
	$R_3 = R_4 = CH_3(OCH_2CH_2)_3$	120–122
	$R_3 = R_4$ = 2-OctylDodecyl	77–78
	R_3 = 2-EthylHexyl; $R_4 = CH_3(OCH_2CH_2)_5$	semi solid
	R_3 = n-hexyl; $R_4 = CH_3(OCH_2CH_2)_5$	83–85

As can be deduced from this study, the melting points of $(Th)_2$-DPP derivatives are dramatically modified in the presence of the branched alkyl chain $R_{3,4}$. The $(Th)_2$-DPP derivatives with branched chains exhibit a lower melting point than derivatives with linear $R_{3,4}$. $(Th)_2$-DPP derivatives with unsymmetrically substituted alkyl chains showed a dramatic decrease in the melting temperature. These authors also observed that $(Th)_2$-DPP derivatives with branched and unsymmetrical substituted DPP derivatives exhibit an amorphous semi-solid state of thin layers [34].

The thermal stability of DPP derivatives determine the stability of organic semiconducting devices. The degree of crystallinity of thin layers strongly influence the final properties of OS devices. The crystallinity of $(Ph)_2$-DPP derivatives of thin layers was studied by Weiter et al. In this study it was observed that the type of substitution, i.e., symmetrical or mono-substituted R_3 and R_4, determine the film morphology. The symmetrical substitution leads to formation of large planar crystallites, whereas the mono-substituted derivatives (substitution only at one N atom) highly rough fibber crystallites. In this and other studies it was reported that the addition of energy such as the higher temperature of the substrate during vacuum deposition increases the size of crystals of DPPs [34; 36].

Charge carrier mobility

Recent studies have shown high charge carrier mobility of various DPP derivatives. The hole mobility of 2.0 cm^2/Vs and electron mobility of up to 0.96 cm^2/Vs are promising values for construction of organic electronic devices. [29; 38]

Factors such as the presence of H-bonds, alkyl chains at $R_{3,4}$ or substitution of electron acceptors influence the charge carrier mobility in DPPs. In this chapter these influences are discussed with respect to two main groups of DPP derivatives, namely phenyl $(Ph)_2$-DPP and thiophenyl $(Th)_2$-DPP.

First, a hole mobility of $1.43 \cdot 10^{-5}$ cm^2/Vs of $(Ph)_2$-DPP was reported by Yanagisawa et al. in 2008 [39]. In 2013, Kojima et al. theoretically predicted a mobility of electrons of $5.1 \cdot 10^{-4}$ cm^2/Vs and of holes of $3.9 \cdot 10^{-3}$ cm^2/Vs in $(Ph)_2$-DPP

[40]. The predicted mobility was experimentally confirmed by Glowacki et al. in 2014, who studied three phenyl DPP derivatives: pristine $(Ph)_2$-DPP, chloride-$(Ph)_2$-DPP and bromide-$(Ph)_2$-DPP without the alkyl substituents on nitrogen atoms. They observed electron and hole mobility up to $1 \cdot 10^{-2}$ cm^2/Vs in high ordered $(Ph)_2$-DPP films [41]. The high crystallinity of $(Ph)_2$-DPP was analysed to be caused by the H-bonds of DPPs. The significant properties of $(Ph)_2$-DPP derivatives are summarized in Table 5. In this study halogenated $(Ph)_2$-DPP derivatives showed higher hole and electron mobilites than non-halogenated $(Ph)_2$-DPP derivatives. This observation was ascribed to a change of the HOMO and LUMO levels.

Table 5 *The electronic properties of (x-$Ph)_2$-DPP derivatives, where x = H, Cl or Br [41].*

Derivate	Band gap CV (eV)	Band gap optical (eV)	HOMO (eV)	LUMO (eV)	Electron mobility [calc.] (cm^2/Vs)	Hole mobility [calc.] (cm^2/Vs)
$(Ph)_2$-DPP	2.1	2.1	-5.4	-3.3	0.01 [0.09]	0.01 [0.08]
(Cl-$Ph)_2$-DPP	2.8	2.1	-6.0	-3.2	0.03 [0.09]	0.01 [0.17]
(Br-$Ph)_2$-DPP	2.7	2.1	-6.1	-3.4	0.06 [0.10]	0.02 [0.20]

The influence of H-bonds on charge carrier mobility was also confirmed by Dhar et al. [29]. They studied the charge carrier mobility of mono and di-hexyl derivatives of $(Ph)_2$-DPP and $(Th)_2$-DPP. It was observed that the mono-hexyl DPP derivatives are tightly bonded due to the H-bonds and thus showed higher hole mobility than di-hexyl derivatives as can be seen in Table 6. The highest reported hole mobility of $(Th)_2$-DPP observed was 2.0 cm^2/Vs.

Table 6 *Hole mobilities of DPP derivatives [29].*

Derivate	Average hole mobility (cm^2/Vs)	Max hole mobility (cm^2/Vs)
$(Ph)_2$-DPP-$(C6)_1$	0.016	
$(Th)_2$-DPP-$(C6)_1$	0.3	2.0
$(Ph)_2$-DPP-$(C6)_2$	0.0002	0.003
$(Th)_2$-DPP-$(C6)_2$	0.004	0.05

Despite DPP derivatives with H-bonding show good charge carrier mobility, they are usually insoluble, which reduces their potential use in large-scale printable electronics. Therefore, the effect of the N-substituted alkyl chain ($R_{3,4}$) on charge carrier mobility has been studied by several researchers. The results of the studies of Palai et al. and Kwon et al. for long alkyl chain DPP derivatives are summarized in Table 7 [42; 43].

Table 7 *Hole mobility for a different length of $(Th)_2$-DPP [42; 43].*

DPP derivate	Gate insulator	Substrate Temp. (°C)	Hole mobility (cm^2/Vs)
$(Th)_2$-DPP-$(C12)_2$	OTS treated SiO_2	25	0.00459
	CL-PVP	25	0.00742
		60	0.00864
		90	0.0132
$(Th)_2$-DPP-$(C16)_2$	CL-PVP	25	0.0113
$(Th)_2$-DPP-$(C18)_2$	CL-PVP	25	0.00477

A comprehensive study of the influence of the alkyl chains' length in $(Th)_2$-DPP derivatives on charge carrier mobility was published by Stolte et al. in 2016 [44]. They studied a broad series of 24 DPP derivatives bearing various dialkyl substituents at NH positions. Butyl, pentyl, hexyl, heptyl, octyl and ethylhexyl with a different electron-withdrawing member as chlorine, bromine and cyano moiety attached to the thiophene ring of $(Th)_2$-DPP were studied.

It was observed that the length of the alkyl chain causes a small or negligible effect on the hole mobility of $(Th)_2$-DPP as is illustrated by the orange curve in the embedded graph in Table 8. This table shows the effect of electron-withdrawing substituents such as chlorine, bromine and cyano-substituted $(Th)_2$-DPP derivatives on hole and electron mobility. The substitutions of halogen atoms on thiophene rings (blue and red curve) led to an increase in hole mobility from 0.01 to 0.1 cm^2/Vs. The cyano-substituted DPP derivatives show ambipolar behaviour. The electron and hole mobility of these derivatives varies without showing a clear tendency with respect to the length of alkyl chains. The observed electron mobility of cyano derivatives was attributed to the electron-poor CN-DPP structure.

Table 8 *Hole mobility of $(Th)_2$-DPP derivatives on the left and electron mobility of (CN-$Th)_2$-DPP derivatives on the right side [44].*

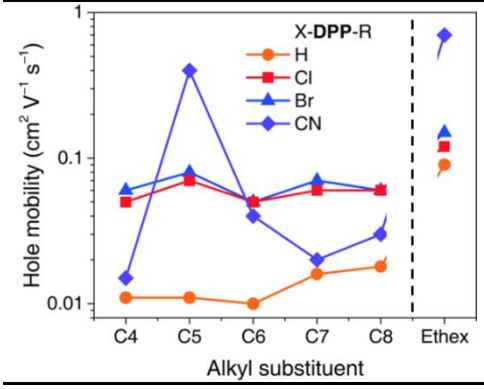

(CN-Th)2-DPP-(x)	Electron mobility (cm^2/Vs)
C4	0.01
C5	0.01
C6	0.04
C7	0.005
C8	0.005
ethylhexyl	Non-measured

The effect of the strong electron-withdrawing groups attached to $(Th)_2$-DPP was observed in the studies of Qiao et al. and Yoon et al. as is shown in Table 9 [45; 46].

Quiao et al. studied two alkyled derivatives ($R_{3,4}$) with substituted dicyanomethylene. Dicyanomethylene is known as an excellent electron acceptor and usually offers low-lying LUMO energy levels, which is suitable for enhanced air stability of n-type organic semiconductors. It was found that the low-lying LUMO level together with the strong electron acceptor led to dominant electron mobility. $(Th)_2$-DPP derivatives with a vinyl component which extends the conjugation without a distorted backbone structure were studied by Yoon et al [46]. This dicyanovinylene derivative with prolongated conjugation and a low-lying LUMO level showed a higher reported electron mobility of 0.96 cm^2/Vs than other $(Th)_2$-DPP derivatives with the strong electron acceptor unit mentioned above.

Table 9 *Electron mobility in dicyano derivate of $(Th)_2$-DPP [45; 46].*

Derivates of $(Th)_2$-DPP	R_3=R_4	Substrate temperature (°C)	Electron mobility (cm^2/Vs)
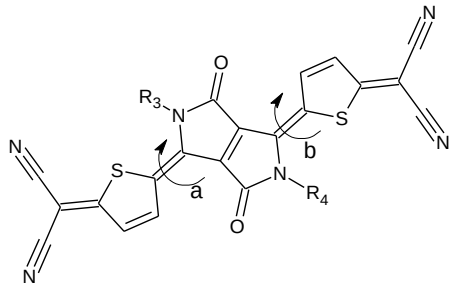	ethylhexyl	room temp.	0.20
		80	0.29
		100	0.45
		120	0.55
		150	0.01
	hexyldecyl	room temp.	0.12
		90	0.18
		120	0.35
		150	0.01
R_3 = R_4 = ethylhexyl 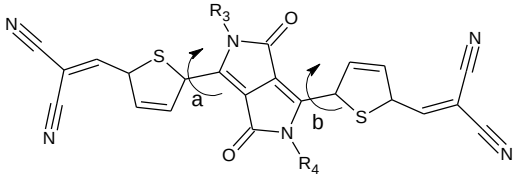		RT-solution	0.96
		RT-sublim.	0.00088
		70	0.11
		100	0.47
		120	0.64
		140	0.55

The high charge carrier mobility was observed in high crystalline films of DPP derivatives with significant hydrogen bonding interactions. In the studies of Quiao et al. and Yoon et al. the dependence of charge carrier mobility on the degree of crystallinity caused by the different temperature of the substrate during vacuum deposition was elucidated as shown in Table 9. In both cases an optimum deposition temperature of 120 °C was observed which led to a maximum electron mobility of 0.55 cm^2/Vs for ethylhexyl and 0.35 cm^2/Vs for hexyldecyl derivatives.

2.5 ARCHITECTURE AND BASIC OPERATION PRINCIPLES OF OFETs

The first FET was proposed by J. E. Lilienfeld, who received a patent for this idea in 1930. He proposed the principle of a field-effect transistor as a capacitor with a conducting channel between a source and a drain electrode [47]. The first silicon-based transistor was developed by William Shockley, John Bardeen and Walter Brattain in 1947 [48]. In 1956 these researchers received the Nobel Prize in Physics for this achievement. The first organic field-effect transistor was reported by Koezuka and colleagues in 1987 based on polythiophene molecules [49].

A simplified scheme of an OFET transistor is depicted in Figure 10, which also includes the basic parameters of the organic field-effect transistors.

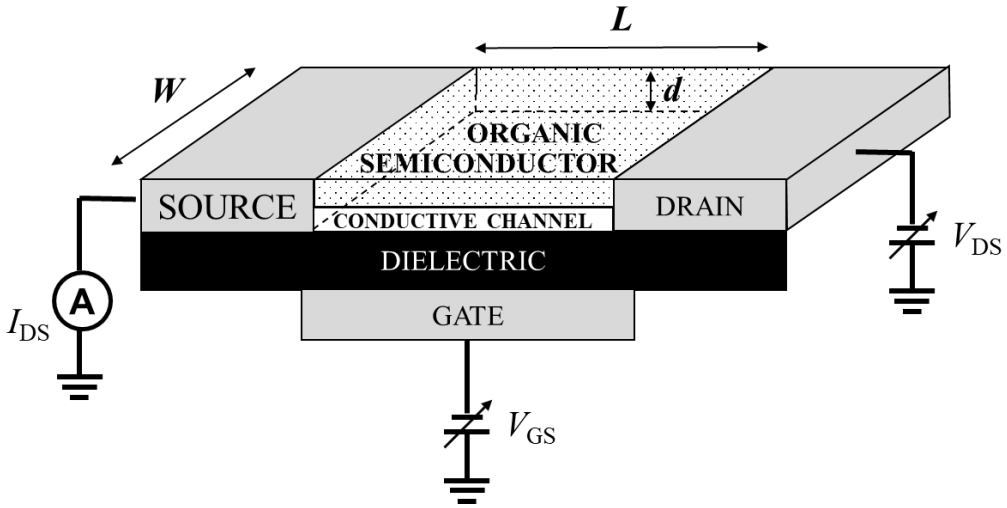

Figure 10 *Simplified scheme of OFET transistors [49]. W denotes channel width, L channel length, d the thickness of semiconductor, V_{DS} applied voltage between the source and the drain electrode, I_{DS} electric current passing through organic semiconductor and V_{GS} the applied voltage between the gate and source electrode.*

The organic field-effect transistor consists of source and drain electrodes that are in contact with organic semiconductors. The organic semiconductor is separated by dielectric layer from gate electrode. The gate voltage V_{GS} applied between the source and gate electrodes induces the formation of an accumulation layer at the interface of the semiconductor/insulator. The accumulation layer forms a conducting channel in organic semiconductors. When the voltage V_{DS} is applied between the source and drain electrodes it causes a charge injection from the source electrode to the OS through a Schottky barrier at the contact. The charges are transported through the conducting channel to the drain electrode. Therefore, the current I_{DS} is dependent on both the V_{DS} and V_{GS} voltages.

The typical characteristics of an organic field-effect transistor based on the p-type of OS are shown in Figure 11. The dependence of current I_{DS} on the applied voltage V_{DS} with constant V_{GS} is called the output characteristic. The dependence of current I_{DS} on the applied gate voltage V_{GS} with constant voltage V_{DS} is called the transfer characteristic. As follows from Figure 11 the output characteristic can be split into a linear region where current increases linearly with the applied voltage V_{DS} and a saturation region where the current is saturated. The current I_{DS} in these regimes can be described by the equations:

$$I_{DS}(\mathrm{LIN}) = \frac{W}{L} C_i \mu \left[(V_{GS} - V_T) V_{DS} - \frac{V_{DS}^2}{2} \right], \tag{9}$$

$$I_{DS}(\mathrm{SAT}) = \frac{W}{2L} C_i \mu (V_{GS} - V_T)^2, \tag{10}$$

where C_i is the capacitance of the insulator, W is the width of the channel, L is channel length, μ is the charge carrier mobility in the OS and V_T is the threshold voltage, which can be expressed as gate voltage when the conducting channel is formed [12].

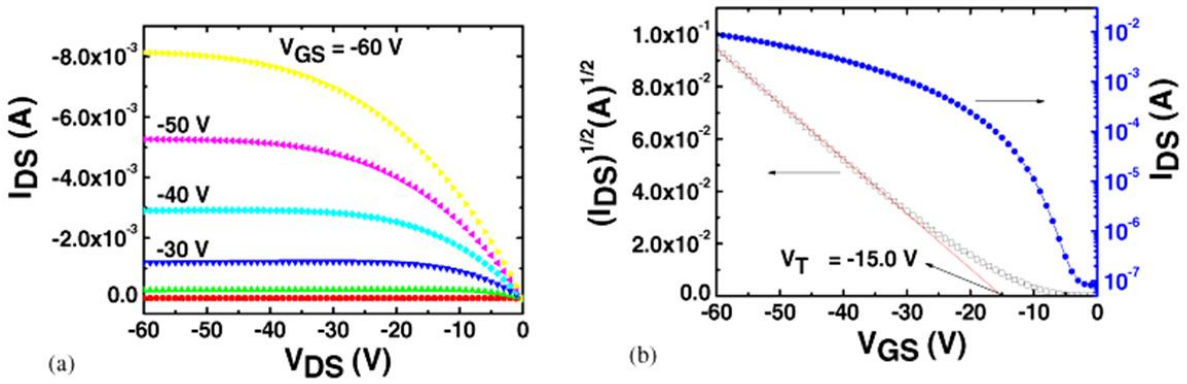

Figure 11 *a) Typical output characteristic b) Typical transfer characteristics of p-type OS [50]*

The simplified scheme for an OFET, which is illustrated in Figure 10, can be practically realized by the four basic architectures depicted in Figure 12. These architectures differ in the ordering of the active, insulating layers and the electrodes constituting the OFET. The configuration in which the source and drain electrodes are placed at the bottom of the OFET, is called a bottom contact OFET. The opposite structure in which the electrodes are placed on the surface of the OS is called a top contact OFET (TC). Similarly, the position of the gate electrode at the bottom or top of the structure indicates a bottom gate or top gate (TG) structure.

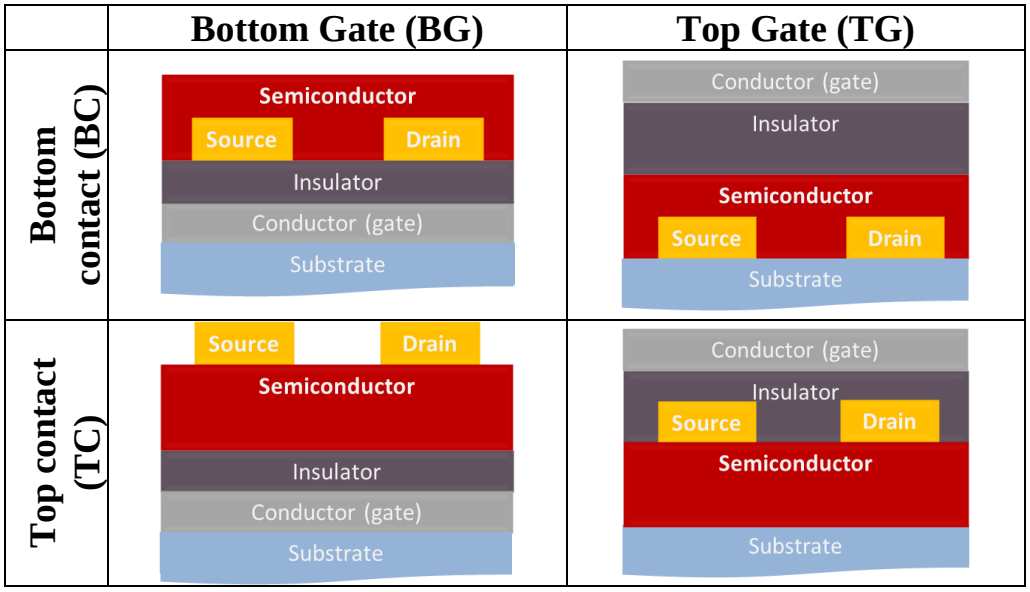

Figure 12 *Architecture of OFETs*

As was described above, the conductive channel in OFET is created at the interface of the OS and gate dielectric. Therefore, the performance of OFETs is strongly affected by this interface. The influence of the interface on the performance of OFETs is given by the "effective" thickness of the OS. This can be illustrated on the relative distribution of charge inside of the active layer for a 30 nm thick pentacene film with the configuration with bottom contact and bottom gate architecture, which is shown in Figure 13. In this calculation, one monolayer of the pentacene is about 1.5 nm thick and thus a 30 nm layer is represented by 20 monolayers. As follows from Figure 13a, the charge carriers are concentrated at the interfaces between the gate dielectric and pentacene. If the gate voltage is increased (Figure 13b), then the concentration of the charges near the interface is also increased [12]. This distribution of charges accumulated at the interface of pentacene layers was confirmed by Kiguchi et al. They studied the dependence of pentacene thickness on OFET performance by continual measurement of current I_{DS} during the gradual deposit of pentacene on the OFET substrate. They observed that at a certain thickness (10–15 nm) saturation of electric current occurs, which was caused by the charge accumulated near the interface of OS and dielectric [51].

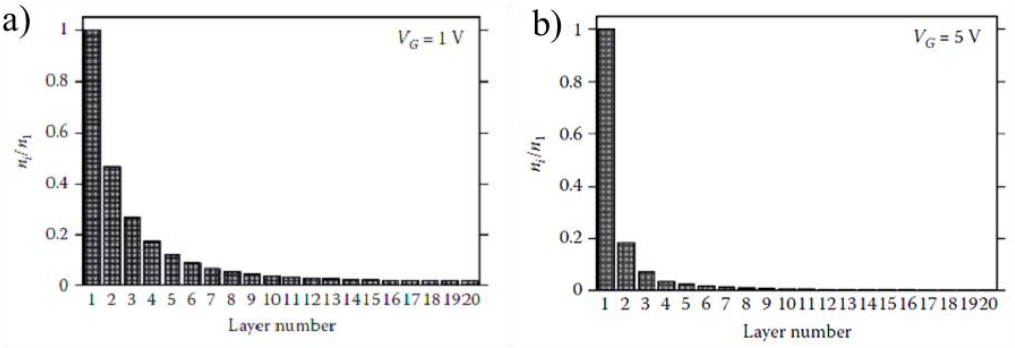

Figure 13 *Relative distribution of charge in 20 layers thick pentacene film [12].*

2.5.1 Charge injection

The processes of charge injection from the source electrode to the organic semiconductor and extraction from the OS to the drain electrode are crucial for OFET performance. Figure 14 shows a simple diagram of the energy level at the metal-OS junction.

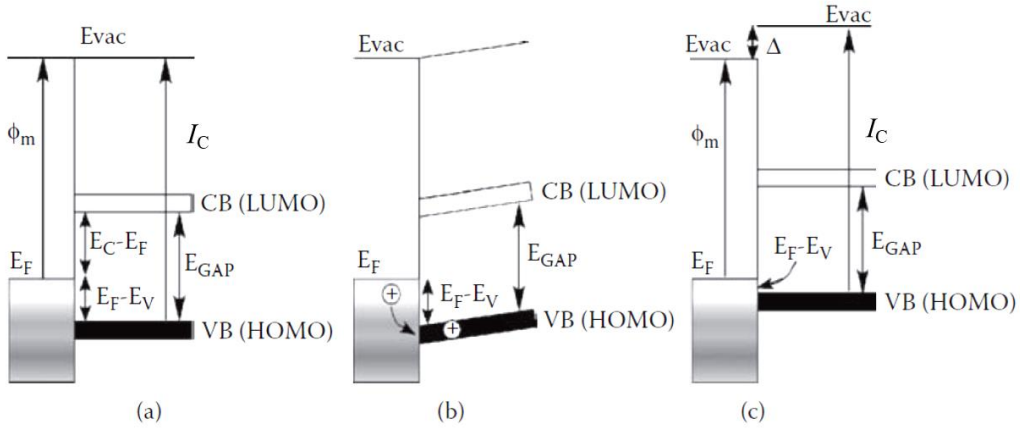

Figure 14 *Simple band diagram for metal-organic semiconductor interface [12]*

The Figure 14a show a simple band diagram of the metal-organic semiconductor interface without an applied electric field. In this figure the offset of the conduction band (CB) and valence band (VB) from the Fermi level are depicted. An energetic barrier for charge carrier injection and extraction can be estimated as the difference between the energy of Fermi level E_F and energy of valence band E_V or conductive band E_C, respectively. Figure 14b shows this energetic scheme with an applied electric field. Application of positive bias to the metal electrode can result in hole injection from the metal to valence band of the OS if the holes overcome the barrier $\varphi_b = E_F - E_V$. This process is known as field-assisted thermionic emission. In reality, the electron structure of the interface is more complicated. Often, an interface dipole Δ is present that shifts the vacuum level of the OS as depicted in Figure 14c. Interface dipoles have several possible origins, including charge transfer between the semiconductor molecules and the metal, reduction of the metal work function by adsorption of the organic layer and population of metal-induced mid-gap states (new energy levels) at the interface [12]. The relation between the barrier high (φ_b), work function of metal (ϕ_m), ionisation potential (I_C) of semiconductors and interface dipoles (Δ) is described as:

$$\varphi_b = E_F - E_V = \Phi_m - I_C \pm \Delta . \qquad (11)$$

In addition to the above-described thermionic injection model, where carriers are thermally excited from the electrodes to overcome the potential barrier, the charge carrier injection can be described by other models. The tunnelling injection model describes the tunnelling of carriers through the potential barrier of the metal–organic contact, while the thermo-activated hopping injection model describes the hopping of carriers from the metal Fermi level into the localised states of the OS.

2.6 PARAMETERS OF OFETS

In this thesis the parameters of OFETs were characterised and evaluated in accordance with the IEEE 1620 standard. This standard comprises methods for characterisation of OFETs, evaluation of conventional sources of measurement errors, as well as methods for the extraction of measured parameters of the devices. Thus, the standard provides tools for systematic characterisation of organic transistors with the aim to maximize the reproducibility of the experimental results [52].

2.6.1 Evaluation of charge carrier mobility

Many techniques focused on determination of charge carrier mobility in organic semiconductors have recently been developed [53]. The charge carrier mobility in thin films deposited in OFETs is derived from transfer characteristics of OFETs. The transfer characteristics can be measured in the linear or saturation region of the output characteristics, which are described in detail in the chapter 0. The charge carrier mobility can be evaluated from the current-voltage characteristics at the saturation regime by the equation:

$$\mu_{SAT} = \frac{I_{DS}}{(V_{GS} - V_T)^2} \frac{2L}{WC_i}, \tag{12}$$

where I_{DS} is the current passing through the channel, V_{GS} is the applied gate voltage, V_T is the threshold voltage, L is the channel length, W is the channel width, and C_i is the capacitance of the dielectric layer. In practice, the dependence of $I_{DS}^{1/2}$ on V_{GS} is shown in Figure 11b, where the slope k of the linear part of current-voltage characteristics is used for the calculation of charge carrier mobility i.e. $k^2 = I_{DS} \cdot V_{GS}^{-2}$.

Within the linear regime, the charge carrier mobility is determined by the equation:

$$\mu_{LIN} = \frac{I_{DS}}{(V_{GS} - V_T)V_{DS}} \frac{L}{WC_i}. \tag{13}$$

Alternatively, the charge carrier mobility can be calculated from the slope of the transfer curve, and the differential of equation 13:

$$\mu = \frac{\partial I_{DS}}{\partial V_G} \frac{L}{WC_i V_{DS}}. \tag{14}$$

2.6.2 Threshold voltage

The threshold voltage V_T is described by the IEEE 1620 standard as the minimum gate voltage required for the creation of the conductive channel. This value can be obtained from the transfer characteristic, where the plot of $I_{DS}^{1/2}$ on V_{GS} is fitted by a straight line. The threshold voltage is obtained by extrapolation of this line to zero current I_{SD}. The fit and extrapolation are depicted in Figure 11b by red line.

Alternative methods for determination of threshold voltage have also been developed [54].

2.6.3 On/Off ratio

The On/Off ratio is defined as the ratio of the maximum ("on state") of the I_{DS} value divided by the minimum ("off state") of the I_{DS} derived from the transfer characteristic. This ratio is dependent on V_{DS} and characterises the ability of the device of OFETs to switch a signal "on" and "off."

2.6.4 Contact resistance

The contact resistance of OFETs should be negligible in comparison to the electrical resistance of the semiconductors. The contact resistance is independent of the channel length and is attributed to the source and drain configuration.

In this thesis, the contact resistance is evaluated by a technique known as the transfer or transmission line method (TLM). This technique is based on the calculation of the total resistance R_{TOT} of OFETs derived from the output characteristics as depicted in Figure 15a. The resistance associated with carrier injection and extraction can be summed up into the "*contact resistance*" (R_c) and the resistance associated with the transport of charges through the conductive OFET channel is called the "*channel resistance*" ($R_{channel}$). The measured total resistance R_{TOT} from the output characteristics is the sum of the channel ($R_{channel}$) and contact resistances (R_c). The contact resistance is obtained by extrapolation of R_{TOT} to zero channel length (Figure 15b This means that several output characteristics for different channel lengths have to be measured in order to obtain R_C. The intersection of the line (at zero channel length) with the y-axis determines the R_C. The methods of evaluation of contact resistance are not determined by the IEEE standard, however alternative methods for evaluating contact resistance have been developed [12].

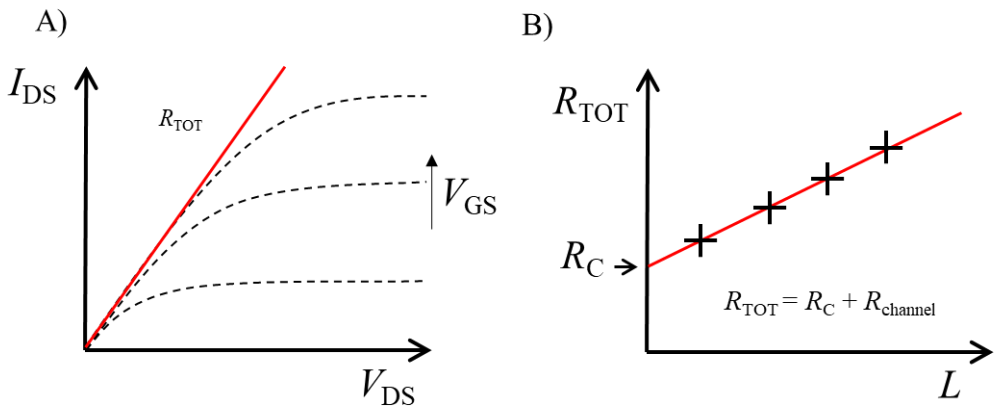

Figure 15 *Transmission line method. A) Evaluation of R_{TOT} from output characteristic B) Evaluation of contact resistance R_C from R_{TOT}.*

3 ORGANIC ELECTROCHEMICAL TRANSISTORS (OECTS)

Organic semiconductors in bioelectronic applications are mostly used as sensors. These OS-based biosensors utilize organic electrolyte-gated field-effect transistors (EGOFET) and organic electrochemical transistors (OECT). Organic electrochemical transistors (OECTs) attracts significant attention due to their simple fabrication and operation in liquid electrolytes with applied voltages below 1V [55; 56]. OECTs provide unique opportunities for application in bioelectronics with a number of benefits such as easy patterning of devices, individual modification of OS and direct interface with biomolecules and living cells [57]. The ability to operate in aquatic environments makes OECTs suitable candidates for a variety of applications, especially biological sensing, detection of ions, glucose, uric acid, dopamine, DNA, bacteria, protein and cells [55].

Comprehensive research into OECTs has been carried out by Rivnay, Owens, Maliaras and Bergren [58; 59]. They realized a large-scale study on the influence of the channel length, width, thickness, PEDOT:PSS volumetric capacitance and many other OECT performance parameters [60; 61; 62; 63].

Recently, OECT sensors have been applied for a study of the action potential in neural and cardiac cells. The first observation of beating cardiomyocytes by OECTs was provided by Hsing et al [64]. Cardiovascular disease has been highlighted by the WHO as the primary cause of death of the global population. The OECT sensors help in screening of drugs used for prevention of arrhythmia which was realized by extracellular mapping of in-vitro cultured cells [65]. In their study Hsing et al. were able to translate the current response of OECTs to an extracellular cardiac action potential within a range of the cardiac voltage drop from 0.2 to 0.6 mV. These OECT sensors measured the increase in cardiomyocyte frequency after the addition of isoproterenol and the real-time propagation of the action potential [64; 65].

3.1 PEDOT:PSS MATERIAL FOR OECTS

The function of the channel of OECTs is typically based on a conducting polymer, most commonly Poly(3,4-ethylene dioxythiophene) PEDOT or polypyrrole, doped with p-type dopants such as small anions or polyanions. The polyanion Poly(styrene sulfonate) PSS is a polymer which is negatively charged, and it is commonly used in a mixture with Poly(3,4-ethylene dioxythiophene) referred to PEDOT:PSS. The chemical structure is depicted in Figure 16a.

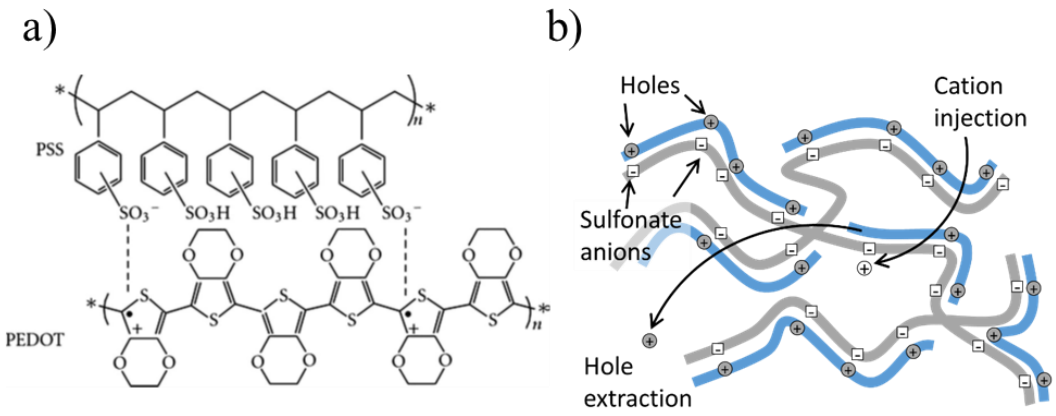

Figure 16 *a) Chemical structure of PEDOT:PSS, b) polymer structure of PEDOT:PSS and principle of ion injection and extraction in PEDOT:PSS [58].*

Today, PEDOT:PSS is the most successful conducting polymer in a wide area of practical applications. It possesses many unique properties, such as good film-forming ability by versatile fabrication techniques, superior optical transparency in the visible light range, high electrical conductivity, intrinsically high work function and excellent physical and chemical stability in air [66].

Principally two types of conformations for PEDOT:PSS exist in the presence of water. The coulomb repulsions among the anions PSS segments and the positively charged PEDOT lead to a coiled conformation of the PSS segments, which are attached to the PEDOT chains. The PSS segments form beads to reduce and prevent contact with the interaction between PEDOT and water. Therefore, the beads have a core/shell conformation with PEDOT in the core and PSS in the shell. Moreover, the excess PSS without attached PEDOT dissociates into PSS anions and protons. These PSS segments adopt a linear conformation to minimise the coulomb repulsions among the PSS anions. The shell of the insulating PSS forms an energy barrier for the charge transport across the PEDOT chains. The coil PEDOT conformation leads to the location of the charge carriers on the PEDOT chains. This is a reason for the low conductivity of as-prepared PEDOT:PSS films from aqueous solution. [66].

Even if PEDOT:PSS is widely used for OECT transistors, the films of PEDOT:PSS have a limited cytologic compatibility, and for this reason other polymers or composites which allow more versatile bio-functionalisation are desirable. Also, the acidity of PSS brings many other consequences such as acidic corrosion. These limitations have motivated researchers to synthesise new materials for OECTs. Replacement of PSS polymer with less acidic polyanions results in similar performance of OECTs in terms of transconductance and response time as PEDOT:PSS based OECT. Conjugated polymers with hydrophilic or ion-transporting side chains can be alternatively used as OECT materials. OECTs made from polythiophene with glycosylated side chains exhibit better transconductance values than PEDOT:PSS-based OECTs [58].

3.2 ARCHITECTURE AND BASIC OPERATION OF ORGANIC ELECTROCHEMICAL TRANSISTORS

Wrighton and colleagues developed the organic electrochemical transistor (OECT) in 1984 [67]. OECT consists of an organic semiconductor film that is in contact with an electrolyte in which the gate electrode is immersed. A schematic picture of an OECT is shown in Figure 17.

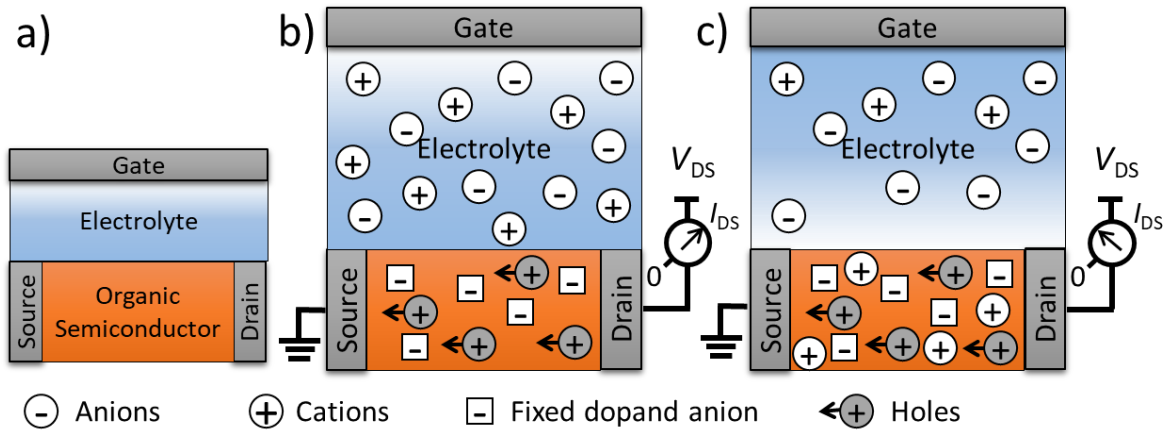

Figure 17 *Schematic picture of OECT transistors taken from Bernards and Maliaras: a) convection scheme of OECT devices, b) OECT without applied gate voltage, c) OECT with applied gate voltage (V_G) [60].*

Bernards and Maliaras in 2007 qualitatively described the operation of OECTs. The model device behaviour of the OECT is divided into an electronic and an ionic circuit. The electronic circuit consists of a p-type organic semiconductor film that transports holes between the source and drain electrodes as depicted in Figure 17b. The current flux J of electronic circuit is described by the Ohm's law equation:

$$J(x) = q\mu p \frac{dV(x)}{dx}, \tag{15}$$

where q is the elementary charge, μ is the hole mobility, p is the hole density, and dV/dx is the electric field. By applying drain voltage V_{DS} current I_{DS} passes through the organic semiconductor. Upon the application of a positive gate voltage (Figure 17c), cations from the electrolyte are injected into the semiconductor film, and each injected cation compensates one acceptor illustrated in Figure 16b. For each cation that enters the organic film, a hole extracted at the source is not replaced by the injection of a hole at the drain. Injection of the cation is attributed to an ionic circuit, which is described as a combination of the linear circuit of a resistor (R_s) and a capacitor (C_d) in series. The resistor is described as the conductivity of the electrolyte (its ionic strength) and the capacitor is ascribed to polarisation at the OS/electrolyte and gate/electrolyte interfaces. The interaction of these two components (electronic and ionic circuit), namely the transport of ions from the electrolyte into the organic semiconductor film, is fundamental to the behaviour of OECTs [60].

The PEDOT:PSS with mixed ion-electron conductivity is most studied and explored conducting polymer in OECTs. A significant contribution to the capacity of a two-phase PEDOT:PSS comes from the electrical double layers created along the interface between the positively charged conjugated PEDOT and negatively charged PSS. Therefore, the organic electrochemical transistors effectively use ion injection from an electrolyte to modulate the bulk conductivity of the PEDOT:PSS. The connection between ionic and electronic charges throughout the channel volume provides OECTs with high transconductance compared to field-effect transistors, but also it limits their response time [58].

3.3 PARAMETERS OF ORGANIC ELECTROCHEMICAL TRANSISTORS

The parameters of organic electrochemical transistors are similar to OFET parameters such as threshold voltage, On/Off ratio and others, which are described in chapter 2.6. The amplification of biological functions by OECT sensors is described by parameter known as transconductance. This amplification of a biological event by an OECT transistor can be obtain by modulation of the gate voltage V_{GS}, which influences the drain current I_{DS}. The transconductance of OECTs from current-voltage characterisation is than determined as = $\Delta I_d/\Delta V_{GS}$. The electronic-ionic model described by Bernards and Maliaras provides a good fit for the output characteristics of OECTs and allows quantitative prediction of the transconductance (g_m) at the saturation regime, where the transconductance can be calculated by the equation:

$$g_m = (W/L) \cdot d \cdot \mu \cdot C^* \cdot (V_T - V_{GS}), \qquad (16)$$

where W, L and d are the channel width, length and thickness of OS, μ is the charge-carrier mobility, C^* is the capacitance per unit volume of the channel and V_T is the threshold voltage. Also minimization of V_{GS} is important when bio-recognition elements such as bilayer membranes and cells are used, that are sensitive to long-term applied voltage [60; 68].

The response time is defined as the interval required by the sensor to display the change of the sensed signal. The response time is represented by a time constant, which can be obtained from the transient behaviour of OECTs, where the gate voltage V_{GS} is modulated in time. The time constant represents the elapsed time required for the system response to decay to the "zero" value. Because of the progressive change in the rate of decay, the time constant is represented by the time where the measured response value is decreased to 1/e (36.8 %) of the final value in the case of a decreasing step. In an increasing step, the time constant is the time for the system's step response to reach 1-1/e (63.2%) of its final value [4; 12].

3.4 BIOCOMPATIBILITY OF ORGANIC SEMICONDUCTORS

Inorganic electronic materials are commonly used in bioelectronics due to a well-established integrated circuit industry and availability of a wide range of inorganic semiconductor devices [69]. The most commonly used materials for the interface between biological tissue and conventional inorganic electronic materials are hydrogels [70]. Abiotic electronic materials have considerable disadvantages in terms of creating a permanent interface with biotic living tissues due to their mechanical stiffness, surface structure, charge transfer nature, biological contamination and a limited number of biocompatible materials. In addition, the inorganic semiconductors conduct electrons and holes, but organic semiconductors can have mixed electronic and ionic conduction [69; 71].

The key to the success of organic semiconductors in bioelectronic applications is in reducing the immune response of living cells or tissue in contact with OS. Ideally, the organic semiconductors are biologically inert and do not activate the immune response but rather allow the integration of target cells with bioelectronic devices. If the OS or device generates an immunological response, they can be encapsulated by the fibrous tissue and the interface between the device and the biological tissue is disturbed or severely impaired. Therefore, the biocompatibility of each component must be tested prior to the creation of organic semiconducting devices and their application to living tissue [72].

The standard tests for the biological evaluation of medical devices to examine the biocompatibility of a material is given by ISO 10993. These test are splitted on the type of body contact and the length of contact time. The type of contact can be surface contact, external communication devices or implant devices. The biocompatibility of the material is assessed by many types of tests such as cytotoxicity, sensitisation, systemic toxicity (acute), chronic toxicity, carcinogenicity and many others. Testing of these responses can be performed in in vitro, ex vivo or in vivo [69; 73].

In vitro experiments allow evaluation of material toxicity to cells, cell adhesion, cell activation, cell death, structural stability, and maintenance of the electronic functionality of the biomaterial in a cell culture medium at 37 °C. The phosphate-buffered saline called PBS is the most-used cultivation medium.

Implantation of a bioelectronic device inserted into a living host (in vivo) can interact with tissues in four ways [69]:

- ***Toxic:*** the biomaterial has adverse effects on surrounding tissues such as cell death, immunological response, organ failure, and inflammation.
- ***Bioinert:*** non-toxic, biologically inactive. The material has no or minimal interaction with the live host. However, fibrous tissue can encapsulate the device, release and separate the device interface from target cells, resulting in device failure.
- ***Bioactive:*** material is non-toxic and biologically active. The device forms an intimate connection with the host tissue.
- ***Bioresorbable:*** the non-toxic material dissolves in the host tissue. Bioelectronic equipment works only temporarily. Surrounding host tissue can eventually replace synthetic devices.

In vitro bioelectronic tests are often performed at an "acute" time up to 10 days. In contrast, in vivo testing typically takes place over a longer "chronic" period, which may be weeks, months or years [69; 74]. The most appropriate cytotoxic assay for the biocompatibility of organic semiconductors is direct contact of primary cells and cell lines with organic semiconductors. Cytotoxicity tests determine whether the biomaterial contains harmful extracts that lead to death or damage to cells. For cytotoxicity testing, the following assays are typically used:

- ***MTT and XTT assay***
- ***Neutral red uptake cytotoxic assay***
- ***Colony formation assay***
- ***Intracellular ATP assay***

These cytotoxic tests assess cell damage by morphological means and take measurements of cell damage, cell growth, and indicators of cell metabolism [75].

4 GOALS OF THE DOCTORAL THESIS

This thesis is focused on the study of the organic semiconductors with respect to their possible applications in organic field-effect transistors (OFETs) and organic electrochemical transistors (OECTs). Therefore, in the part related to the preparation and characterisation of OFETs, the attention is paid to the understanding of the relationship between the properties of novel semiconducting organic materials used as active layer, their molecular structure and final properties of OFETs. In the part related to preparation and characterisation of OECTs, the work is focused on characterisation of suitable materials and their subsequent utilization for optimisation of OECTs structures for application with living cells and for detection of the physiological response of cardiomyocytes.

The particular tasks of the thesis are:

1. description of the state of the art and progress in the development of organic semiconductors used in organic field-effect transistors and organic electrochemical transistors,
2. development and optimisation of the methods and procedures for preparation of thin active layers and characterization of OFETs and OECTs,
3. studies of the relationship between the molecular structure of novel organic semiconductors, their optical and electrical properties and final properties of OFETs,
4. characterisation of selected organic semiconductors with respect to their application in bioelectronics devices,
5. optimisation of OECT structures for detection of the physiological response of cardiomyocytes.

5 EXPERIMENTAL

5.1 STUDIED MATERIALS

5.1.1 Thiophene-benzo-furan DPP derivative

The (3,6-bis(5-(benzofuran-2-yl)thiophen-2-yl)-2,5-bis(2-ethyl-hexyl)pyrrolo[3,4-c]pyrrole-1,4-dione) referred as DPP(TBFu)$_2$ was selected as reference material. The structure of the material can be seen in Figure 18. This material was supplied by the Centre for Organic Chemistry Ltd. (COC Ltd.). In this work the SAM monolayers were used to optimize thin film formation prepared by spin-coating technique with subsequent exploring OFET performance with DPP(TBFu)$_2$ as active layer.

This material has earlier been used in organic solar cells with an efficiency exceeding 5% and organic field-effect transistors with a hole mobility of up to $2.8 \cdot 10^{-3}$ cm^2/Vs in a bottom gate/top contact OFET architecture [76; 77; 78].

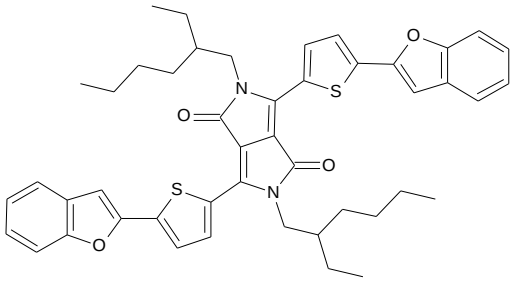

Figure 18 *Structure of 3,6-bis(5-(benzofuran-2-yl)thiophen-2-yl)-2,5-bis(2-ethyl-hexyl)pyrrolo[3,4-c]pyrrole-1,4-dione) referred as DPP(TBFu)$_2$*

5.1.2 Diphenyl-amino-stilbene DPP derivatives

The properties of novel synthesised soluble diphenyl-amino-stilbene-based DPP derivatives illustrated in Figure 19 were studied as hole transport material for photovoltaic applications. Four DPP derivatives with 4-phenylaminostilben-4-yl substituents at the DPP dilactame core were supplied by the Centre for Organic Chemistry Ltd. (COC Ltd.).

The unsymmetrically substituted phenyl-amino-stilbene and symmetrically substituted phenyl-amino-stilbene DPP derivatives were used to study the influence of conjugation length on the performance of OFETs. The ethylacetate (EtAcet) and ethylhexylacetate (EtHexAcet) DPP derivatives were used to study the effect of length of solubilizing alkyl chains on performance of OFETs. The systematic names of the organic compounds illustrated in Figure 19 are as follows:

- **(Ph)$_1$-(PhAmStb)$_1$-DPP-(EtAcet)$_2$**: diethyl (E)-3-(4-(4-(diphenylamino)styryl)phenyl)-6-phenyl)-1,4-dioxopyrrolo[3,4-c]pyrrole-2,5(1H,4H)-diyl)diacetate

- **(PhAmStb)$_2$-DPP-(EtAcet)$_2$**: diethyl 2,2'-(3,6-bis(4-((E)-4-(diphenylamino)styryl)phenyl)-1,4-dioxopyrrolo[3,4-c]pyrrole-2,5(1H,4H)-diyl)diacetate
- **(Ph)$_1$-(PhAmStb)$_1$-DPP-(EtHexAcet)$_2$**: bis(2-ethylhexyl) (E)-3-(4-(4-(diphenylamino)styryl)phenyl)-6-phenyl)-1,4-dioxopyrrolo[3,4-c]pyrrole-2,5(1H,4H)-diyl)diacetate
- **(PhAmStb)$_2$-DPP-(EtHexAcet)$_2$**: bis(2-ethylhexyl) 2,2'-(3,6-bis(4-((E)-4-(diphenylamino)styryl)phenyl)-1,4-dioxopyrrolo[3,4-c]pyrrole-2,5(1H,4H)-diyl)diacetate

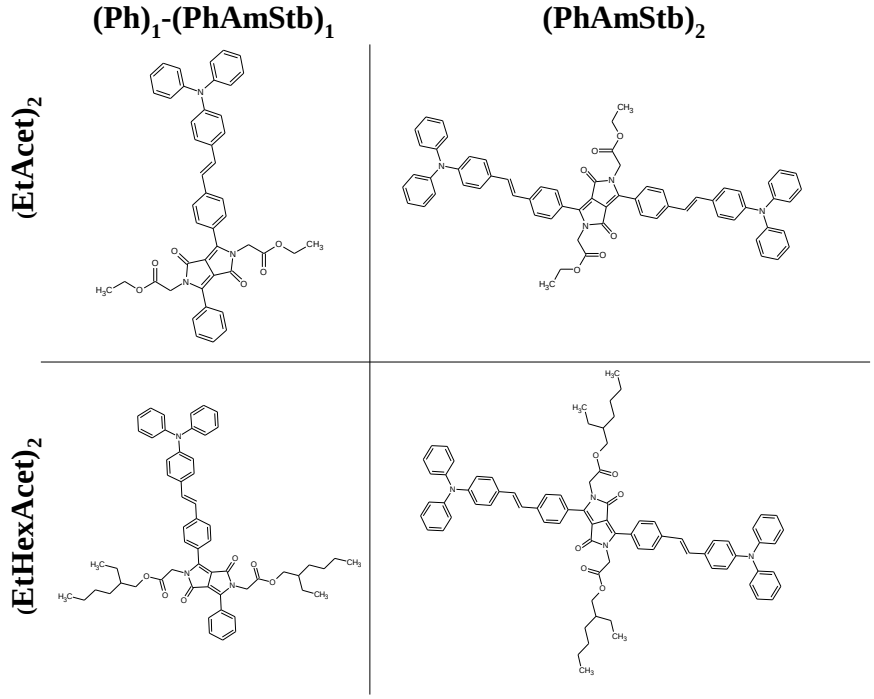

Figure 19 *The mono and diphenyl-amino-stilbene DPP derivatives with shorter and longer solubilizing alkyl chain (Frebort, et al., 2014), (Honová, et al., 2016).*

5.1.3 Alkyl substituted DPP derivatives

The group of newly synthesized (Th)$_2$-DPP derivatives with an ethyladamantane alkyl side chain novel synthesised was choose to characterize the charge carrier mobility. The shorter butyl (C4) and longer dodecyl (C12)$_2$ derivatives were added to the group of novel synthesized DPP derivatives to recognise the effect between the robust ethyladamantane solubilising groups and the substitution position (N, O). New materials were supplied by the syntetic group at FCH VUT in Brno under the leadership of Ing. Jozef Krajčovič, Ph.D. The other two materials without bonded alkyl chain and derivative with bonded ethyl-2-hexyl alkyl chain are part of study in chapter 6.1.4. The studied materials and their systematic names are shown in Table 10.

Table 10 *DPP derivatives under study*

Title and systematic names	**Molecular structure**
(Th)$_2$-DPP-(H)$_2$ 3,6-di(thiophen-2-yl)-2,5-dihydropyrrolo[3,4-c]pyrrole-1,4-dione *Basic reference structure*	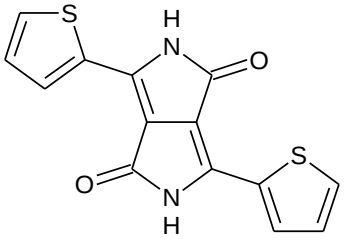
N, N – (Th)$_2$-DPP-(C4)$_2$: 2,5-dibutyl-3,6-di(thiophen-2-yl)-2,5-dihydropyrrolo[3,4-c]pyrrole-1,4-dione	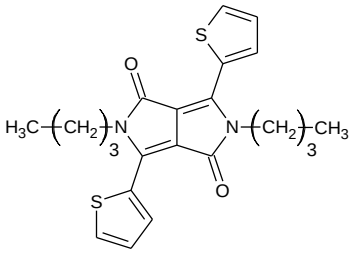
N, N – (Th)$_2$-DPP-(C12)$_2$: 2,5-didodecyl-3,6-di(thiophen-2-yl)-2,5-dihydropyrrolo[3,4-c]pyrrole-1,4-dione	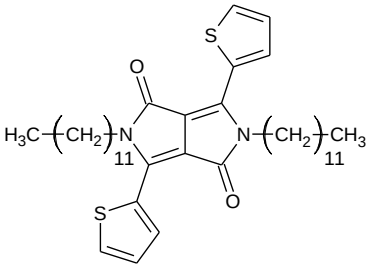
N, N – (Th)$_2$-DPP-(EtHex)$_2$: 2,5-diethyl-2-hexyl-3,6-di(thiophen-2-yl)-2,5-dihydropyrrolo[3,4-c]pyrrole-1,4-dione	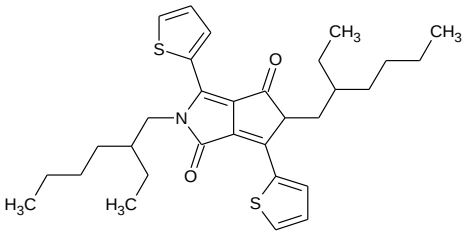
N, N – (Th)$_2$-DPP-(EtAd)$_2$: 2,5-bis(2-(adamantan-2-yl)ethyl)-3,6-di(thiophen-2-yl)-2,5-dihydropyrrolo[3,4-c]pyrrole-1,4-dione	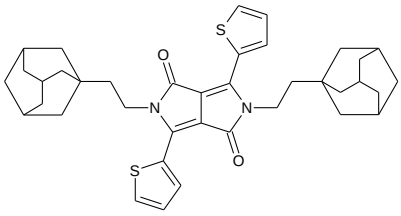
N, O – (Th)$_2$-DPP-(EtAd)$_2$: 4-(2-(adamantan-2-yl)ethoxy)-2-(2-(adamantan-2-yl)ethyl)-3,6-di(thiophen-2-yl)-4,5-dihydropyrrolo[3,4-c]pyrrol-1(2H)-one	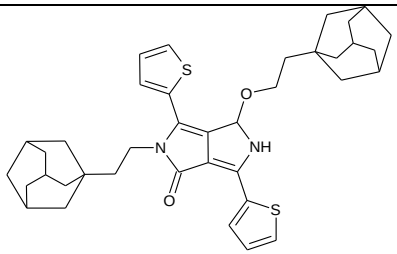
O, O – (Th)$_2$-DPP-(EtAd)$_2$: 1,4-bis(2-(adamantan-2-yl)ethoxy)-3,6-di(thiophen-2-yl)-1,2,4,5-tetrahydropyrrolo[3,4-c]pyrrole	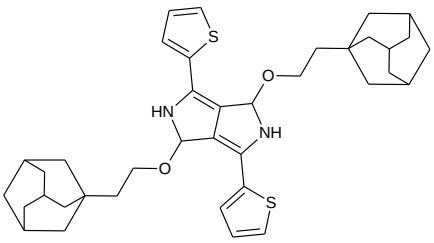

5.1.4 Naphthalene derivatives with ethynylene linker

The charge carrier mobility properties of three new naphthalene derivatives with (5´-hexyl-2,2´-bithiophene-5-yl)ethynyl side arms attached to the central naphthalene core illustrated in Figure 20a were investigated. A series of naphthalene derivatives:

- 1,4-Bis{[50-hexyl-(2,20-bithiophen)-5-yl]ethynyl}naphthalene (H2TA14N),
- 1,5-Bis{[50-hexyl-(2,20-bithiophen)-5-yl]ethynyl}naphthalene (H2TA15N),
- 2,6-Bis{[50-hexyl-(2,20-bithiophen)-5-yl]ethynyl}naphthalene (H2TA26N)

were supplied by the Department of Organic Chemistry, Faculty of Natural Sciences at the Comenius University in Bratislava. The observed properties of naphthalene derivatives with incorporate ethynylene block are compared to the properties of naphthalene derivatives without ethynylene published early. A comparison of the molecular structure of new derivative with ethynylene and old derivatives is illustrated in Figure 20b. The ethynyl group in novel derivatives should decrease torsion angle the between acene core and thiophenyl group as was disclosed via previous derivatives [79].

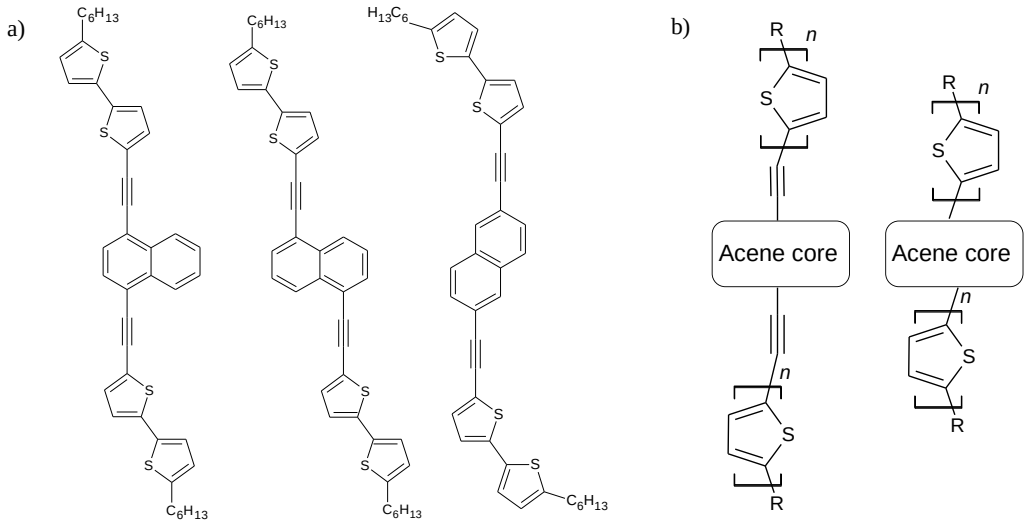

Figure 20 *a) The materials H2TA14N, H2TA15N and H2TA26N under study, b) new and old naphthalene derivatives used in this study [79; 80].*

5.1.5 PEDOT:PSS inks

Today many PEDOT:PSS commercial inks are available. The differences between them can lie in the ratio between PEDOT and PSS, the pH of inks, the ratio of PEDOT:PSS at solutions, the conductivity of the prepared PEDOT:PSS layer, etc. The aim of this work was to study the selected PEDOT:PSS inks to for bioelectronic applications. The appropriate electronic properties, biocompatibility properties and also environmental stability of PEDOT:PSS over a longer period were studied. The available commercial PEDOT:PSS inks A-F and one synthesised by COC Ltd are described in Table 11.

Table 11 *PEDOT:PSS inks under study*

Notation	**Commercial name**	**Conductivity /Resistivity**	**Description**
Ink A	Heraeus CleviosTM P VP AI 4083	500-5000 ohm·cm	Standard dispersion for hole injection layers (OPV, OLED), pH acidic, PEDOT:PSS ratio 1:6
Ink B	Heraeus CleviosTM P JET HC V2	300 S/cm	Ink-jet formulation, high conductive version of CleviosTM P, acidic
Ink C	Sigma Aldrich 739 316	110 ohm/sq	Optimized for ink-jet, contains 1–5% ethanol, 5–10% diethylene glycol, concentration 0.8% in H_2O, acidic (pH 1.5–2.5)
Ink D	Sigma Aldrich 483 095	1 S/cm	Conductive grade, contains PEDOT 0.5 wt %, PSS 0.8 wt %, concentration 1.3 wt % in H2O
Ink E	PEDOT/PSS-AS	150 S/cm	Contains PEDOT 0.4 wt %, PSS 0.6 wt %, concentration 1 wt % in H2O, no additives
Ink F	Sigma Aldrich 560 596	10000-300000 ohm·cm	Hole injection layer in OLED, low conductivity grade, contains PEDOT 0.14%, PSS 2.6%, concentration 2.8 wt %, acidic (pH 1.2–1.8)

The ink G and ink H in Table 12 were used for the construction of prototype of printed OECTs.

Table 12 *PEDOT:PSS inks for printed OECT transistors*

Notation	**Commercial name**	**Conductivity /Resistivity**	**Description**
Ink G	CLEVIOS™ S V 3	350 - 500 ohm/sq	PEDOT:PSS dispersion in glycols, blue paste for screen-printing
Ink H	CLEVIOS™ S V 4	250 - 300 ohm/sq	PEDOT:PSS dispersion in glycols, blue paste for screen-printing

5.1.6 Organic semiconductors used as reference

The four reference materials were used to characterise the biocompatibility of organic semiconductors and to identify aspects that may improve their compatibility with living cells. These OS were chosen as they are frequently used in organic electronic devices prepared by solution deposition techniques. The structures of materials are shown in Figure 21.

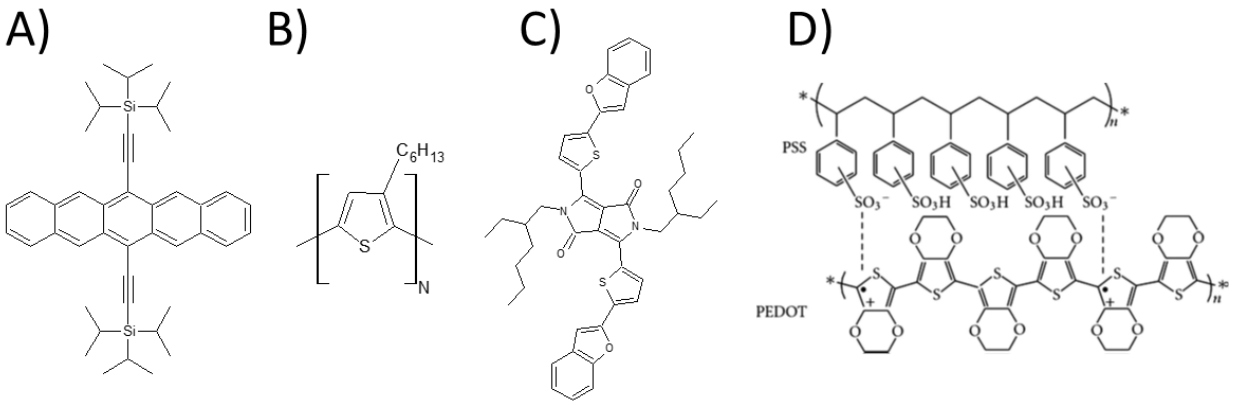

Figure 21 *Reference materials used in biocompatibility study: A) 6,13-bis (triisopropylsilylethynyl) pentacene (Tips-pentacene) purchased from Ossila Ltd., B) Poly(3-hexylthiophene-2,5-diyl) (P3HT) purchased from Ossila Ltd., C) 3,6-bis(5-(benzofuran-2-yl)thiophen-2-yl)-2,5-bis(2-ethyl- hexyl)pyrrolo[3,4-c]pyrrole-1,4-dione) DPP(TBFu)$_2$ synthesised by COC Ltd., D) Poly(3,4-ethylenedioxythiophene):polystyrene sulfonate PEDOT:PSS – purchased from Sigma Aldrich 739 316*

5.1.7 Supporting materials

In order to construct OECT transistors, electrodes and protecting layers must be used. The gold ink and silicon ink were used to construct electrodes and prototypes of OECT transistors.

Gold ink for ink-jet printing

Gold resin solution RL Au 01913 (art. no. 89960429, an experimental product under development in 2014) was purchased from Heraeus. It is based on the Heraeus RP 181208 ink which contain 15% of gold. This ink resin has poor properties for inkjet printing technique. Therefore, the cyclohexanol was added to the ink for excellent jettability with no clogging and satellite droplet formation for ink jet technique. The modified ink contains 20 vol.% of cyclohexanone and 80 vol.% of the gold resin solution [81].

Silicon Ink

The commercially available silicon Sylgard 184 was used for masking the supply electrodes to prevent leakage current and it was used to define the active area of the organic electrochemical transistors. Sylgard 184 was also used to prefabricate silicon wells with a 3D-printed negative form.

5.2 THIN FILM PREPARATION

The fabrication process of organic electronics devices is affected by the presence of impurities and dust in the ambient atmosphere. The preparation of thin films was carried out in clean laboratories to protect against unwanted impurities. The clean laboratory is equipped with MB-200B MBRAUN glove boxes, which allow the preparation of samples in a nitrogen atmosphere with an oxygen and water content of less than 0.1 ppm (Figure 22).

Figure 22 *The glovebox equipment in the clean lab*

5.2.1 OFET substrates

The tested organic semiconductors were prepared in thin films on the commercially available silicon/silicon dioxide standard substrate purchased from Fraunhofer IMPS (see Figure 23). The n-doped silicon substrate with thermally grown silicon dioxides contains 16 transistors with channel length 20, 10, 5 and 2.5 μm (each channel length for four transistors) and 30 mm channel width of gold interdigital electrodes (30 nm of gold on 10 nm ITO adhesion layer).

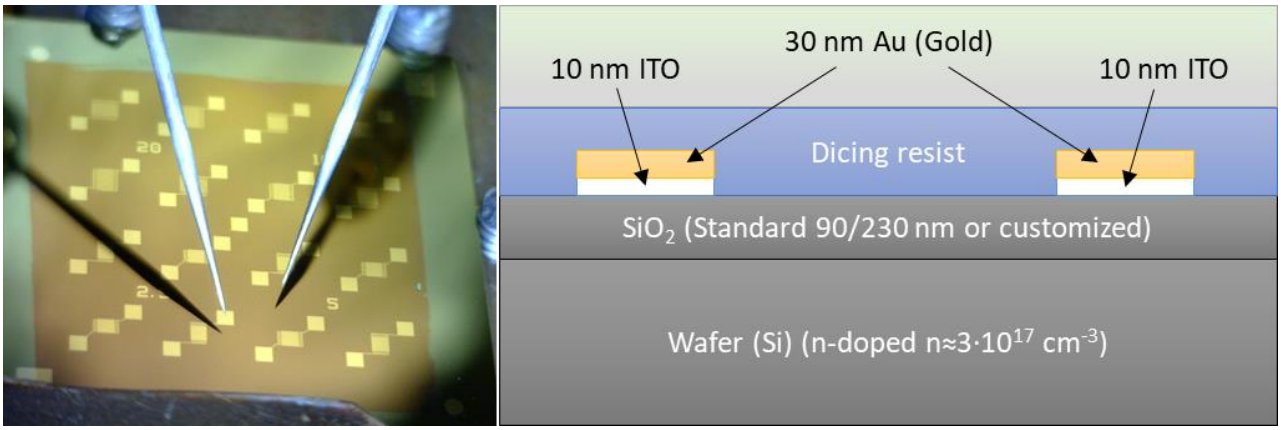

Figure 23 *Left image of Fraunhofer substrates with 16 interdigital gold electrodes; right cross-section view.*

5.2.2 OECT substrates

For preparation of OECT devices with gold printed electrodes, Ultra-flat Quartz Coated Glasses from Ossila Ltd were purchased. These ultra-flat glass substrates are coated with a 20 nm layer of synthetic quartz. These substrates have a roughness of 1 nm RMS.

For preparation of flexible electronics, the PEN foil ES361150 (250 μm) purchased from GoodFellow was used. These substrates were used to construct the OECT devices by printing techniques.

Glass substrates

For characterization of prepared thin layers by optical, profilometer and atomic force measurements, quartz glass purchased from Ossila Ltd. and Sigma Aldrich was used.

5.2.3 Cleaning routine

The OFETs substrates were cleaned with the following routine for better reproducibility of results:

- 15 minutes in an acetone ultrasonic bath at room temperature
- Washed by acetone from a wash bottle
- 15 minutes at 2% NaOH (or Neodisher) in an ultrasonic bath at room temperature
- Washed by distillate water from a wash bottle
- 15 minutes in isopropanol ultrasonic bath at room temperature
- Washed by isopropanol from a wash bottle
- Blown dry by nitrogen

The cleaning of glass for optical measurement was performed similarly, but without the first two cleaning steps, i.e. cleaning by means of acetone, which is important for removing the photoresist protecting layer from Fraunhofer substrates.

The ultra-flat glasses for gold ink-jet printing (purchased from Ossilla ltd.) were cleaned under 2% Neodisher in an ultrasonic bath for 10 minutes, then immersed into deionised water in the ultrasonic bath for 10 min and blown dry by nitrogen.

Self-assembled monolayers

The parameters of OFET transistors are affected by the barrier between the work function of electrodes and the HOMO or LUMO level of the OS. The gold surface of the substrates can be modified by monolayers which can change the work function of electrodes and thus can change the barrier high. The pentafluorobenzenethiol (PFBT) self-assembled monolayers (SAM) were formed by immersing the silicon wafers in a 5 mM solution of anhydrous toluene for 5 min at 20 °C. After the formation of the PFBT SAMs, the substrates were rinsed with isopropyl alcohol (IPA) and dried with N_2.

The traps on the interface of dielectric and active OS layers decrease the performance of the OFETs. The modification of a SiO_2 dielectric layer by monolayers can effectively increase the measured charge carrier mobility. The OTS monolayers were formed on silicon wafers by immersion in a 10 mM solution of OTS in anhydrous toluene for 20 min at 70 °C. The substrates were then rinsed with IPA and dried with N_2. The HMDS was dropped on the substrate and left there for 1 min. Then, the substrate was spun at 1000 rpm, and a drop of chlorobenzene was dynamically spin-coated until dry. The preparations of all monolayers proceeded in a nitrogen glove box. The coverage of the SiO_2 layer by OTS and HMDS was monitor by measuring the contact angle.

5.2.4 Spin-coating and physical vapour Deposition

The spin-coating is frequently used technique in laboratory for deposition of thin film from solution. The spin coating process was performed by the KW-4A spin coater (Chemat Technology, Northridge CA, USA shown in Figure 24). The spin-coating parameters (rpm, duration, etc.) and the organic semiconductor solution determine the thickness, surface morphology and packing of the organic semiconductors of prepared layers. For the experiments, the following set up conditions were used.

In most cases, solutions of the studied soluble organic semiconductors were prepared at a concentration of 15 mg/ml in anhydrous chloroform. The organic semiconductors were dissolved for several hours with the spinning of magnetic stirrer bars at elevated temperature (50 °C) on a hotplate in vials. The organic semiconductor solutions were then filtered through 0.45 μm PTFE syringe filters before their spin-coating (after their cooled down to laboratory temperature). On cleaned silicon wafers the 50–100 μl of OS solution was deposited by spin-coating at 1500 rounds per minute.

Figure 24 *The spin-coating thin layer deposition equipment on the left and physical vacuum deposition equipment in the glovebox on the right.*

Physical vapour deposition technique was used to prepare thin films for sparingly soluble and insoluble organic semiconducting materials. The vacuum depositions were performed in a MB-ProVap-5 chamber from MBRAUN (MB-ProVap-5) in the glovebox controlled via the SQC 310 TF evaporation controller with a quartz microbalance controller from Inficon Co., Syracuse NY, USA. The spin-coating and physical vapour deposition equipment can be seen in Figure 24.

5.2.5 Printing techniques

Ink-jet and screen-printing deposition techniques have been used as an alternative to spin-coating. The printing techniques have become very popular in organic electronics because they allow mass production, low weight and cheap fabrication of devices.

A Dimatix Ink-jet DMP 2831 material printer from Fujifilm Dimatix Inc., Santa Clara, CA, U.S.A. was used (see Figure 25 on the left) for printing of gold resin (used in chapter 6.2.4) onto the glass slides with printing head 10 pl in size. The printing was performed in a closed box which provides an atmosphere without any unwanted dust. The commercially available gold resin ink (5.1.7) was printed by Dimatix material printer on a cleaned ultra-flat glass substrate.

The printed gold resin layers were left for 2 hours at a vacuum 1 Pa to dry the printed films. After drying, substrates were put on hotplate and temperature was increased continuously from 25°C to 550°C with a rate of 1.5 °C/min in a fume hood to firing the resin. The firing temperature of the resin starts at 350 °C, which provides a covering of the substrate with gold particles. After cooling down to the ambient temperature, the substrates were overprinted with PEDOT:PSS (ink G and ink H in Table 11) and silicon layers (Sylgard 184) by screen-printing machine RokuPrint. Silicon provides hydrophobic surface and set the district of the active area of OECT. The silicon well was glued on the substrate again by silicon to finalise the OECT devices. The final device can be seen at the inset of Figure 27 at chapter 6.2.4. Both material printing devices can be seen in Figure 25.

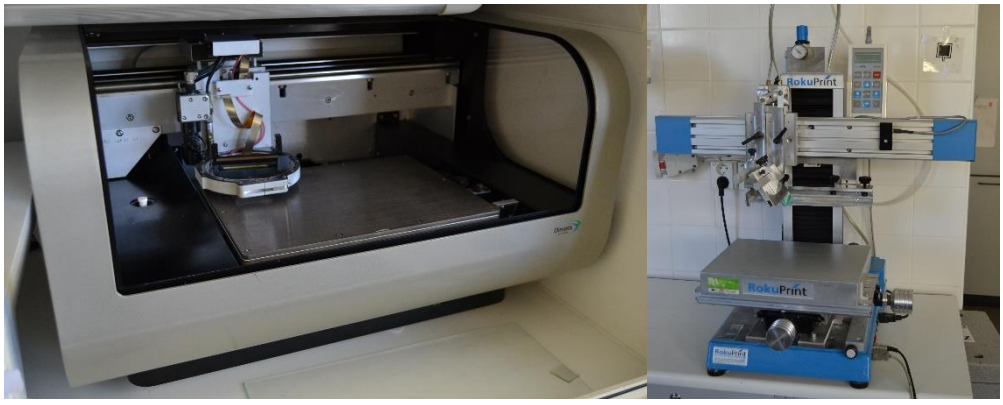

Figure 25 *Ink-jet DMP 2831 material printer on the left and RokuPrint screen printer on the right*

Bitmap

The bitmap is map of pixels, where each one may store more than two colours. In this study a bitmap is referred to as raster according to which materials is printed. The bitmap produced by exporting from CAD software involves many bits around the precise structure, and it is not suitable for material pattern printing. For this reason, the clear bitmap pattern was prepared at Adobe Illustrator directly (differences can be seen in Figure 26).

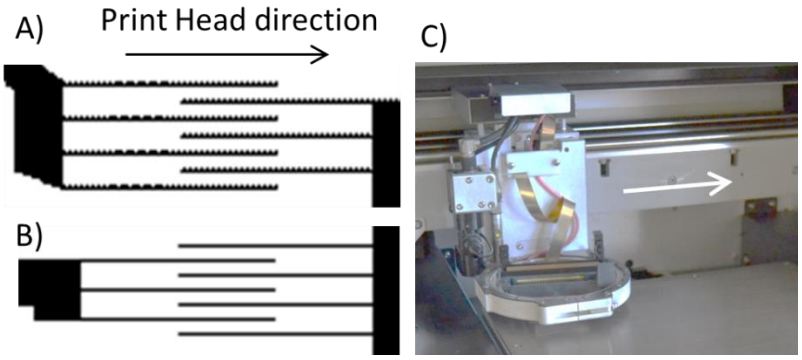

Figure 26 *The bitmap preparation for material printing: A) Bitmap exported from CAD software, B) Bitmap prepared directly at Adobe Illustrator, C) Dimatix printer head direction*

The bitmap of interdigital electrodes was designed with respect to the direction of movement of inkjet head. It gives more precision and smooth line of interdigital electrodes. Bitmap images (Figure 26) were prepared as an array of interdigital electrodes with one common source electrode, 10 pieces of drain electrodes and one gate electrode. Device and profilometry structure of interdigital electrodes can be seen on the inset of Figure 27.

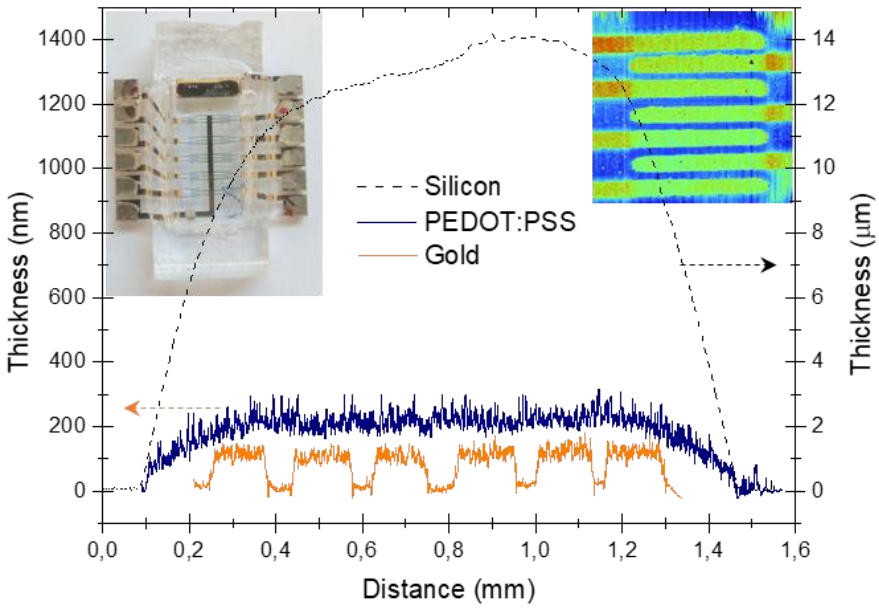

Figure 27 *The profilometry of printed layers*

The dimension of interdigital electrodes was designed to fit 847 dpi resolution (i.e. 30 μm for each bit). The channel length was designed with decreasing space as a distance of bits from 210 μm to 90 μm, i.e. structures of 30 μm difference (180, 150, 120 μm) are formed. The one printed layers of gold analysed by Bruker Dektak XT has approximately 110 ± 10 nm thickness. The screen-printed PEDOT:PSS (ink G in Table 12) layer has a thickness of 200 ± 10 nm and screen printed silicon layers has approximately 14 ± 2 μm.

The structures of OECT interdigital electrodes had to be optimised due to "spilling" of gold printed layers. The gold ink showed constant spilling about 35-40 μm on each side. This spilling limits the designed channel length between printed electrodes as a bit without inks on 120 μm result in 50 ± 5 μm of channel length. The printed interdigital electrodes were very often merged below this limit. The spilling can be seen in Figure 27, where 30 μm designed width electrode results into 110 μm one.

5.3 MATERIALS CHARACTERISATION

5.3.1 OFET characterisation

The Probe Station for measurement of organic field-effect transistors was constructed by the author. The Probe Station was designed to measurement in semi-automatic mode. The measurement device consists of three micro linear stepper motors, two Peltier modules with ethylene glycol cooling system, one NTC 100k ohm thermistor, Arduino Mega microcontroller with Ramps 1.4 extension and a 12-volt voltage source. The microcontroller can work separately without a PC. The position of the 2D micro-positioner table and lift of the source and drain electrodes/probes can be controlled with two joystick controllers. First joysticks control the position of the 2D table and second joystick control lifts of the source and drain electrodes together. By joysticks can also be set pulse width modulation (PWM) value to fans, pump and Peltier. The USB microscope help to contact the two probes. The probe station is placed in a nitrogen glove box to protect the measured sample against the air oxygen and water. The probe station system is shown in Figure 28.

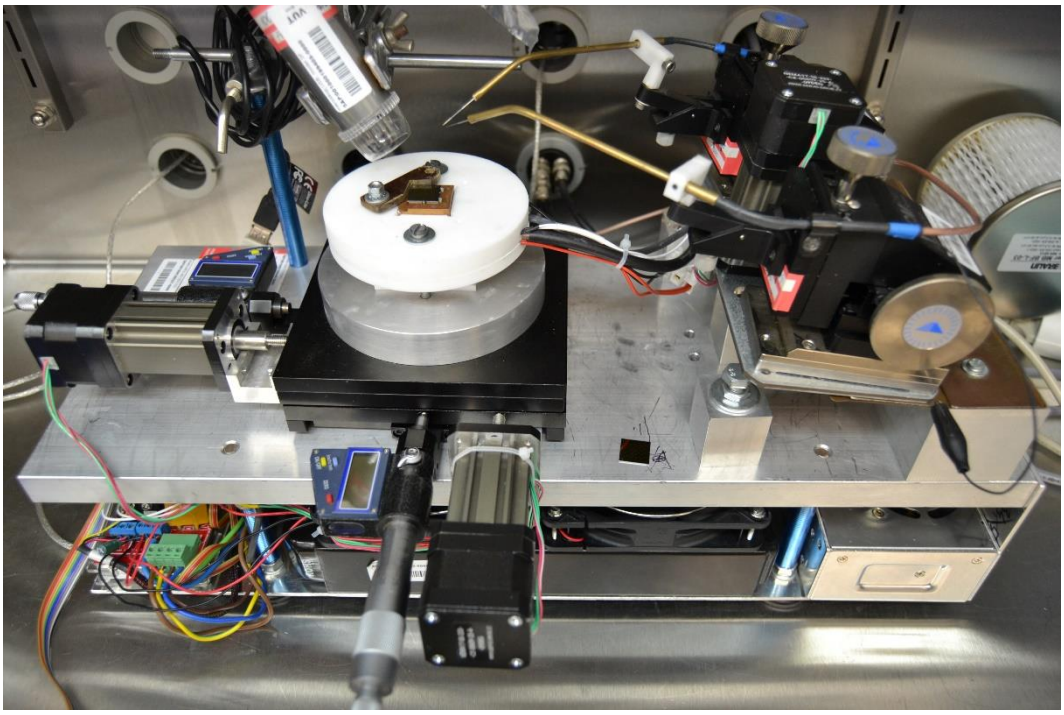

Figure 28 *The photo of probe station*

The current-voltage characteristics are measured by multimeter Keithley 6487 and Keithley 617 which are controlled by PC via programmed software in LabVIEW. The multimeter Keithley 6487 drive voltage between Source and Drain electrodes and measure the current through the channel. Keithley 617 sets the voltage on the gate electrode and both meters are grounded to the Source electrode. The measurement is provided under dark to avoid photo-induced effect during current-voltage characterisation. The measuring software was programed to export the measured data

into an excel template. In excel template the transistor parameters are automatically calculated such as charge carrier mobility, on/off ratio, contact resistance etc. The screenshot of measuring software is shown in Figure 29:

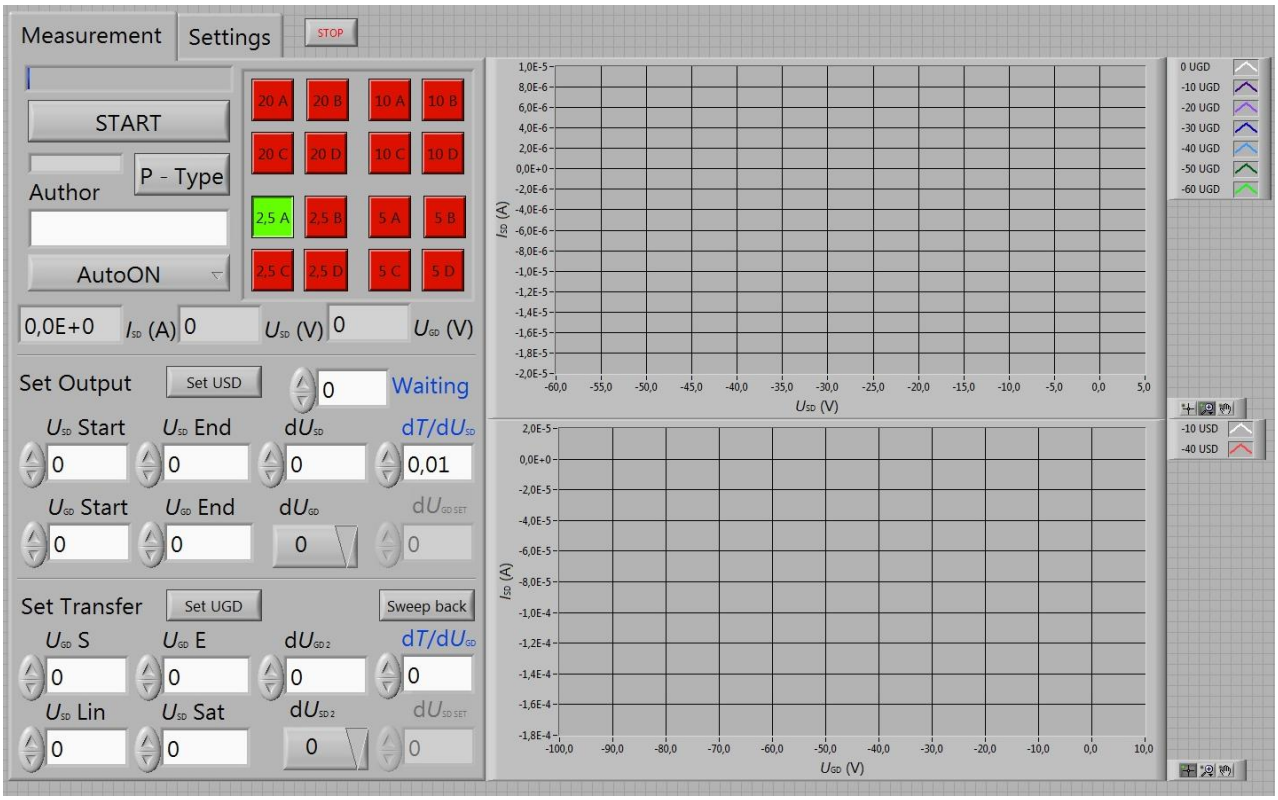

Figure 29 *Programmed software for measurement OFET devices.*

Calculation of charge carrier mobility

The charge carrier mobility can be evaluated from the measurement of transfer characteristics of OFETs as it is described in 2.6.1. The transfer characteristics can be measured in linear or saturation regime of output characteristics (0). The transfer characteristics are measured in saturation regime, measured data are modified as square root of I_{DS} and both I_{DS} and $I_{DS}^{1/2}$ are plotted with dependence on V_{GS} as it is illustrated in Figure 11b. The linear part of curve $I_{DS}^{1/2} = f(V_{GS})$ is fitted by line and the slope (k) of line is used for the calculation of charge carrier mobility i.e. $k^2 = I_{DS} \cdot V_{GS}^{-2}$. Then the equation for calculation of charge carrier mobility from measured data is modified to equation:

$$\mu_{SAT} = k^2 \cdot \frac{2L}{WC_i}, \qquad (17)$$

where k is the slope of fit line of curve $I_{DS}^{1/2} = f(V_{GS})$, L is channel length, W is channel width and C_i is capacitance of dielectric layer. In practice, the absolute value $|I_{DS}|$ and square root $I_{DS}^{1/2}$ are calculated and plotted as it is illustrated in Figure 30. For fitting of linear part of curve $I_{DS}^{1/2} = f(V_{GS})$, its numerical derivative is calculated.

The numerical derivative of $dI_{DS}^{(1/2)}/dV_{GS}$ is plotted as the grey curve in Figure 30. The V_{GS} data for maximum of derivative are found and their appropriate $I_{DS}^{(1/2)}$ data are used for calculation of charge carrier mobility.

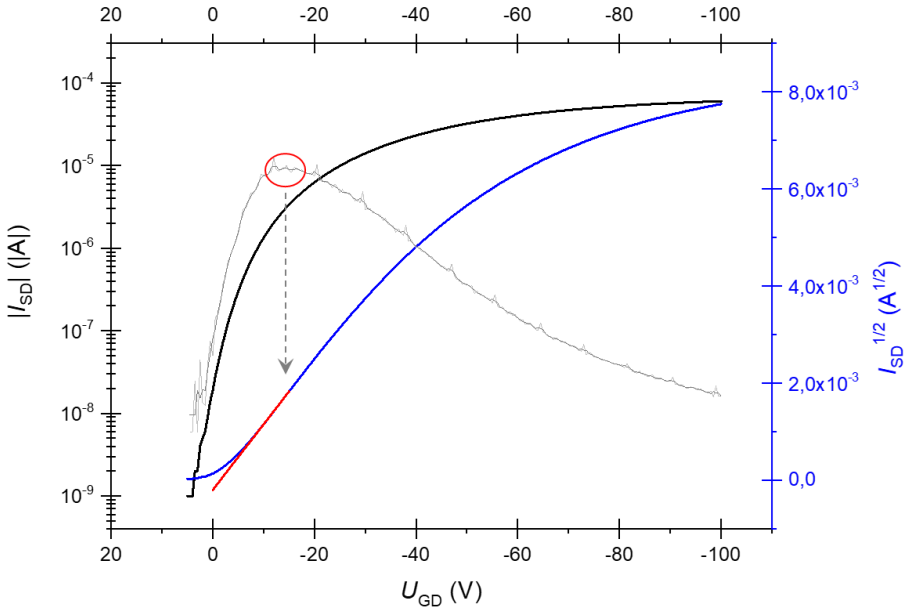

Figure 30 *The example of transfer characteristics of OFETs for calculation of charge carrier mobility*

5.3.2 OECT characterisations

A new apparatus for characterisation of OECT devices was constructed. The apparatus consists from a shield steel box with BNC connectors and four modules from National Instruments (ammeter Ni 9203, 2 x voltage source Ni 9263 and voltmeter Ni9201). The apparatus is shown in Figure 31.

Figure 31 *Apparatus for characterisation of OECT devices. The noise shield steel box with BNC connectors on the left and National Instruments connected modules on the right.*

This apparatus has the following properties:

- Voltage range ± 10 volts, the 1-bit resolution is 305 μV.
- Voltage stability is 260 μV_{rms}
- Current supply is 1 μA per channel (2 x 4), max 8 μA
- Current ammeter range ± 20 mA / 0-20 mA, resolution 660 nA or 330 nA
- Sampling frequency up to 100 kS/s

The software was programmed by the author at the LabVIEW graphical programming environment. The software is able to measure transient behaviour of OECT and modulate V_{DS} or V_{GS} voltage in time. Screen-print of OECT measurement software is shown in Figure 32. The supply voltage from Ni voltage source can be replaced by battery with a potentiometer for reducing of the electric noise. The measurement of OECT parameters was provided at phosphate buffer (PBS).

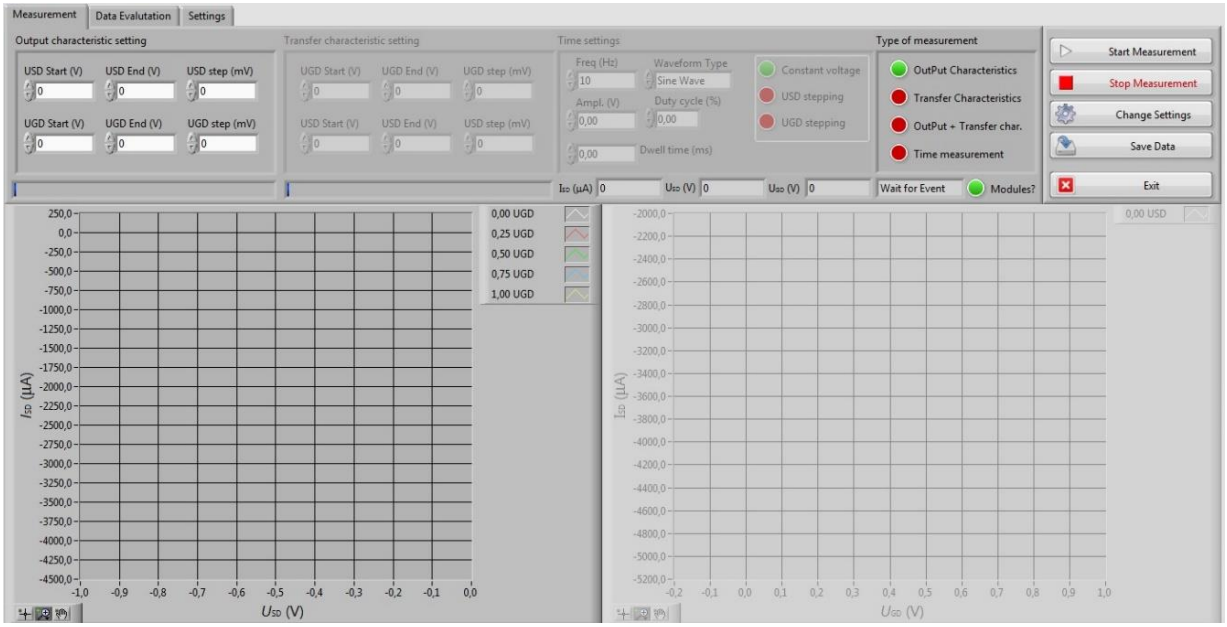

Figure 32 *Screen-print of OECT software measurement.*

5.3.3 Optical spectroscopy

Optical methods the UV-VIS spectroscopy and Fluorescence spectroscopy were used to investigate fundamental optical properties of studied materials. The absorption of organic semiconductors were investigated by Varian Cary 50 UV-VIS spectrometer (Agilent Technologies Inc., Santa Clara, CA, U.S.A.). The fluorescence spectra were measured by Thermo Spectronic Aminco Bowman AB-2 fluorescence spectrometer. The solutions and thin layers were measurements by both techniques. The solutions were studied in 10 mm quartz cuvette (Hellma GmbH, Mühlheim, Germany). The preparation of thin film for optical measurement is described in chapter 5.2.

5.3.4 Supplementary characterisations

Thermal properties

The thermal properties such as temperature stability, melting point, sublimation point and transient glass point of organic semiconductors were performed using a TA Instruments TGA Q5000 (New Castle, DE, U.S.A.). Calorimetric analyses were carried out employing a TA Instruments DSC Q200 calorimeter equipped with an external cooler RCS90. These methods were used as background information for vacuum deposition of organic semiconductors.

Thin-film characterisation

The thicknesses of prepared layers were determined by Bruker Dektak XT contact profilometer. The topography of organic semiconductors surfaces was investigated by atomic force microscopy. The samples were measured using an NT MDT (Moscow, Russia) NTEGRA Prima ambient AFM microscope with ETALON tips (tip curvature radius < 10 nm, tipping frequency = 140 kHz, force constant = 3.5 Nm) in a semi-contact mode in cooperation with Institute of Physics, Academy of Sciences Czech Republic v.v.i,.

Biocompatibility study

Biocompatibility study was performed in cooperation with the Institute of Biophysics of the Czech Academy of Sciences. For testing biocompatibility of organic semiconductors, mouse 3T3 fibroblasts and Cardiomyocytes were used. These cells were differentiated from the mouse HG8 line of embryonic stem cells. A solution of reference materials (Figure 21) in concentration 15 mg/ml in chloroform (except PEDOT:PSS) was spin-coated onto cleaned circular glass slides (Greiner 15 mm, No. 1) at 1500 rpm. Others coatings were carried out by the Institute of Biophysics of the Czech Academy of Science to improve the interface between organic semiconductors and living cells. i.e. to increase biocompatibility.

Wetting angle

The measurement of the wetting angle was performed with a Dataphysics OCA-10 system. The wetting angle was determined by the sessile droplet method. The contact angle was evaluated per six variant droplets of 5 μl water drop. The contact angle was used for measurement of coverage monolayers on OFET substrates and as a preliminary study to predict the biocompatibility of the surface of studied materials with a living cells.

6 RESULTS AND DISCUSSIONS

6.1 ORGANIC FIELD-EFFECT TRANSISTORS

The parameters of OFETs are partially dependent on the active layer of the OS. However, the overall parameters of transistors depend not only on the properties of the OS but also on the construction of the whole device. The optimisation of thin films of individual organic semiconductors significantly affects the parameters of OFET devices. The first section 6.1.1 is focused on the study of the effects of the various methods used for preparation and optimisation of active layers prepared from solution on the performance of OFETs.

The following paragraphs briefly describes a study of the relationship between the molecular structure of novel organic semiconductors, their properties and the final properties of OFETs.

The results related to the studies of novel soluble diphenyl-amino-stilbene-based DPP molecules are discussed in section 6.1.2. These stilbene DPP derivatives were studied with respect to their possible application in bulk heterojunction photovoltaics as hole transport materials.

In the following section 6.1.3, the charge carrier mobility of novel DPP derivatives with ethyl-adamantyl bonded in the -N, N; - N, O and -O, O position of the DPP core are studied. The different bonding of the alkyl chain on the DPP core can change the conjugation length and consequently also the charge carrier mobility in DPP derivatives.

A novel DPP derivative with a bulk ethyl-adamantyl group bonded in the -N, N position of the DPP core was studied in detail as described in section 6.1.4. In chapter 2.4.2 was described the charge carrier mobility of DPPs derivatives and its strong influence in the presence of intermolecular interactions. The ethyl-adamantyl group can promote high coulombic interaction which can lead to high packing property and consequently it can effectively increase charge carrier mobility.

The results of studies of ethynylene (C-C triple bond) as a building block for OS are described in the last section 6.1.5. The influence of ethynylene is studied in naphthalene derivatives. The observed properties of naphthalene derivatives with an incorporated ethynylene block are compared to the properties of naphthalene derivatives without ethynylene published early.

6.1.1 Development and optimisation of OFETs based on DPP(TBFu)$_2$

The goal of this study is to elucidate the effect of different methods used for thin-film preparation from solution on the performance of OFETs. For this study the reference material (3,6-bis(5-(benzofuran-2-yl)thiophene-2-yl)-2,5-bis(2-ethyl-hexyl)pyrrolo[3,4-c]pyrrole-1,4-dione) [referred as DPP(TBFu)$_2$] was supplied by the Centre for Organic Chemistry Ltd. (COC).

The thin active layers of DPP(TBFu)$_2$ were prepared by means of the spincoating technique on a commercially available OFET platform mentioned at 5.2.1. This platform represents the bottom-gate/bottom-contact architecture which is advantageous for use when the OS is in direct contact with the environment.

Several process for device optimisations were used. First, high vacuum treatment (cleaning) after standard solution cleaning was introduced in order to reduce residue on the surface. The self-assembled monolayers (SAMs) hexamethyldisilazane (HMDS) and octadecyl trichlorosilane (OTS) onto silicon dioxide dielectric and pentafuorobenzenethiol (PFBT) onto gold electrodes, and combinations thereof were used as another tool for optimisation. In the last step, thermal annealing of the used DPP(TBFu)$_2$ was introduced. The architecture of the OFET used in this study is depicted in Figure 33.

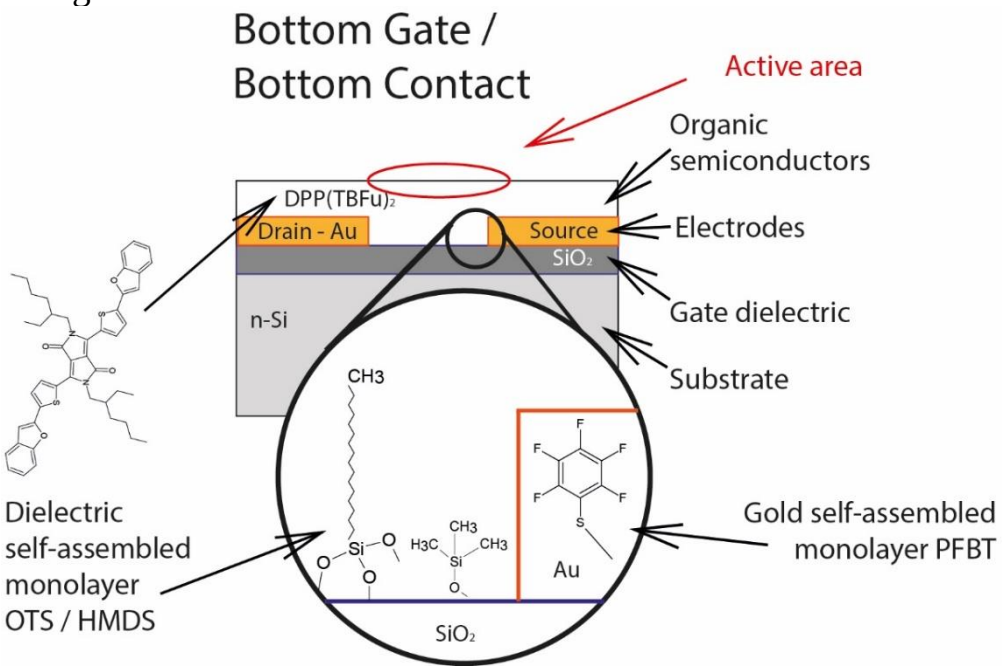

Figure 33 *The solution-processed device architecture.*

The effect of vacuum treatment on the performance of the OFET is depicted in Figure 34A (without vacuum) and Figure 34B (with vacuum). The contact resistance obtained from the slope of output characteristics depicted in Figure 34B show eight-times-lower contact resistance (R_c) for vacuum treatment ("cleaning") of OFET platforms from which we can assume that during the fabrication process, some residue or absorbed gasses were present on the surface [82].

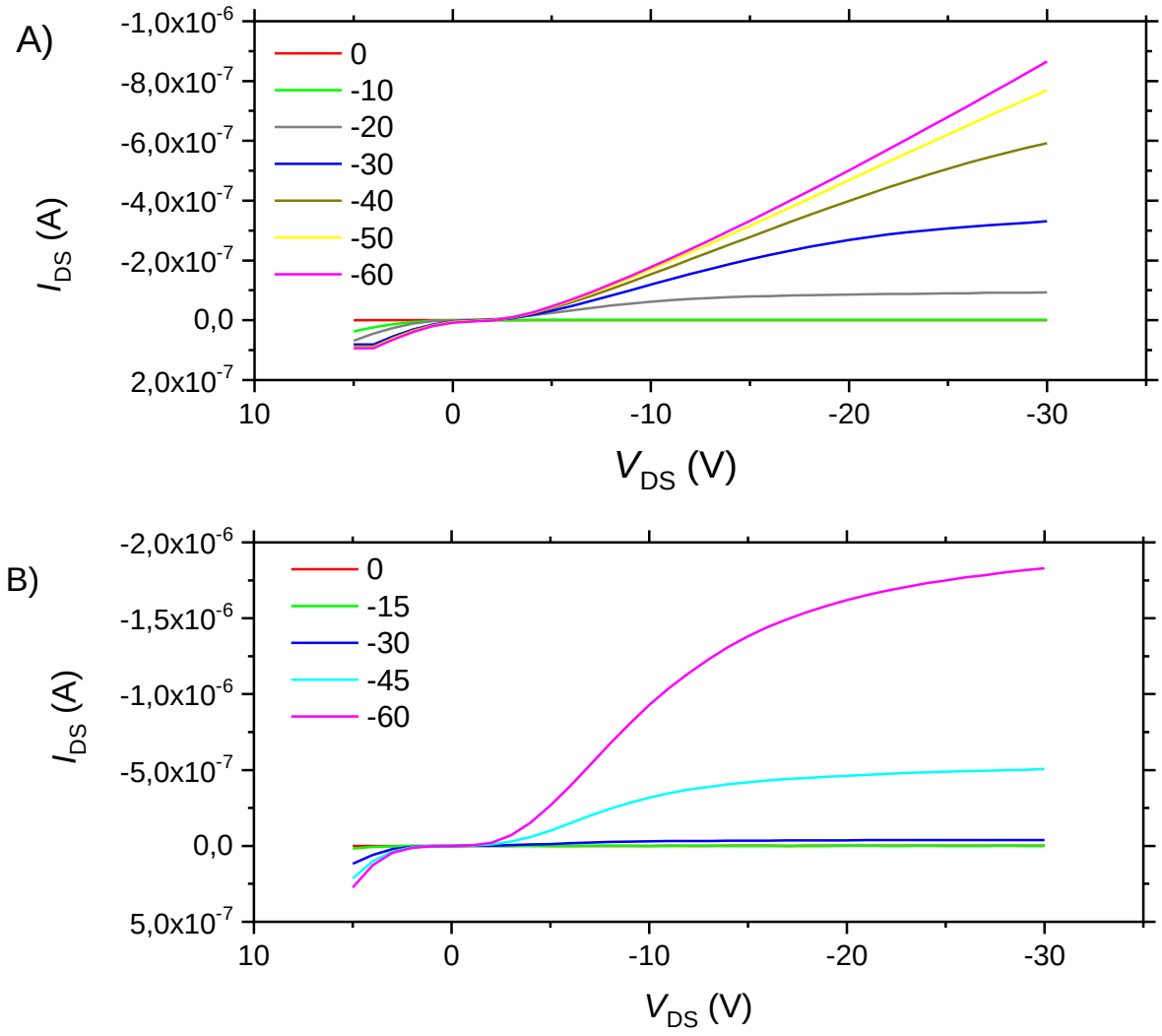

Figure 34 *Comparison of output characteristics of OFETs A) without vacuum cleaning and B) with vacuum cleaning.*

The applied monolayers on gate dielectrics effectively decrease the charge trapping states on the interface between the dielectrics and OS [83]. The comparison of transfer characteristics with and without a HMDS monolayer on the gate dielectric can be seen in Figure 35. Silicon dioxide as a dielectric contains many traps for charge carriers, and thus influences the properties of OFET transistors. Hexamethyldisilazane represents a silazane containing Si–NH–Si groups. The other SAM used in this study is octadecyl trichlorosilane (OTS) which represents a halosilane with Si–Cl groups. Both compounds react with surface silanol groups (–Si–OH) on a SiO_2 dielectric and form strong siloxane Si–O–Si bonds. Both SAM materials are known to decrease the polarity of the surface, and this reduces the charge trapping states [84]. In every case, the OTS and HMDS layers increase one order of magnitude measured hole mobility as can be seen for samples I and IV in Table 13.

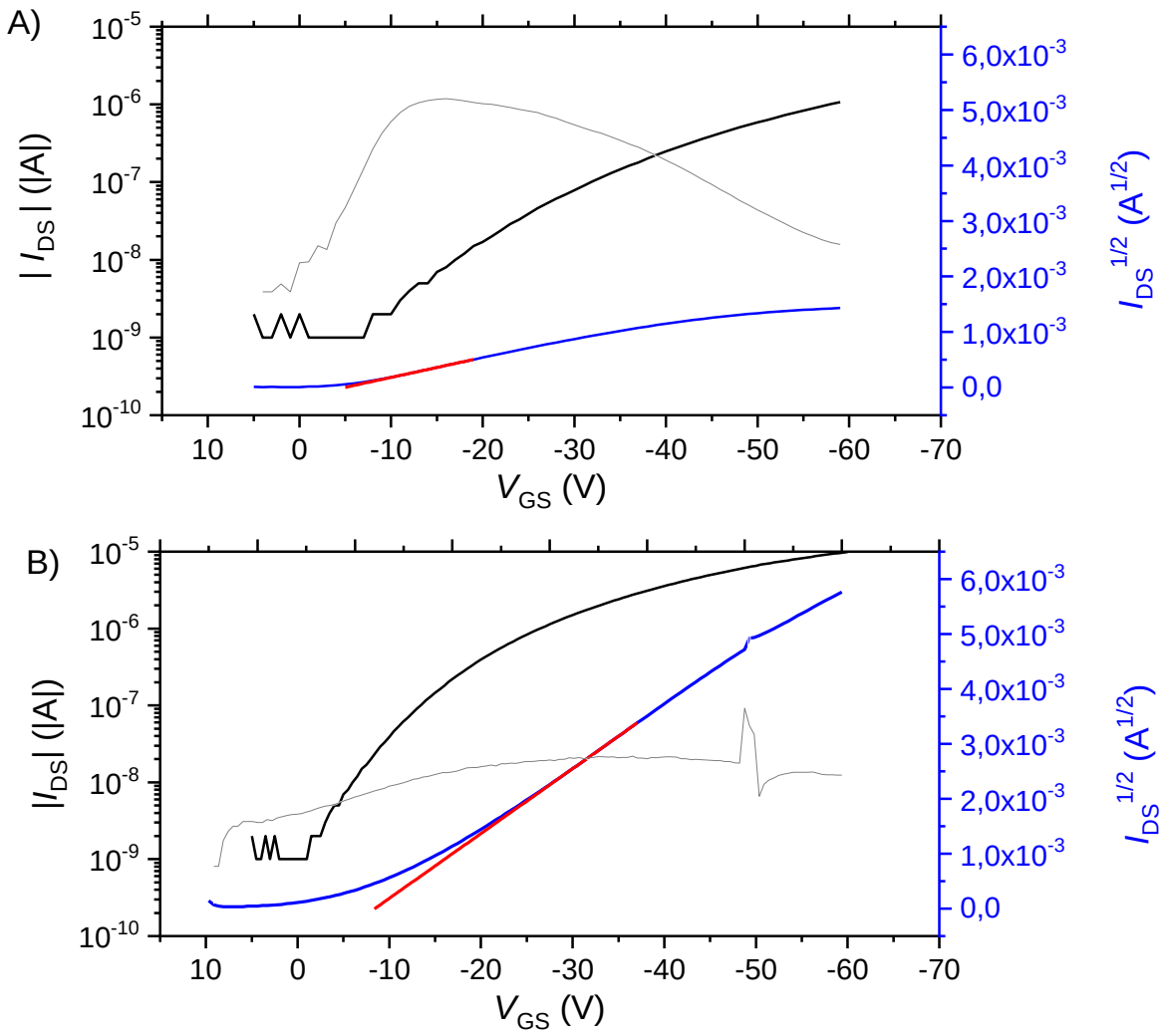

Figure 35 *Comparison of transfer characteristics of OFETs A) without HMDS SAM and B) with HMDS SAM*

The output characteristics of OFETs with and without PFBT self-assembled monolayers and with OTS are shown in Figure 36. Figure 36A shows the output characteristics of a vacuum-treated substrate with an applied OTS SAM. The Figure 36B shows the output characteristics with an applied OTS (without vacuum treatment) and PFBT. The present gold interdigital electrodes without PFBT SAM (Figure 36A) have a work function in the range 4.8 – 5.2 eV depending on the cleaning routine, absorbed gasses, etc. [82]. By applying a PFBT monolayer, the contact resistance is reduced as can be seen in Figure 36B. The PFBT monolayer creates dipoles on gold that increase the electrode work function and reduce injection barriers between the work function of the gold electrodes and the HOMO level of $DPP(TBFu)_2$ [85]. The PFBT monolayer on gold leads to a greater decrease in R_c than vacuum treatment and it works for both HMDS and OTS pretreated substrates as can be seen from Table 13. Thus, it can be concluded that PFBT treatment is more efficient than vacuum treatment.

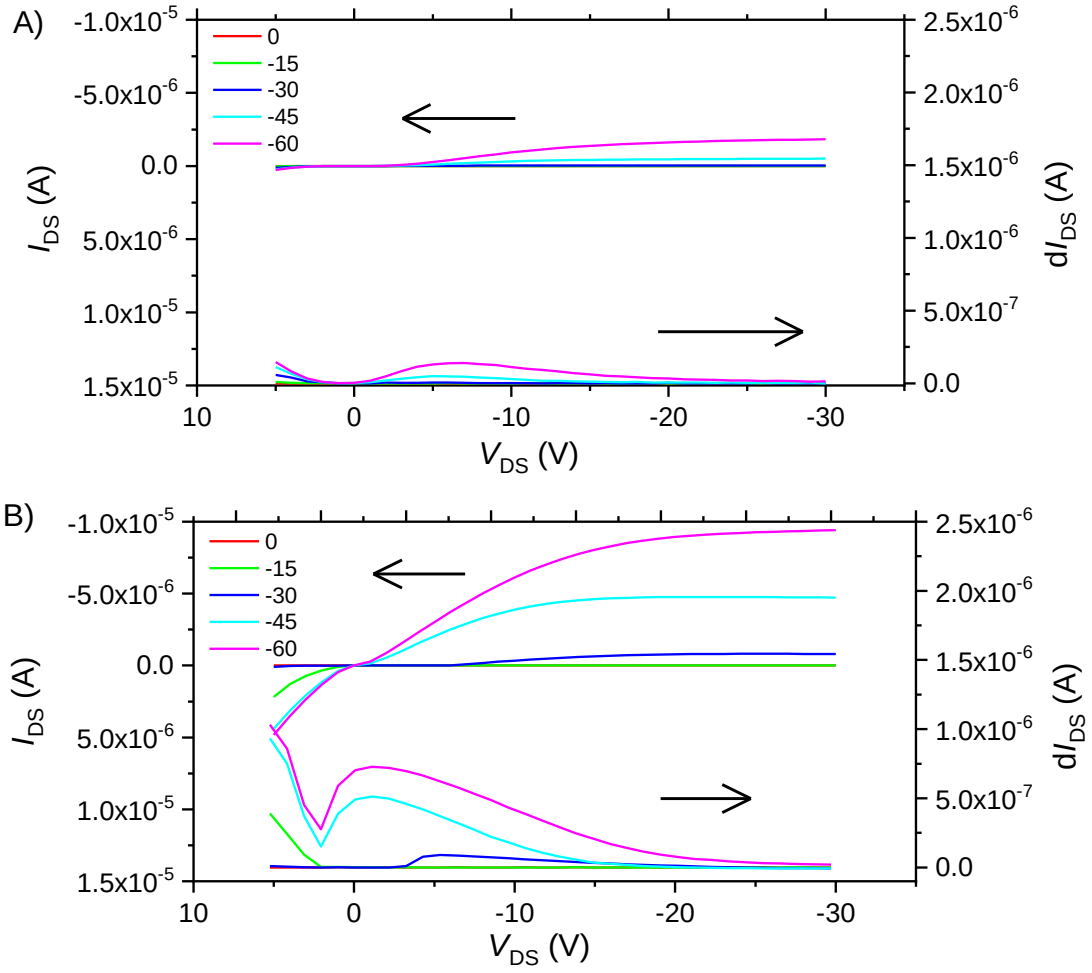

Figure 36 *Comparison of output characteristics of OFETs A) with vacuum treatment and B) with PFBT SAM, both with OTS SAM.*

The AFM measurements performed in cooperation with the Institute of Physics, Academy of Sciences Czech Republic shown in Figure 37 showed an increases the amount of microcrystals after thermal annealing of DPP(TBFu)$_2$ [76]. Thus the thermal annealing increases the amount of microcrystals, which improves measured charge carrier mobility of DPP(TBFu)$_2$ as can be deduced from Table 13.

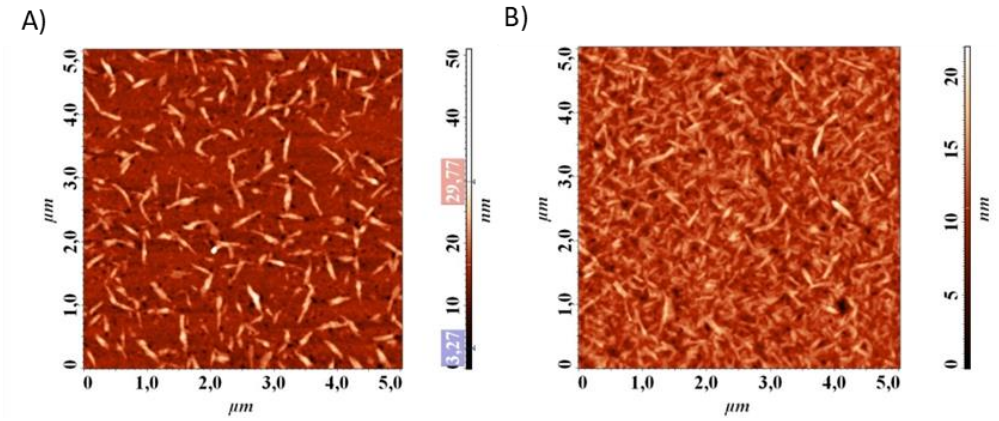

Figure 37 *AFM pictures of the active layer (for sample III) for A) as-cast B) annealed for 10 min at 110 °C.*

Table 13 *Properties of DPP(TBFu)2 under different fabrication conditions.*

Sample	Treatment		TA[a)]	Hole Mobility	V_T[b)] (V)	R_C[c)] (Ω)	On/Off ratio
	Au	SiO_2		($cm^2V^{-1}s^{-1}$)			
I	-	-	110 °C	$2.3 \cdot 10^{-4}$	-4.8	$8.86 \cdot 10^{6}$	$1.9 \cdot 10^{4}$
II	vac	vac	-	$1.9 \cdot 10^{-5}$	-11.9	$1.10 \cdot 10^{6}$	$4.9 \cdot 10^{4}$
			110 °C	$2.7 \cdot 10^{-4}$	-19.5	$1.08 \cdot 10^{6}$	$5.3 \cdot 10^{4}$
III	vac	OTS	-	$8.2 \cdot 10^{-4}$	-5.5	$3.74 \cdot 10^{6}$	$2.4 \cdot 10^{4}$
			110 °C	$1.3 \cdot 10^{-3}$	-11.5	$3.00 \cdot 10^{5}$	$6.3 \cdot 10^{4}$
IV	-	HMDS	-	$6.7 \cdot 10^{-4}$	-9.5	$6.73 \cdot 10^{5}$	$7.7 \cdot 10^{3}$
			110 °C	$2.0 \cdot 10^{-3}$	-10.3	$7.22 \cdot 10^{5}$	$9.5 \cdot 10^{3}$
V	PFBT	OTS	-	$8.5 \cdot 10^{-4}$	-2.9	$3.08 \cdot 10^{5}$	$2.7 \cdot 10^{4}$
			110 °C	$2.8 \cdot 10^{-3}$	-3.6	$9.61 \cdot 10^{4}$	$3.7 \cdot 10^{4}$
VI	PFBT	HMDS	-	$1.3 \cdot 10^{-3}$	-13.3	$3.99 \cdot 10^{5}$	$2.9 \cdot 10^{4}$
			110 °C	$3.6 \cdot 10^{-3}$	-15.9	$3.66 \cdot 10^{5}$	$1.1 \cdot 10^{5}$

[a)] The TA values thermal annealing, [b)] V_T is the threshold voltage, [c)] R_C is the contact resistance at V_G = -60 V.

Due to a combination of SAMs and thermal annealing, the highest charge carrier mobility $5.5 \cdot 10^{-3}$ cm^2/Vs was achieved. This value represents the highest hole mobility experimentally achieved so far for the $DPP(TBFu)_2$ material. It is even slightly higher than the mobility observed for the stereoisomer (mesomer form) isolated by preparative chiral high-performance liquid chromatography HPLC, namely a value of $2.8 \cdot 10^{-3}$ cm^2/Vs [77].

Several methods for thin-film preparation from solution were used. Their influence on the performance of OFETs were studied. To eliminate contact barriers, vacuum treatment and a PFBT monolayer on the gold electrodes were used. The applied self-assembled monolayers of OTS and HMDS on gate dielectrics increased measured hole mobility. By the combination of self-assembled monolayers and thermal annealing, a higher charge carrier mobility $5.5 \cdot 10^{-3}$ cm^2/Vs than the best previously reported value $2.8 \cdot 10^{-3}$ cm^2/Vs can be achieved [77].

The complete results were published in the journal *Chemical Papers*. The paper is enclosed. The overview and contribution of the author is also described [S1].

6.1.2 Diphenyl-amino-stilbene DPPs

The aim of this study is to characterise the properties of novel synthesised soluble diphenyl-amino-stilbene-based DPP derivatives as hole transport materials for photovoltaic applications. Bulk-heterojunction organic solar cells have become one of the most attractive photovoltaic technologies due to their colour tunability, flexibility, low mass, and simplicity of production. The active layer of these solar cells is mostly based on a solution-processed mixture of electron and hole transport semiconductors [86]. While fullerene derivatives remain the most successful electron transport/acceptors in these cells, over the past decade great progress has been made in the search for new, more efficient electron donors and hole transport materials. The hole transport materials are mostly conjugated polymers or small molecules with an extended conjugated system incorporating sulphur molecules such as a thiophene ring, but sulphur-free OS materials are rarely used. For this reason, the study of four soluble diphenyl-amino-stilbene-based diketo-pyrrolo-pyrrole molecules as hole transport materials has been carried out. The DPP-based hole materials shown in Figure 19 were synthesised by Centre for Organic Chemistry Ltd. (COC).

The basic optical properties of stilbene DPP derivative films were studied. The optical bandgap of OS can be obtained from the UV-VIS absorption curve. The solid-state spectra of thin films are shown in Figure 38.

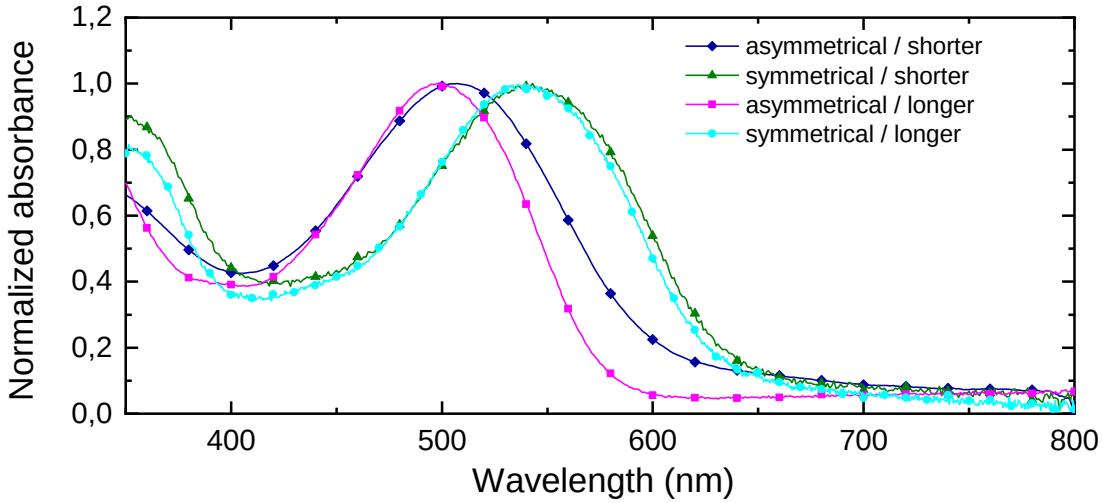

Figure 38 *Solid-state spectra of asymmetrical/shorter (diamond), symmetrical/shorter (triangle), asymmetrical/longer (square), and symmetrical/longer (circle)DPP derivatives [87].*

As was described in chapter 2.4.2, the presence of phenyl in the structure of DPP molecule enables its rotation, intermolecular π–π interaction is weaker and its spectra are shifted to the blue region as can be seen for asymmetrical derivatives in Figure 38.

These materials were applied as films in OFETs in the bottom-gate/bottom-contact architecture. A comparison of the transfer characteristics of the studied materials is shown in Figure 39.

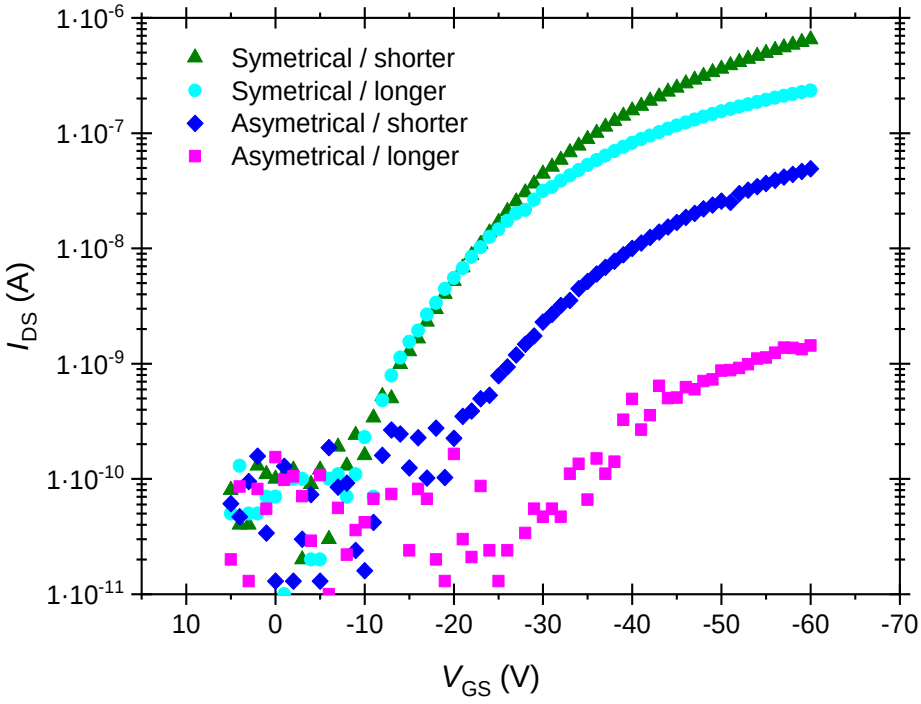

Figure 39 *Comparison of transfer characteristics of studied diphenyl-amino-stilbene-based DPP derivatives.*

The average hole mobilities, threshold voltages of OFETs and chemical structures of the studied materials are shown in Figure 40.

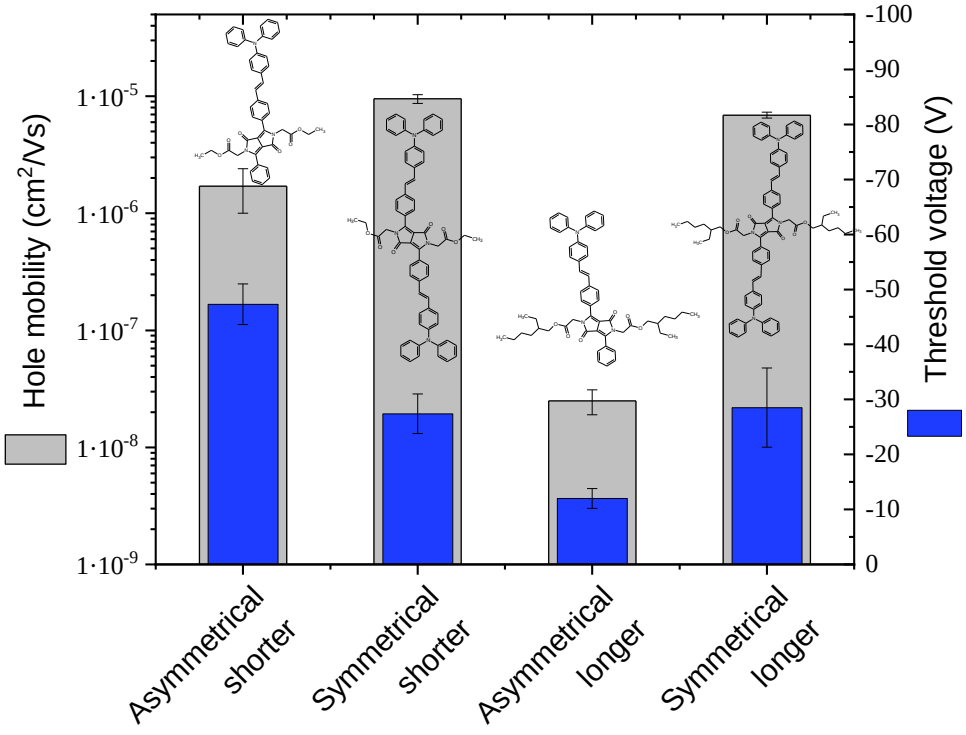

Figure 40 *Charge carrier mobility of thiophene-free DPP derivatives.*

It has been reported that the performance of organic solar cells (OSC) directly depends on the mobility of the photoactive materials. For bulk heterojunction solar cells with fullerene as an electron acceptor and transport material, the optimal hole mobility of donor/hole transport materials is in the interval between 10^{-3}–10^{-4} cm^2/Vs [88]. As it is shown in Figure 40, the hole mobility values determined by the characterisation of thin-film transistors are significantly lower than the optimum (2–4 magnitudes lower) for OSC.

As follows from Figure 40, higher hole mobility can be observed for symmetrical derivatives than for the asymmetrical ones. This effect can be ascribed to the longer conjugated chain and corresponds well with the results of the optical measurements in Figure 38 [89]. A shorter alkyl chain undoubtedly has a positive effect and improves the hole mobility for a symmetrical derivative. However, lower hole mobility were found for unsymmetrical DPP derivatives in comparison to the symmetrical derivative.

The symmetrical and asymmetrical diphenyl-amino-stilbene-based DPP derivatives were compared. Phenyl compared to the stilbene group is more susceptible to rotations, and this effect is thus more emphasised in asymmetrical derivatives. Comparison of longer (2-ethyl-hexyl acetate) and shorter (ethyl acetate) alkyl chains showed an interesting effect: the shorter alkyl chain has been proven to provide higher mobility. Even if the hole mobilities are significantly lower than the optimum for an organic solar cell, these derivatives were successfully used as hole transport materials and donors in the bulk heterojunction solar cells with a solar cell efficiency of up to 1.5%.

The complete results were published in the journal *Chemical Papers*. The paper is enclosed. The overview and contribution of the author is also described [S2].

6.1.3 Ethyladamantane derivatives of the DPPs

The aim of this part of the work was to characterise the charge carrier mobility in newly synthesised $(Th)_2$-DPP derivatives with an ethyladamantane alkyl side chain. The study was performed on thiophene DPP derivatives where an ethyladamantane chain was bonded through oxygen (O) or nitrogen (N) to the central dilactam core of DPPs. The bonding of ethyladamantane is possible in three ways, i.e. the position in N-N, N-O and O-O.

As was described in chapter 2.4.2, the size of the solubilising alkyl chain can influence the morphological structure, packing of molecules and electronic coupling of DPPs. The other derivatives with shorter butyl and longer dodecyl alkyls bonded in the N-N position of the $(Th)_2$-DPP derivatives were also studied in order to determine the influence between the robust ethyladmantane groups and the bonding position. The charge carrier mobility of DPP derivatives shown in Figure 41 were studied.

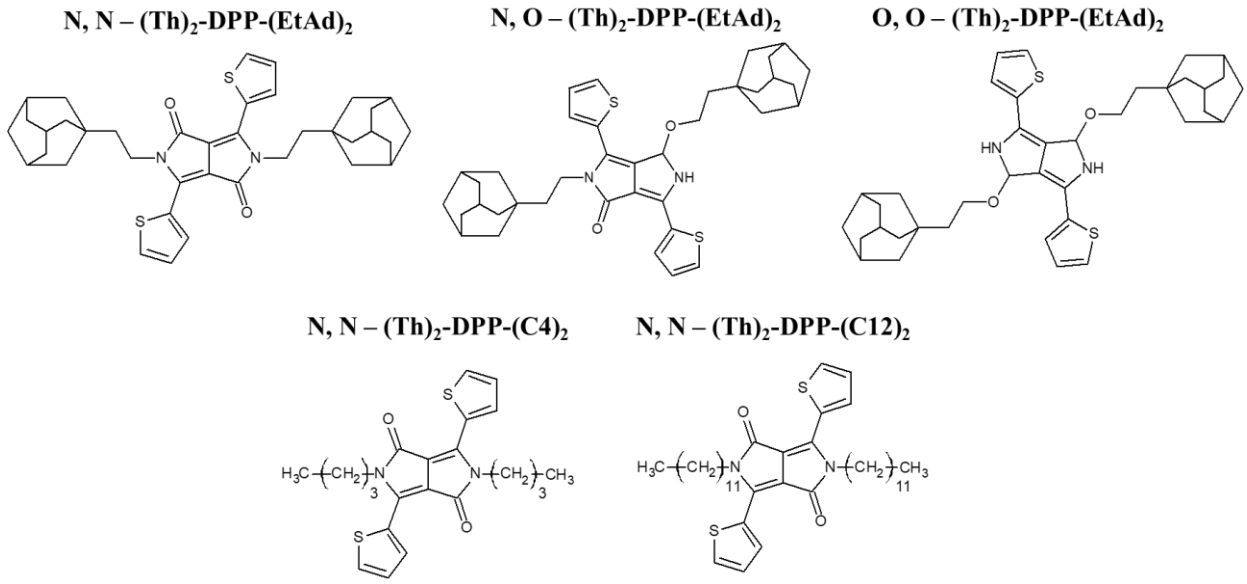

Figure 41 *Structures of the studied ethyladmantane DPP derivatives.*

The optical spectra of solutions and thin films were studied, which can reveal the bandgap and suggest the packing of molecules and electronic coupling. The comparison of the solution absorption spectra of butyl and ethyladamantyl derivatives in Figure 42 shows the same optical properties, i.e. the alkyl chain does not participate in conjugation in the N,N bonding position. The more significant bathochromic shift for butyl derivatives in the solid state indicates better intermolecular interaction [89]. On the other hand, the narrow and clearly identifiable peaks in optical spectra for the ethyladamantyl derivative suggest a more rigid structure.

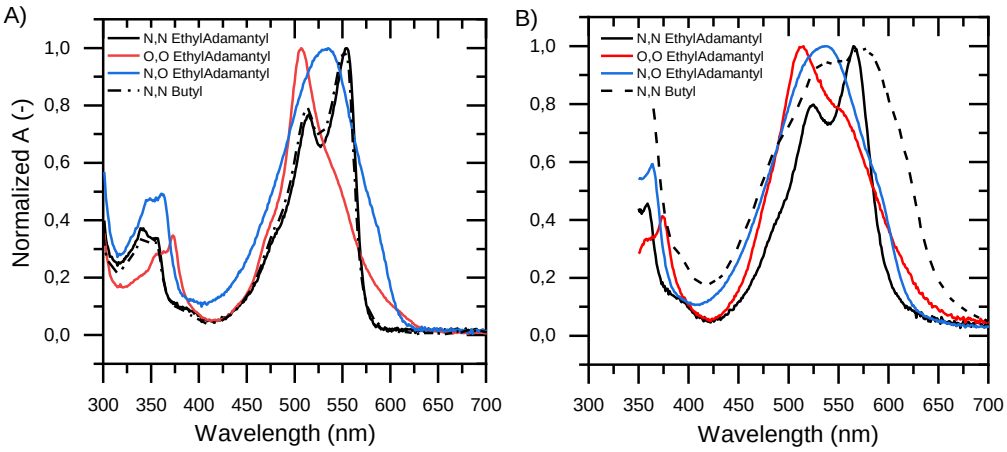

Figure 42 *Normalised absorption spectra of the A) solution and B) thin film of the studied DPP derivatives.*

The different state is evident between the bonding of ethyladamantyl in the N-N, N-O and O-O position of DPP derivatives. The N, N ethyladamantyl derivative showed a lower optical bandgap than the other N, O and O, O derivatives as can be deduced from the absorption spectra of solutions and thin film in Figure 42. The optical spectra of N, O derivatives suggest better conjugation. However, the better

recognised vibrational spectra of O, O substituted ethyladamantyl suggest its rigid and higher packing properties [90]. The conjugation of bonded ethyladamantyl derivatives decrease in the order N N < N, O < O, O.

The influence of the size of the ethyladamantyl group on hole mobility can be observed in the comparison of DPP derivatives with bonded alkyl chains in the N,N position in Figure 43. The thin films of DPP derivatives were prepared onto an OTS-treated OFET substrate by means of the spincoating technique.

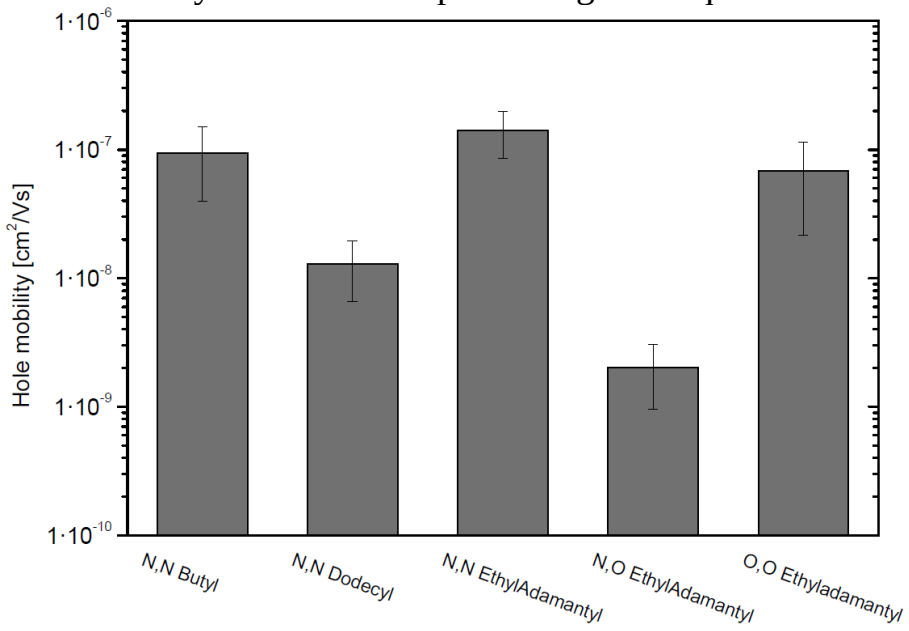

Figure 43 *Hole mobilities of studied DPP derivatives [91].*

As can be deduced from Figure 43, the higher hole mobility in N,N–ethyladamantyl derivative than N,N–dodecyl derivative was observed even if the ethyladamantyl group is relatively greater than or equal to the size of the dodecyl. In spite of the differences in the solid-state optical spectra between the butyl and ethyladamantyl derivatives, the DPP derivative with a bulkier ethyladamantyl group shows similar hole mobility at $1 \cdot 10^{-7}$ cm^2/Vs as the smaller "butyl" derivative.

The worst result hole mobility $2 \cdot 10^{-9}$ cm^2/Vs was observed for the N, O ethyladamantyl DPP derivative and a higher hole mobility by two magnitudes at $1 \cdot 10^{-7}$ cm^2/Vs was observed for the O, O ethyladamantyl DPP derivative.

The ethyladamantyl group represents relatively bulky substituents; the ability to induce rigid and good organisation leads to better hole mobility than dodecyl derivative and similar mobility as butyl derivatives. The N, N ethyladamantyl bonded thiophene DPP derivatives show two magnitudes higher charge carrier mobility than the N, O substituted derivative and one magnitude higher than the N, N dodecyl derivative. It can be thus concluded that although the ethyladamantyl group represents bulky substituents it can be an alternative when the high solubility and high molecular packing in the solid state are required.

The complete results were published in *Materials Science Forum*. The paper is enclosed. The overview and contribution of the author is also described [S3].

6.1.4 The charge carrier mobility in N,N Ethyladamantyl DPP

As was shown in chapter 6.1.3, the ethyladamantyl solubilisation side groups bonded at the N,N position of the DPP core have a relatively good ability to induce self-organisation. The capability for self-organisation of the adamantyl group has been several times published, and the induced π–π interactions between the conjugated cores through adamantyl–adamantyl stacking in the diketo-pyrrolo-pyrrole derivative has been studied [92].

This study was performed by author at the Linz Institute of Organic Solar Cells (LIOS) at the Johannes Kepler University in Linz. For this study, the three DPP derivatives with thiophene groups were chosen (see Figure 44). Basic thiophene DPP derivatives without bonded alkyl chain derivative "A" in Figure 44 should promote high H-bonding stacking properties. An ethyl-2-hexyl thiophene DPP derivative "B" in Figure 44 was chosen as an alternative soluble material.

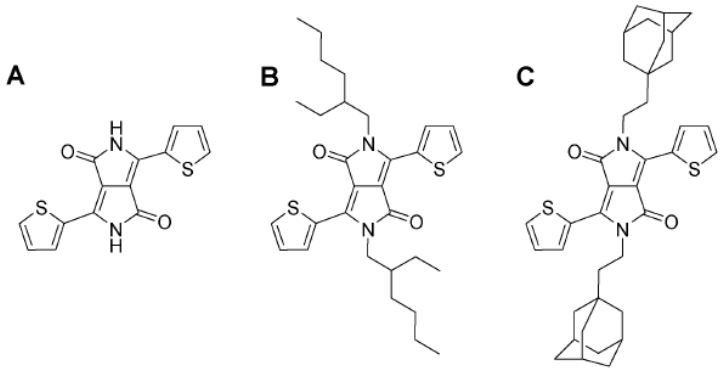

Figure 44 *Transfer characteristics of (A) H; (B) 2-ethylhexyl and (C) ethyladamantyl N,N-bonded $(Th)_2$-DPP-$(x)_2$ derivatives.*

The absorption, emission and excitation spectra of vacuum deposited thin films of DPP derivatives in this part were also studied. Regarding the optical spectra shown in Figure 45, the alkyl chain engineering of DPP derivatives usually does not result in any significant changes because of the absence of side-group/core conjugation.

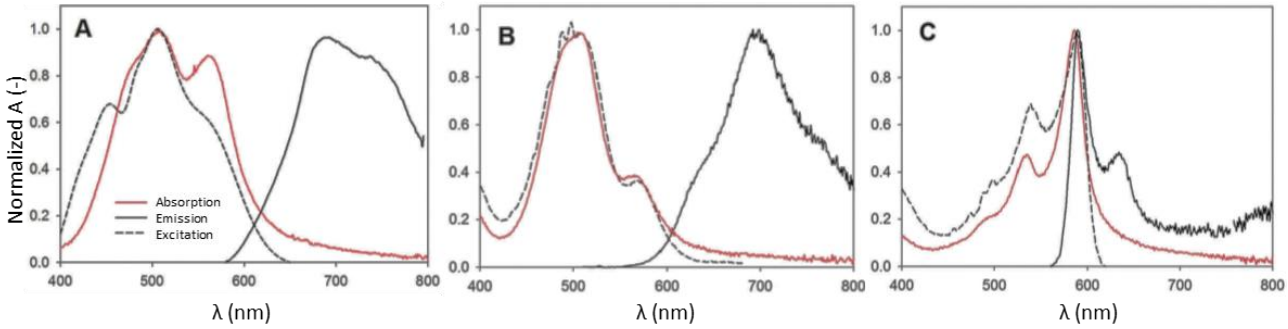

Figure 45 *Absorption (solid red), Emission (solid black) and Excitation (dash black) of the molecular structures of (A) H; (B) 2-Ethylhexyl and (C) ethyladamantyl N-substituted DPP(Th)2 [93].*

However, distinctively from other compounds, the ethyladamantyl-substituted derivative (C) exhibited solid-state blue-shifted fluorescence in comparison with 2-ethylhexyl (B) and hydrogen-substituted derivatives (A). The optical spectra depicted in Figure 45C show a small Stokes shift. A negligible Stokes shift alongside well-defined vibrational peaks in the spectra is also evidence of the high crystallinity of the layer [94].

In this study, the fabrication of organic field-effect transistors was modified as follows. The OFETs were fabricated by a vacuum deposition technique. Glass slides used for the device fabrication were sequentially cleaned with detergent, deionised water, acetone and isopropanol. The aluminium gate electrodes (100 nm) were evaporated through a shadow mask. The aluminium was oxidised by the potentiostatic method of anodised alumina (32 nm AlOx). The AlOx layer was then passivated by evaporating oligoethylene tetratetracontane (C44H90, TTC) to create an inorganic/organic composite gate dielectric with a capacitance of 20 nF/cm^2. Films of the DPP derivatives were evaporated at a pressure of $1 \cdot 10^{-6}$ mbar at a rate of 0.2–0.3 Å·s^{-1}. Finally, gold source and drain electrodes were evaporated using a shadow mask with a thickness of 80 nm (L = 60 μm, W = 2 mm). The current-voltage characteristics of prepared OFETs were measured in the dark and under nitrogen. The transfer characteristics are shown in Figure 46.

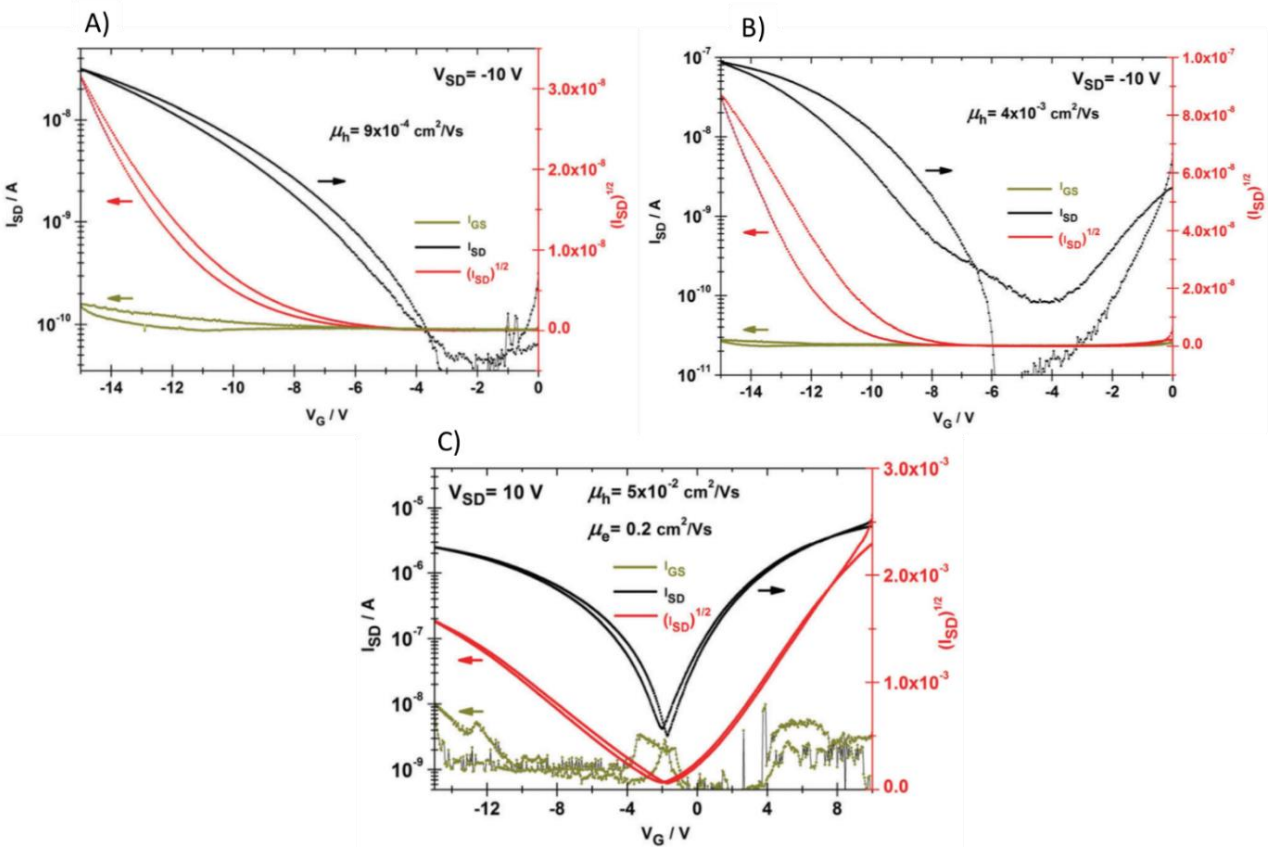

Figure 46 *Transfer characteristics of (A) H; (B) 2-ethylhexyl and (C) ethyladamantyl N,N-bonded $(Th)_2$-DPP-$(x)_2$ derivatives [93].*

The high organisation of DPP derivatives on the TTC interlayer results in the closeness of the DPP cores, which facilitates the charge transfer in the material, as evidence of the observed high measured charge carrier mobility in Figure 46. As a consequence of vacuum thin film preparation and high stacking properties, higher hole mobility by five orders of magnitude than for the solution-prepared thin film (chapter 6.1.3) of N,N ethyladamantyl derivatives was observed. The $(Th)_2$-DPP derivatives containing adamantyl-derived solubilisation side groups (C) possessed mobilities which are also higher than the hole mobilities of H-bonded $(Th)_2$-DPP (A) and $(Th)_2$-DPP-$(EtHex)_2$ (B) derivatives at $9 \cdot 10^{-4}$ cm^2/Vs and $4 \cdot 10^{-3}$ cm^2/Vs, respectively. Moreover, due to the high crystallinity and co-planarity of the conjugated cores, electron transfer was preserved with an electron mobility of 0.2 cm^2/Vs, as is illustrated in Figure 46 C and summarized in Table 14.

Table 14 *Properties of DPP derivatives measured at LIOS.*

Material	**μ_e (cm^2/Vs)**	**μ_h (cm^2/Vs)**
A	-	$9 \cdot 10^{-4}$
B	-	$4 \cdot 10^{-3}$
C	0.2	$5 \cdot 10^{-2}$

Interestingly, as distinct from all the derivatives under investigation, the material with ethyladamantyl containing side groups showed an ambipolar behaviour. The electron transport of thiophene DPP derivatives was theoretically predicted in the case of high co-planarity with a low torsion angle of the thiophene substituent and this behaviour was first confirmed in this study [95].

The complete results were published in *Journal of Materials Chemistry C*. The paper is enclosed. The overview and contribution of the author is also described [S4].

.

6.1.5 Naphtalane derivatives with ethynylene building block

This study is focused on a series of new naphthalene derivatives with an incorporated ethynylene building block, which could enhance our knowledge about the relationship between molecular structures and their properties, mainly charge carrier mobility.

The naphthalene derivatives with (5-hexyl-2,2-bithiophene-5-yl)**ethynyl** side arms attached to the central naphthalene core at positions 1 and 4 (H2TA14N), 1 and 5 (H2TA15N), and 2 and 6 (H2TA26N) were synthesised by the Department of Organic Chemistry, Faculty of Natural Sciences, Comenius University in Bratislava. A comparison of the molecular structure of the new and previously published derivatives without an ethynylene building block is illustrated in Figure 48A.

The normalised absorption and emission spectra of solutions and thin films shown in Figure 47 revealed the change in conjugation (bandgap) compared to the ethynylene-free naphthalene derivatives [80].

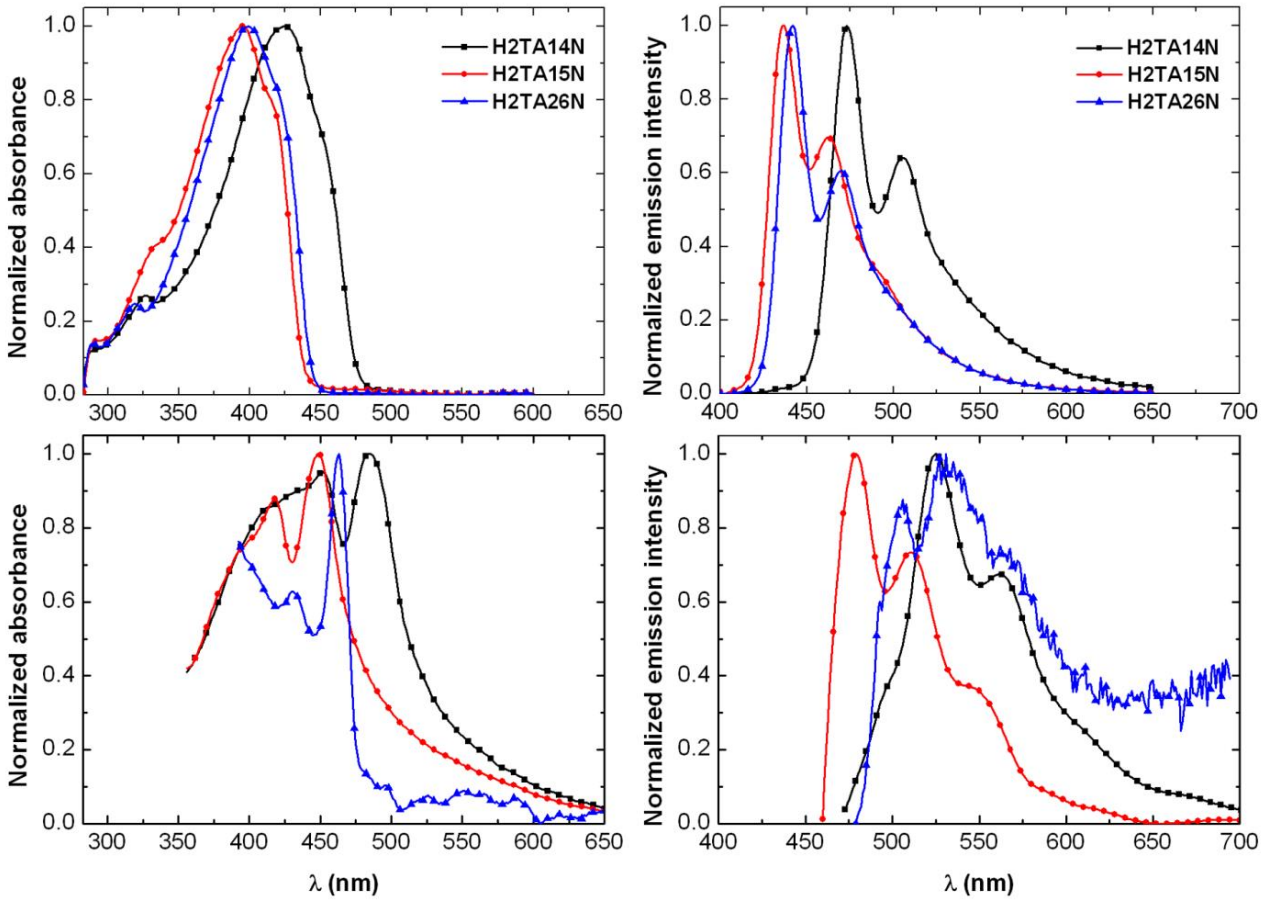

Figure 47 *Normalised absorption (left) and emission (right) spectra of the studied compounds: solutions in toluene (top) and vacuum-deposited films (bottom) [80].*

The ethynylene linker ensures the planarity of the molecules and the conjugation (bandgap) of derivatives in the order H2TA15N ≈ H2TA26N < H2TA14N, as can be seen from the optical spectra of solutions and thin films. In the previous study the

conjugation of ethynylene-free derivatives was in the order 1,5 < 1,4 < 2,6 of the naphthalene bonding position. In both cases the highest conjugation was observed for derivatives with 2,6 bonding positions of naphthalene, which ensured the planarity of the molecule.

The absorption and fluorescence maxima of thin films of derivatives with ethynylene building block H2TA14N, H2TA15N and H2TA26N show a bathochromic shift compared to the spectra in solution (Figure 47, top vs. bottom). This red shift of materials with ethynylene linkers indicates the formation of a different type of molecular aggregation (J-aggregates), while the thin films of the ethynylene-free derivatives exhibit hypsochromically shifted spectra (H-aggregates).

From a general point of view, the slip angle between two adjacent molecules **α** is important and substantial. It has been proposed that aggregates with α, which can be smaller than 54.7° and larger than 54.7°, correspond to J and H aggregates, respectively. Head-to-tail and parallel aggregates are formed when α = 0° and α = 90°, respectively [96]. The face-to-face arrangement of organic molecules is considered to be suitable for the transport of charge carriers since the degree of overlap of π-electrons in adjacent molecules should be larger for H-aggregates. From the viewpoint that overlapping of the frontier orbital should be larger in H-aggregates than in J-aggregates, it is probable that the transport of carriers in H-aggregates is superior to that in J-aggregates [97; 98; 99].

The charge carrier mobilities were analysed from the saturation regime of OFETs. The transfer characteristics are shown in Figure 48B. All investigated organic semiconductors H2T**A**xyN exhibited hole transport behaviour.

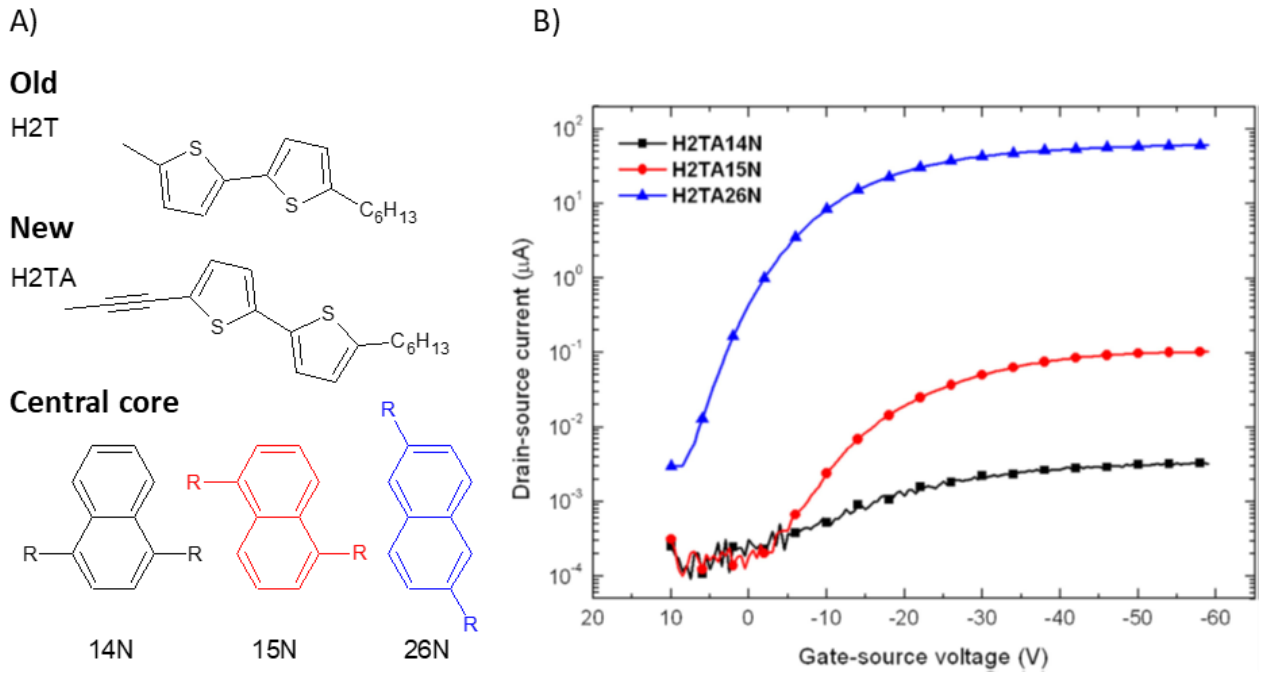

Figure 48 *A) Comparison of molecular structure and B) transfer characteristics of studied compounds H2TAxyN on the right. These characteristics were measured at a saturation regime with a drain-source voltage of -40 V [80].*

Table 15 summarised extracted device parameters of studied materials and data for previously published ethynylene-free analogue H2TxyN derivatives [79]. The hole mobility in all naphthalene derivatives with an ethynylene building block are two magnitudes lower than derivatives without an ethynylene building block (J-aggregates). The hole mobility of the newly synthesised derivatives decreases in the same order 2,6 > 1,5 > 1,4 of the bonding position of naphthalene as in the previously published materials.

Table 15 *Comparison of evaluated OFET parameters of H2T(A)xyN derivatives.*

	Compound	Conditions	Mobility μ (cm^2/Vs)	V_{th} (V)	$I_{on/off}$
In this study	**H2TA14N**	(i)	$1.8 \cdot 10^{-8}$	-6	10^1
	H2TA15N	(i)	$1.1 \cdot 10^{-6}$	-11	10^2
	H2TA26N	(i)	$5.5 \cdot 10^{-3}$	-6	10^5
	H2TA26N	(ii)	$2.2 \cdot 10^{-4}$	-1	10^3
In previous study	**H2T14N**	(ii)	$5.1 \cdot 10^{-6}$	-3	10^2
	H2T15N	(ii)	$1.6 \cdot 10^{-2}$	-23	10^5
	H2T26N	(ii)	$1.2 \cdot 10^{-1}$	-15	10^6

(i) OTS-treated SiO_2/Si; PFBT-treated Au electrodes; PVD by radiative heat; BG/BC with 90 nm SiO_2; (ii) HMDS-treated 40 nm SiO_2/Si; untreated top contact 40 nm Au electrodes [79].

The OFET with semiconducting material H2TA26N was also prepared by the same previously published methods. The one order of magnitude higher hole mobility of OFET preparation methods, as was described in chapter 6.1.1 (conditions "i" in Table 15) than in previously published fabrication procedure, was observed (conditions "ii").

Although conjugation of H2TA materials was changed in comparison to previous derivatives, the order of derivatives by the hole mobility in a field-effect transistor remains unaltered (i.e. H2TA14N < H2TA15N < H2TA26N). The tendency in hole mobility can be explained by different packing motifs affected by molecular symmetry and was revealed by single crystal X-ray analysis, 2D X-ray GIWAXS and AFM characterisation of the thin films in cooperation with colleagues from the Department of Organic Chemistry, Faculty of Natural Sciences, Comenius University in Bratislava.

The crystal structure analysis of the derivatives with ethynylene building blocks H2TA14N and H2TA26N revealed a herringbone packing motif. H2TA15N molecules are packed into slipped columnar structures evoking a brick-wall motif, but with a parallel orientation to the substrate. The derivative H2TA26N is the only one that exhibits a perpendicular orientation of the molecules with respect to the substrate

surface. This molecular orientation, together with the tightest intermolecular interactions and the best film-forming properties led to the highest hole mobility $\mu = 5.5 \cdot 10^{-3}$ cm^2/Vs of H2TA26N. However, the hole mobility of the derivatives H2TA26N with an ethynylene building block is two orders of magnitude lower than those previously determined for the ethynylene-free analogues H2T26N ($\mu_h = 1.2 \cdot 10^{-1}$ cm^2/Vs), which can be attributed to the formation of J-aggregates.

The complete results were published in the journal *Synthetic Metals*. The paper is enclosed. The overview and contribution of the author is also described [S5].

6.2 ORGANIC ELECTRO-CHEMICAL TRANSISTORS

The OECT chapter focuses on the characterisation of selected OS with respect to their application in bioelectronics devices, in particular, biocompatibility, stability and the electrical conductivity of the organic semiconductors were studied. Subsequently, the OECT devices were optimised for the detection of the physiological response of living cells.

6.2.1 Biocompatibility of reference materials

This study aims to determine and verify the biocompatibility of reference organic semiconductors and to identify aspects that may improve their compatibility with living cells. The four reference organic semiconductors depicted in Figure 21 were used. These four materials represent two the small-molecular organic semiconductors TIPS-pentacene and DPP(TBFu)$_2$ and the two semiconducting polymers P3HT and PEDOT:PSS.

In the context of OS working with living cells, the biocompatibility is defined in terms of the absence of cytotoxicity and the ability to provide support for cell adhesion and spreading. These aspects are usually determined by the release of potentially cytotoxic compounds as well as by wettability and the presence of specific surface functional groups or molecular structural motives [100].

First, the wetting angles of TIPS-pentacene, DPP(TBFu)$_2$, P3HT, and PEDOT:PSS in physiological medium are shown in Figure 49.

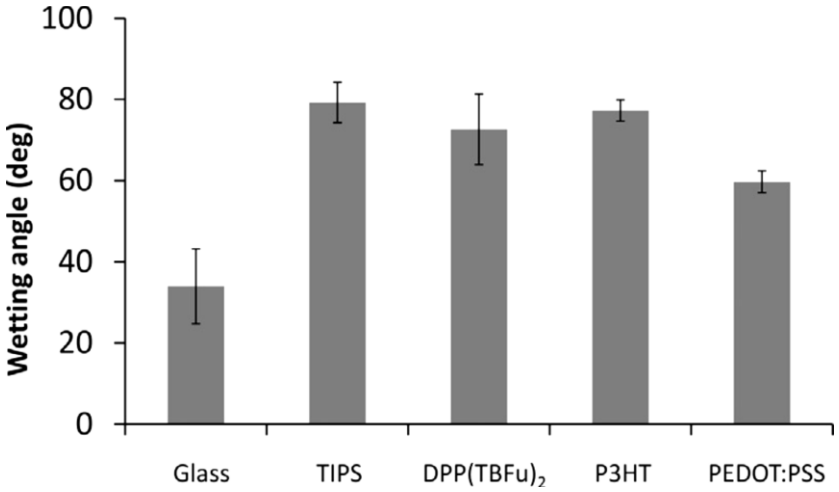

Figure 49 *Wetting angles of reference materials [101].*

The wettability can play a significant role in a material's biocompatibility. TIPS-pentacene, DPP(TBFu)$_2$ and P3HT were rather hydrophobic, as demonstrated by the measured contact angles of between 70 and 80°. Such levels of wettability could be limiting for some cell lines. In contrast, the contact angle of PEDOT:PSS layer was about 60°. The wetting angle of around 60° for these materials should be suitable for culturing a wide range of cells [100].

The application of organic semiconductors in a bioelectronic device requires that the material possess good stability in the aqueous physiological environment, which has a pH of 7.4 and the relevant concentration of salts. An assay of stability in phosphate-buffered saline (PBS) solution was carried out by means of determining the release of UV-VIS absorbing matter, as all tested materials show intense absorption in the UV-VIS spectrum. TIPS-pentacene, DPP(TBFu)$_2$ and P3HT were stable, whereas PEDOT:PSS showed the minor release of compounds.

The determination of the biological compatibility of reference organic semiconductors was performed in cooperation with the Institute of Biophysics of the ASCR. The biocompatibility tests were performed with murine 3T3 fibroblasts cells. These cells require contact with a substrate and are commonly used in biocompatibility testing. 3T3 fibroblasts were grown on standard culture plastic, glass, TIPS-pentacene, DPP(TBFu)$_2$, P3HT and PEDOT:PSS deposited on glass slides. The cells grown on culture plastic and glass were used as standard. The biocompatibility of 3T3 fibroblasts is tested on the correct morphology and sustained viability of cells. Images of cells on reference semiconducting materials are shown in Figure 50.

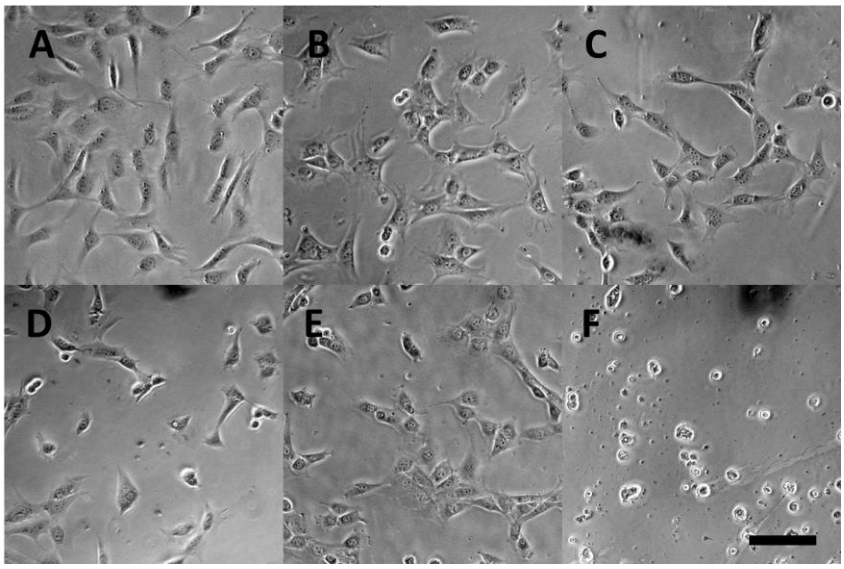

Figure 50 *The coverage with 3T3 fibroblast on (A) Standard culture plastic, (B) Glass, (C) TIPS-pentacene, (D) DPP(TBFu)$_2$, (E) P3HT, (F) PEDOT:PSS. Bar represents 50 μm [101].*

TIPS-pentacene, DPP(TBFu)$_2$ and P3HT exhibited lower coverage by cells and some non-adherent cells (round shape of cells) when compared to the shape and viability of 3T3 fibroblasts on the standard culture plastics and glass as can be seen in Figure 50. Attached cells showed slight morphological disturbances compared to standard culture plastics. This indicates that these materials caused minor stress to cells. Strikingly, the coverage of PEDOT:PSS by cells was very low. The ATP and MTT cell viability tests were also performed to obtain measurable values of biocompatibility. Both tests provided similar data and revealed no interference with the tested materials as can be seen from Figure 51.

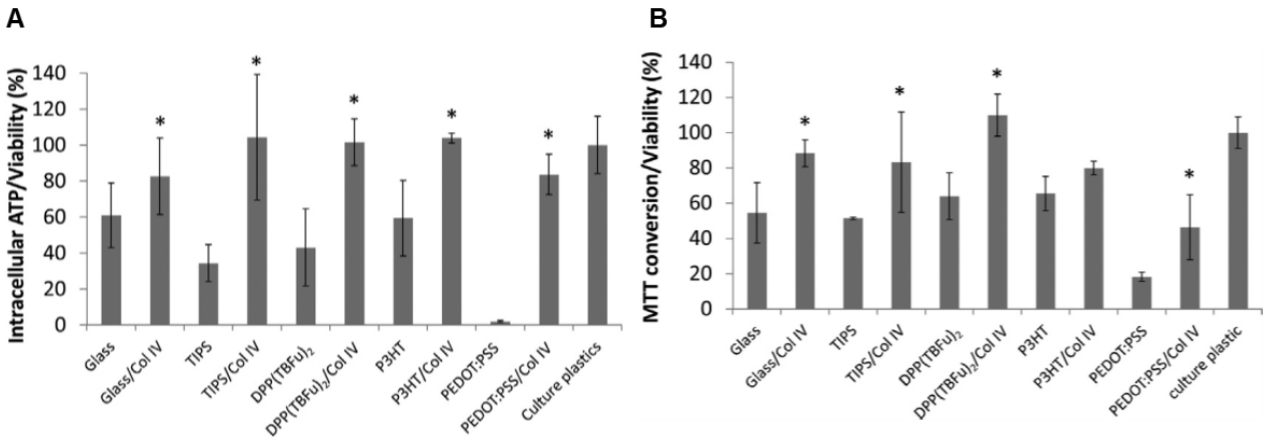

Figure 51 *The ATP (A) and MTT (B) tests on the viability of 3T3 fibroblast before and after collagen IV coating [101].*

In order to increase the biocompatibility of the materials, surface coating by the self-assembled layer of collagen IV was applied. To further support the benefits of using collagen IV, 3T3 fibroblasts with and without a collagen IV coating were grown on each material. Viability assays indicated that collagen IV significantly increased biocompatibility towards 3T3 fibroblasts. The wetting angle of all tested organic semiconductors coated with collagen IV was about 60° in a dry state; such a value is suitable for animal cells. Compared to cells grown on standard cell culture plastics and the viabilities of cells grown on the glass on Figure 51, TIPS-pentacene, $DPP(TBFu)_2$ and P3HT were lower but similar among themselves with collagen coating. The viability of cells grown on PEDOT:PSS was considerably lower than the viabilities of cells grown on glass and the other organic semiconductors without collagen coating.

The reference organic semiconductors were tested to determine and verify biocompatibility. Since the tested organic semiconductors were mostly stable, the possible explanation for the lower compatibilities of these materials lay in their surface properties. The biocompatibility of a surface towards adherent cells is largely dependent on wettability. The hydrophobic or extremely hydrophilic surfaces usually do not support cell adhesion. The other factor is the quantity and quality of surface functional groups or structural motives. The lower biocompatibility of TIPS-pentacene, $DPP(TBFu)_2$ and P3HT found in this study can be attributed to the rather hydrophobic character of their surfaces (a wetting angle of 70–80°) and a lack of cell adhesion promoting functional groups or structural motives. The unexpected drop in biocompatibility of the more hydrophilic semiconductor PEDOT:PSS compared to standard cell culture plastics (a wetting angle of about 60°) can be linked to the presence of sulfonate groups that restrict contact with cells. The limited biocompatibility of moderately hydrophilic PEDOT:PSS towards 3T3 fibroblasts was probably caused by the presence of cell adhesion-restricting sulfonate groups of PSS moiety. The work emphasised the need to manipulate surface wettability and to introduce cell adhesion promoting functional groups or structural motives. The

collagen IV coating improved the biocompatibility of all tested organic semiconductors to the level of standard cell culture plastics.

The complete results were published in *Sensors and Actuators B: Chemical*. The paper is enclosed. The overview and contribution of the author is also described [S6].

6.2.2 PEDOT:PSS The study of biocompatibility, stability and electrical properties

The poly(3,4-ethylenedioxythiophene): poly(styrene sulfonate) (PEDOT:PSS) has already been successfully used in a spontaneously beating cardiomyocytes sensor [64; 65]. However, the previously discussed data in chapter 6.2.1 showed limited biocompatibility of PEDOT:PSS. Therefore, the aim of this study was to establish suitable procedure for preparation of thin active layers, and to characterise the electrical properties and stability of several PEDOT:PSS inks.

Six electroactive polymer inks based on PEDOT:PSS shown in Table 11 were studied. The stability and electrical properties of such films were characterised on organic electrochemical transistor (OECT)-based sensor platforms purchased from Ossila Ltd. Their biocompatibility was evaluated in assays with 3T3 fibroblasts and murine cardiomyocytes in cooperation with the Institute of Biophysics of the Czech Academy of Science.

Conductivity

The resistance of PEDOT:PSS layers can be seen in Figure 52.

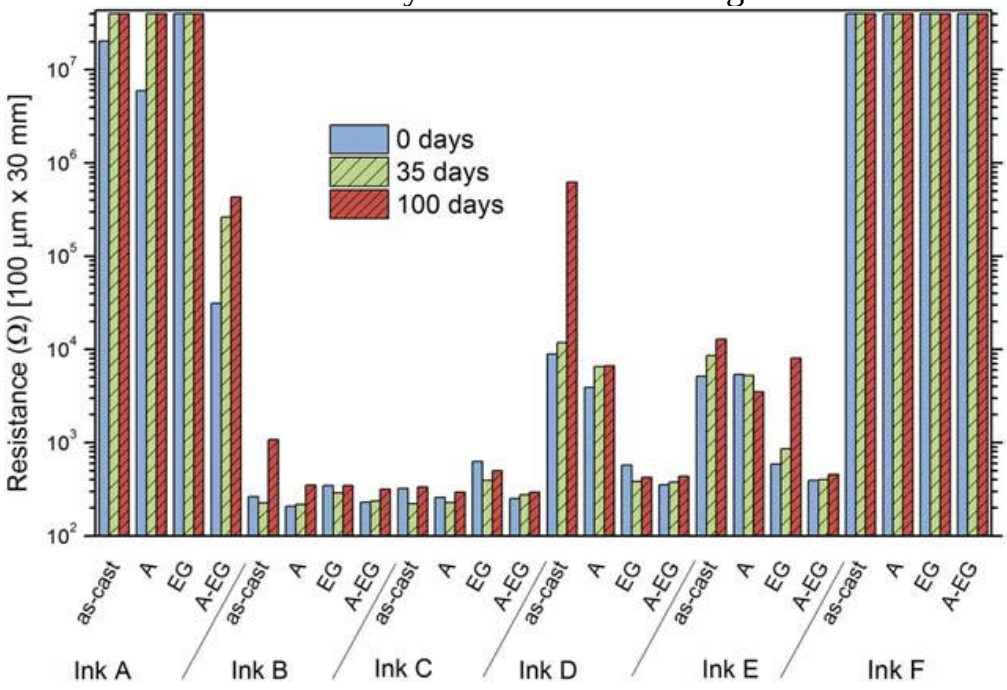

Figure 52 *Resistance of PEDOT:PSS layers with different coatings. "As-cast" is fresh film dried at room temperature, while "A" is thermal annealing and "EG" is ethylene glycol annealing [102].*

Figure 52 shows the measured resistance of the thin films prepared from the studied inks immediately after thin film preparation, after 35 and 100 days of storage in the dark at room temperature. The resistance was measured for (i) spincoated films only (as-cast), (ii) thermally annealed films (A), (iii) ethylene glycol treated films (EG), and (iv) both thermal annealed and ethylene glycol-treated films (A–EG).

The conductivity of PEDOT:PSS is primarily dependent on the ratio of the two components. The higher the PSS content, the lower the conductivity. This can also be seen from our results shown in Figure 52, where higher resistances by several orders of magnitude were measured for Ink A and Ink F than for the rest of the formulations in the test. While the PEDOT:PSS ratio used in Ink A is not known (the supplier does not provide it), Ink F can be directly compared to Inks D and E with significantly lower PSS concentration (2.6% vs. 0.8%) and thus with higher conductivity.

The other factors that influence the PEDOT:PSS films' conductivity are mainly related to the polymer chains' conformation, which is affected by the preparation method and conditions during the film formation [103].

The influence of immersing the films into ethylene glycol can be seen from the results obtained for Ink D and the reference Ink E. In both cases the ethylene glycol treatment led to a substantial reduction of the initial films' electrical resistance. On the other hand, Ink C that already contained ethylene glycol shows neither reduction nor increase of the electrical resistance. Ink B for which the supplier does not provide the exact composition showed similar results, suggesting that ethylene glycol or another additive is already included in the ink formulation. The resulting electrical resistances for as-cast films of Ink B and Ink C, which have ethylene glycol added already in the solution, are comparable to the resistances of Ink D and Ink E after the annealing and ethylene glycol treatment.

It can be concluded that it does not matter how the ethylene glycol is applied either directly in the ink or after the preparation of the thin layer. It can also be concluded that the additional treatment (neither annealing nor ethylene glycol) does not help in further reduction of electrical resistance once the ethylene glycol is included in the ink formulation. The thin films prepared from inks without any additive will not provide sufficient performance (electrical conductivity) and stability for use in bioelectronics applications. This can be solved by the treatment that offers thin films with sufficiently low electrical resistance and its stability over time.

Stability of thin films in water

Electrical stability and performance in dry conditions are necessary prerequisites for bioelectrical sensors, but stability in a cell cultivation medium is even more important. PEDOT:PSS thin films immersed in water can swell quickly and be partially dissolved because they are water-based. As a result, such a layer undergoes changes to its mechanical and electrical properties and a PEDOT:PSS-based sensor can release compounds that are not naturally occurring in living tissues or culture

media. Therefore, a simple method to determine PEDOT:PSS thin film dissolution by UV-VIS spectrophotometry was adopted.

The inks with higher electrical resistance are not suitable for bioelectronic applications (e.g., OECT) and were not further analysed (Inks A and F). The prepared thin films were immersed in deionized water and absorption was measured as a function of time. The measured absorption at 226 nm was compared against the calibration curve and a relative percentage of the dissolved material was evaluated (Figure 53).

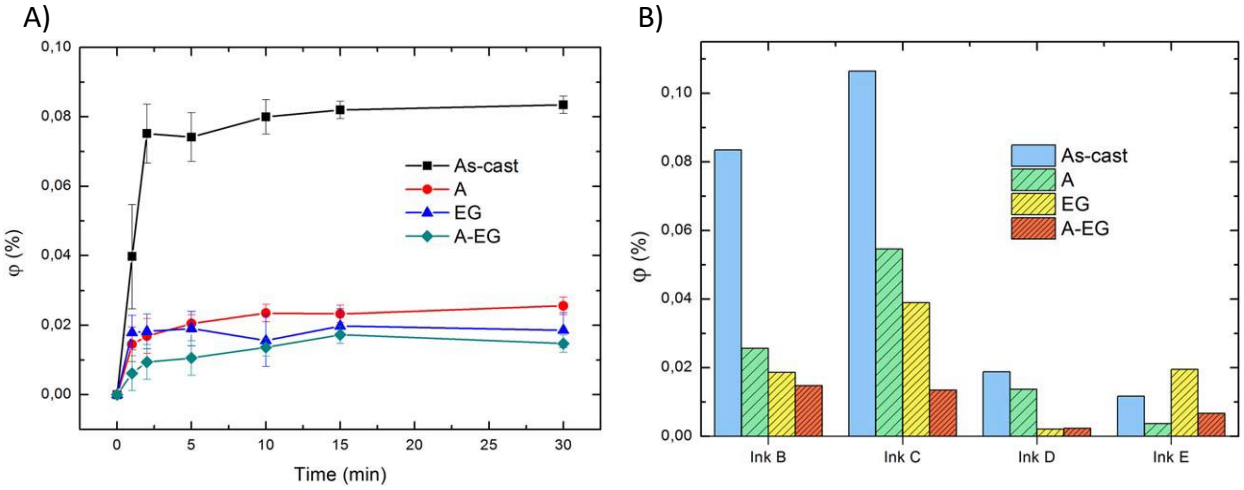

Figure 53 *A) Dissolved PEDOT:PSS of Ink B over time and B) fraction of leached material after 30 min exposure to water from thin films prepared by different methods [102].*

The typical observed response of PEDOT:PSS thin film leakages to water and its evolution over time is shown in Figure 53A. The main increase of the released films occurs within the first few minutes. After this rapid change, the films slowly stabilised. It is also apparent that films which were thermally annealed (A and A–AG) show slower initial leaching.

The summarised data of the influence of the treatments on Inks B–E is shown in Figure 53B. The figure shows the amount of released material after 30 min of exposure to water. As can be seen, any annealing has always been beneficial for the stability of tested thin film in water. Ethylene glycol treatment also improved films' stability for Ink B, C, and D, but an increase of the released material was observed for Ink E. The combination of the two treatments had a further positive influence in Ink B and Ink C. The subsequent treatment of the thin films by each of the methods used here or by a combination of them brings improved film stability against water and potential cultivation media.

Long-term stability

The duration of contact of the sensor with the biological material is highly variable depending on the specific application. In the case of animal cells, it can cover a period of up to several days. Conductive PEDOT:PSS films were tested for their stability for

300 hours. Prior to the resistance measurement after the 300-hour test, the samples were dried with dry air. The obtained data are displayed in Figure 54.

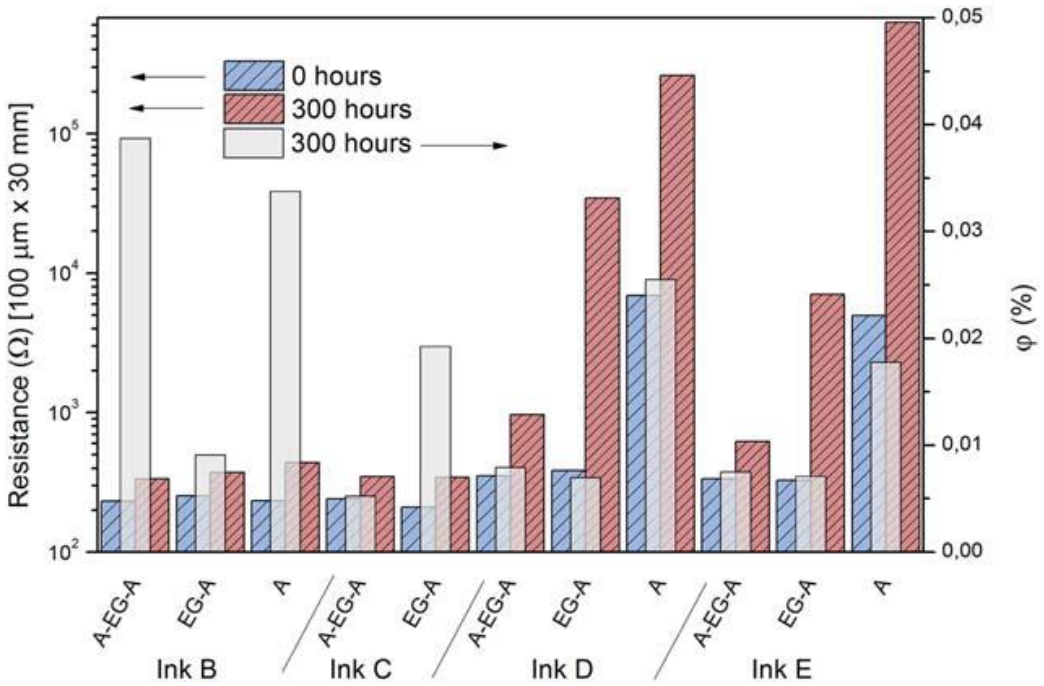

Figure 54 *Electrical resistance (left axis) and material leaching from the films (right axis) prepared by different methods after 300 h exposed to deionized water [102].*

Films without any post-treatment and films treated with ethylene glycol showed limited stability as they were completely released from the substrate after 300 h. As can be deduced from Figure 54, thermal annealing is always necessary to obtain films stable for several days. However, thermal annealing alone is not always sufficient for stability of layers. A combination of thermal annealing after the ethylene glycol treatment was in all cases beneficial and improved the films' electrical resistance and stability. The best results were obtained for Ink C and a combination of annealing–ethylene glycol–annealing.

In summary, it has been observed that a small proportion of the PEDOT:PSS layer can be released into the aqueous environment. The released compounds may potentially be toxic to living cells. Such leaching reaches a plateau within a few minutes.

Biocompatibility studies

The post-processing procedure based on EG and annealing treatment, which results in the lowest degree of leaching and an electrical resistivity well stable over time regardless of whether in a dry or wet state was used to prepare PEDOT:PSS films on OECT sensor platforms for biocompatibility assays. The water-soluble components of PEDOT:PSS layers were washed out during the sterilisation and subsequent washing steps and their release into the culture medium during the biocompatibility assay was negligible.

Organic semiconductors are generally regarded as biocompatible, but in the previous chapter 6.2.1. the biocompatibility of reference materials was observed to be limited. The coatings with collagen IV remarkably increased the ability of PEDOT:PSS to host animal cells. Thus, to maximise the biocompatibility of PEDOT:PSS ink-based thin films on OECT sensor platforms, coating by collagen IV was carried out as well. Figure 55 shows the correct shape and viability of 3T3 fibroblasts cells cultured on the prepared thin films of PEDOT:PSS inks as well as on a reference culture dish and glass.

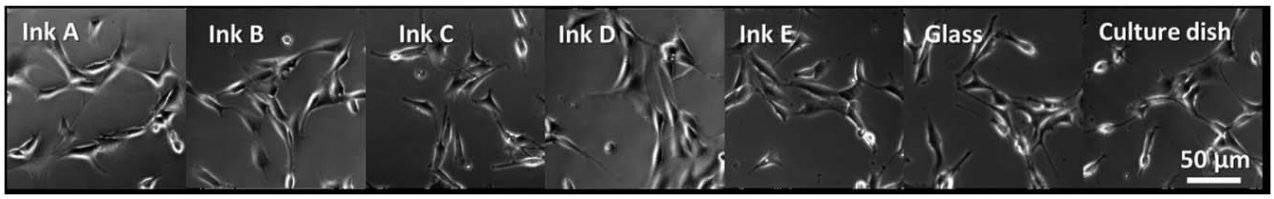

Figure 55 *Biocompatibility assay of PEDOT:PSS inks: PEDOT formulation spincoated on OECT substrates were treated with collagen IV [102].*

These films coated with collagen IV showed good biocompatibility in the assay with 3T3 fibroblasts when compared to standard cell culture plastics. Selected films (Inks B–E) were then used in assays with murine cardiomyocytes. We observed that these cells were able to attach to the PEDOT:PSS films and form an active sensor element. Spontaneously beating syncytia were formed, indicating a good physiological status for the cardiomyocyte cells.

Summary

It could be concluded that the thin films prepared from PEDOT:PSS inks without an additive (ethylene glycol in this work) will not provide sufficient conductivity and stability for use in biomedical applications as exemplified by the OECT-based bioelectrical sensor platform tested in this work. The observed high resistance for as-cast films was successfully reduced by the treatment proposed in this work: additional exposure to ethylene glycol in combination with thermal annealing provided thin films with electrical resistance and its stability in aqueous media comparable to the inks with additives. However, the long-term test of thin films exposed to water revealed that addition of ethylene glycol to ink rather than subsequent treatment of the films is favourable. While the initial resistances are comparable, long-term exposure to water (12.5 days) is much less harmful to the films prepared from inks with ethylene glycol included directly in ink.

Furthermore, the resistance toward water is mostly poor for as-cast films. We observed leaching of the PEDOT:PSS into the water above the films for all of the studied PEDOT:PSS ink formulations. After an initial release, the films are stabilised within a few minutes. The films' stability was greatly improved using treatment with ethylene glycol and annealing. Both procedures can decrease the leaching and improve the films' electrical properties and resistance against water, but the actual

influence differs for the ink formulations. Generally, in order to obtain stable films, mainly thermal annealing is necessary. After 12.5 days, non-annealed films were completely released from the surface. The best electrical stability was achieved using a combination of thermal annealing followed by ethylene glycol treatment and again thermal annealing. These results open the door to construction of cheap printed electronic devices for bio-interfacing in biomedical applications such as sensors of beating cardiomyocytes.

The complete results were published in *Journal of Biomedical Materials Research Part A*. The paper is enclosed. The overview and contribution of the author is also described [S7].

6.2.3 The printed prototype of OECT arrays for real-time cell culture monitoring

The aim of this study was to prepare a prototype of OECT arrays, test its performance, biocompatibility and try to measure biological response of living cells to an external stimulus.

A microplate with a multielectrode array of 96 organic electrochemical transistors (OECTs) based on the polymer poly(3,4-ethylenedioxythio-phene):poly(styrene sulfonic acid) PEDOT:PSS (ink G in Table 12) was developed and fabricated by the screen-printing method. It consists of a microplate of a 12 × 8 chimney–well array with transistors on the bottom. The OECT is circular with a channel of 1.5 mm^2 in the centre surrounded by the circular gate electrode. The fabrication of screen-printed OECTs was provided by Ing. Lukáš Omasta, Ing. Michal Hrabal and Ing. Jiří Ehlich. A detail of the OECT device with a living 3T3 fibroblast can be seen in Figure 56 A.

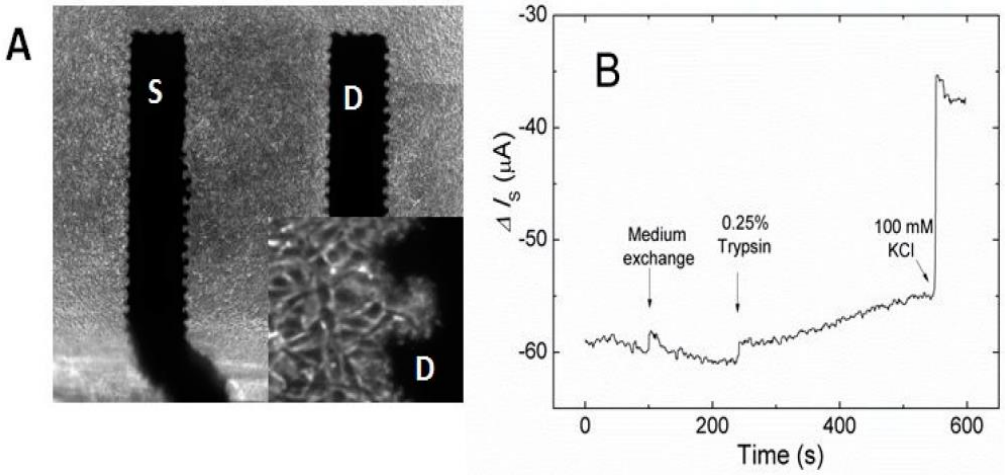

Figure 56 *A) The detail of screen printed OECT transistor (inset of 3T3 fibroblast) and B) OECT sensor response of environmental changes [104].*

The average transconductance g = 1.4 mS was achieved in the wide range of gate voltages V_{GS} = ±0.4 V when the drain potential V_{DS} = −0.735 V was set. The time constant 0.15 s limited by the channel-electrolyte charge electrical double layer

capacitance was achieved. The device was tested with a 3T3 fibroblast cell culture. The current response of OECT transistor was recorded for exchange of cultivation medium, adding trypsin and KCl solution to medium (Figure 56B). The response of living cells can be observed on the channel of the OECT during electrical stimulation by gate voltage, as well as during the source current response on the inset of the left side of Figure 56A. The added solution of enzyme trypsin cleaved the collagen of 3T3 fibroblasts and the attached cells were released from the OECT sensor to the cultivation medium. The added solution of KCl caused depolarisation of the cell membrane and the death of the cells. With the help of the printed OECT prototype, it was possible to measure these two procedures

The biocompatibility of the OECT transistor prototype with a 3T3 fibroblast was demonstrated. The device showed high biocompatibility and a good response to the trypsin-mediated detachment of cells. This printed prototype OECT array is a good starting point for the efficient monitoring of cells in biological applications, such as a sensor of beating cardiomyocytes.

The complete results were published in the journal *Applied Sciences*. The paper is enclosed. The overview and contribution of the author is also described in [S8].

6.2.4 Gold printed electrodes for OECT sensors of beating cardiomyocytes

The goal of this study was to prepare optimised large-scale printed OECT sensors with high performance, stability and biocompatibility for sensing of beating cardiomyocytes. One of the ways for increasing the performance of OECT transistors rests in decreasing the serial resistance of the supply electrodes. Only a few low-resistance inorganic materials for conductive electrodes are biocompatible. Among them, the gold electrode is very popular, but it has the drawback of predominant fabrication by the lithography process. Gold resin ink was used for the construction of high-resolution interdigital electrodes.

The structures of OECT transistors are designed as an array of 10 transistors with one common source electrode and one gate electrode with the size of the sensing area being 1 mm^2. The OECT transistors were designed with an increasing channel length of interdigital electrodes from 50 to 170 μm. A picture of the OECT sensors is shown in Figure 57.

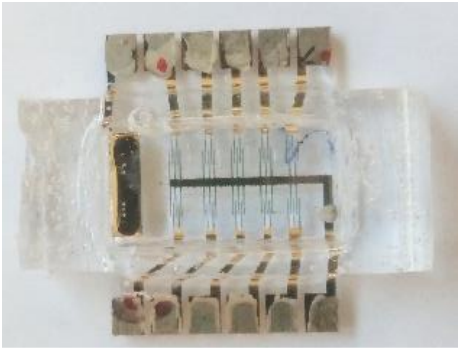

Figure 57 *The picture of OECT sensor with printed gold electrodes.*

The OECT transistors were measured in a phosphate buffer in the steady-state mode. The steady-state characteristics can be seen in Figure 58.

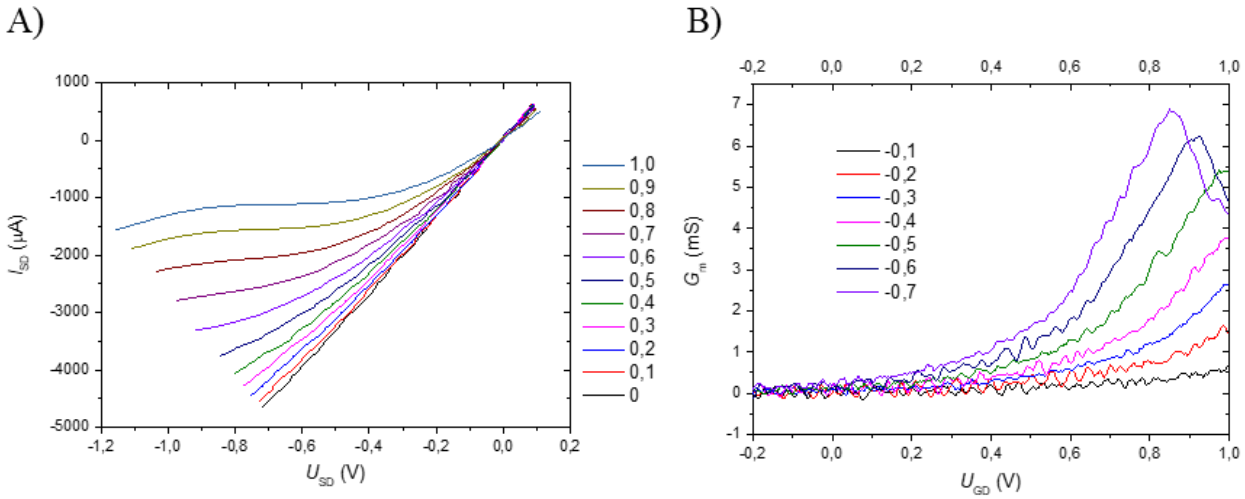

Figure 58 *A) Output characteristics and B) transconductance of the OECT sensor.*

Transconductance up to 7 mS was achieved. The maximum of transconductance is shifted almost to 0.8 volt for a higher *Wd*/*L* ratio of the interdigital electrode as is shown in Figure 58B [61]. The higher the *Wd*/*L* ratio, the higher the transconductance can be expected [68; 105]. The obtained data are summarised in Table 16.

Table 16 *Achieved transconductance of OECTs; W is channel width, L is channel length, d is PEDOT:PSS thickness, g_m is transconductance.*

W **(mm)**	***L*** **(µm)**	***Wd*/*L*** **(µm)**	**Maximum of g_m (mS)**
6	50	24.0	7
4	80	10.0	6
4	110	7.3	5
4	140	5.7	4
4	170	4.7	3.5

The *Wd*/*L* ratio of up to 24 µm of prepared OECTs is similar to the lithography-prepared OECT with published 24 millisiemens of transconductance [105]. The measured transconductance (purple triangle dots in the ring) were plotted in Figure 59 over the transconductance of lithography-prepared OECT (black square dots), peak transconductance (red round dots) published by Donahue [105] and printed OECTs (blue pyramid dots).

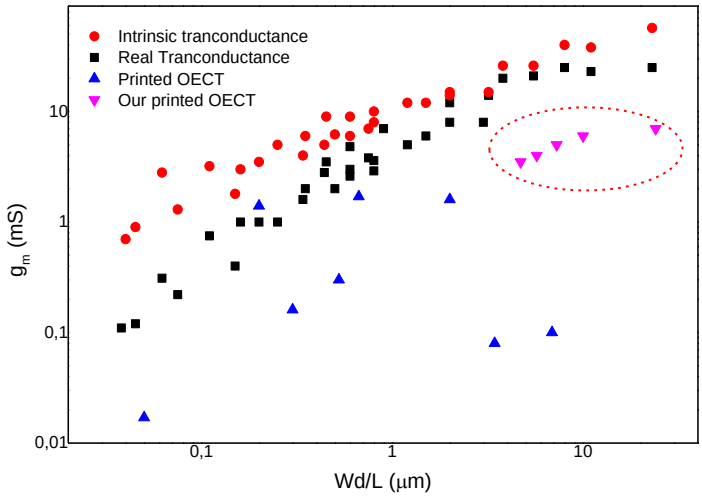

Figure 59 *OECT transconductance values overlaid on previously published OECT data [105].*

The transconductances of printed OECT sensors are lower in comparison to lithography-prepared OECTs. However, the external gate electrodes immersed in the solution have been used in the published literature in comparison to our designed OECTs with one gate electrode printed in the same plane as the source and drain electrode, which is a big advantage for fabrication of large amount number of screening sensors. Although the transconductance of the printed OECT devices is lower than for lithography-prepared OECTs, the obtained OECT parameters in this study should be sufficient for the measurement of beating cardiomyocytes [64].

The time constant of the prepared OECT sensors was also determined. The time constant determines the speed of the sensor response to the external signal. The measured transient response of printed OECT transistors as voltage drops (peak to peak 20 mV) on the gate electrode is depicted in Figure 60.

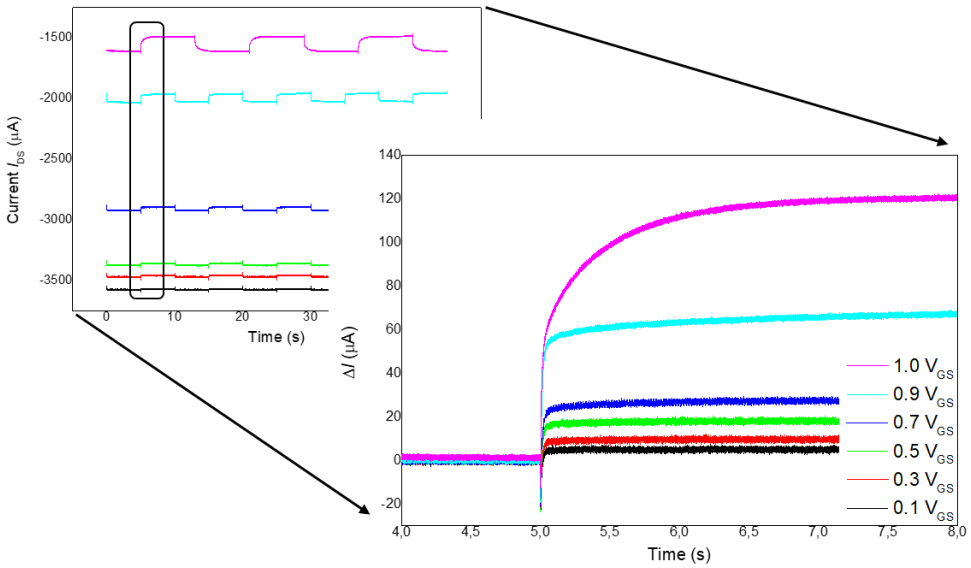

Figure 60 *Transient characteristic of OECT transistors at V_{DS} = 0.6 volts and different V_{GS} with pulsing 20 mV peak to peak.*

As can be deduced from Figure 60, the change of the time constant depends on the applied gate voltage, which is inconsistent to the theory of transient behaviour in the OECT depletion mode [60]. The transient characteristics for a wide range of V_{DS} and V_G voltages were measured and the transconductance and the frequency (inverted time constant) as a 3D plot was plotted in Figure 61.

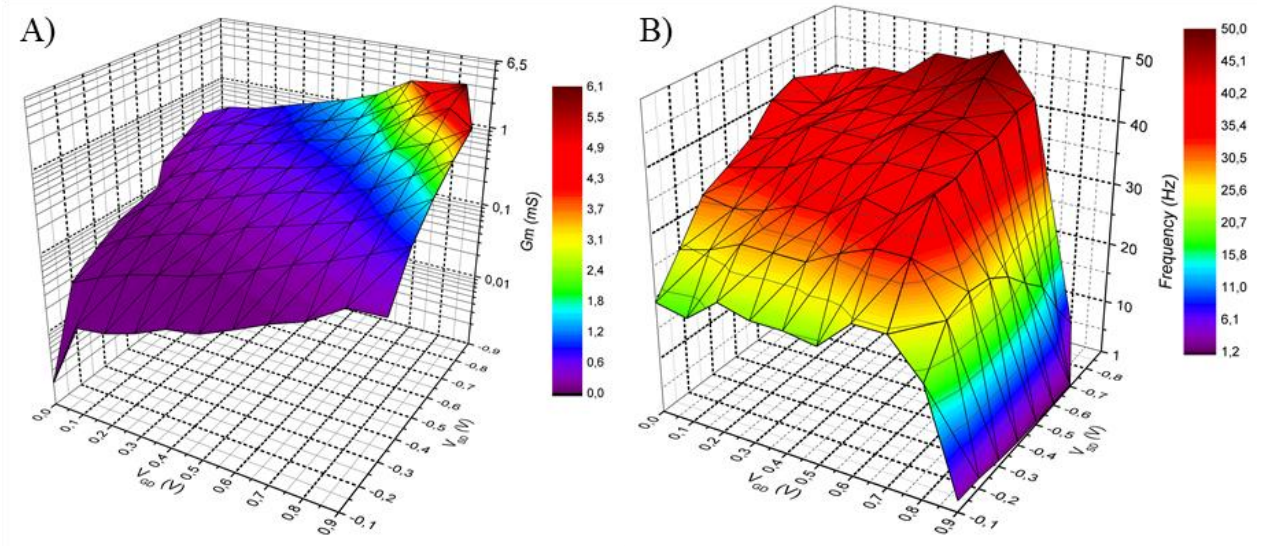

Figure 61 *A) Scan of the transconductance and B) frequency (inverted time constant, 1/e and 1-1/e) for a set of voltages obtained from the transient characteristics.*

As can be seen from Figure 61A, the transconductance linearly increases with the applied voltages and the maximum of transconductance can be observed at V_{DS} = -0.8 volts and V_{GS} = 0.8 volts. The maximum frequency (the lowest time constant) was measured at V_{GS} = 0.6 volts and the decreasing frequency (increasing the time constant) above this voltage was observed. The time constant of the OECT sensor decreases at high gate voltages 0.9 volts (Figure 61B), yet it does not have big impact on measured transconductance.

The biocompatibility test of printed OECT sensors was performed in cooperation with the Institute of Biophysics of the Czech Academy of Sciences. The cardiomyocytes were cultivated on printed OECTs and lived for two weeks. The cardiomyocytes syncytia can be seen in Figure 62, which lay on interdigital electrodes.

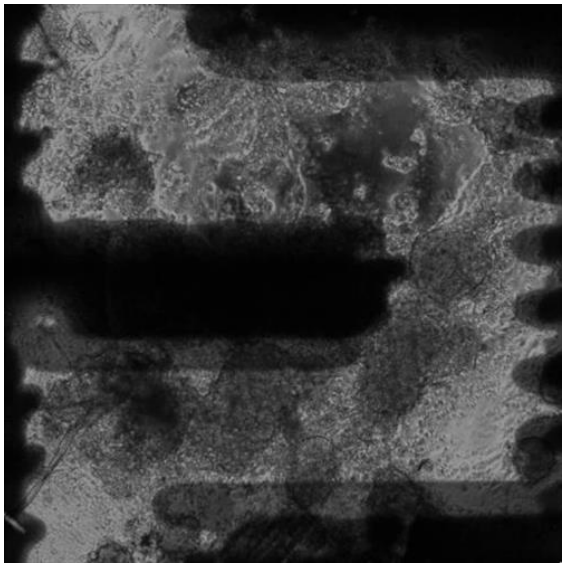

Figure 62 *Image of cardiomyocytes syncytia lying on the printed interdigital electrodes of OECT sensor.*

Summary

Gold printed electrodes were used to construct high-performance OECT devices. An OECT sensor with a channel length of up to 50 μm of printed interdigital electrodes, 7 mS of transconductance and a time constant down to 20 milliseconds was achieved. The OECT sensor prepared in this study should be sufficient for measurement of beating cardiomyocytes. The fabrication process is straightforward and compatible with the methodology for the preparation of sensitive organic semiconducting devices. It allows exceptional control over the transistor channel length, width and easy modification of the printed pattern. This novel approach is also suitable for large-scale, fast and easily prototyped devices, such as sensors, OFETs, OLEDs, organic solar cells and many other applications.

7 CONCLUSIONS

This thesis was focused on the study of the novel organic semiconductors with respect to their possible applications in organic field-effect transistors (OFETs) and organic electrochemical transistors (OECTs). The main goal of this thesis was to elucidate the relationship between the chemical structure of organic semiconductors and their properties. The second aim of this thesis was to bring new knowledge which enable and enhance the utilization of novel organic semiconductors in bioelectronics applications. The main results of this thesis can be highlighted as follows:

- The Probe station for electrical characterisation of OFETs and determination of charge carrier mobility of novel organic semiconducting materials was build-up. Several methods used for thin-film preparation and characterisation of OFETs were developed and optimised.

- All novel studied materials showed hole transport. Higher hole mobility was observed for materials with a symmetric, planar and rigid molecular structure.

- It was found that thin layers of N, N ethyladamantyl thiophene DPP derivative prepared by vacuum deposition show five orders of magnitude higher hole mobility than the spin-coated layer. For the first time electron mobility of thiophene DPP derivative was observed.

- The biocompatibility of two reference small-molecular organic semiconductors TIPS-pentacene and DPP(TBFu)$_2$, and two semiconducting polymers P3HT and PEDOT:PSS was characterised. Limited biocompatibility of reference organic semiconductors was observed. The possibility of enhancement of the biocompatibility of studied materials by collagen IV coatings was demonstrated.

- The six electroactive polymer inks based on PEDOT:PSS suitable for construction of OECT was characterized with respect to their electrical properties, stability and biocompatibility. PEDOT:PSS inks without additive do not provide sufficient conductivity and stability for use in bioelectrical applications. The best conductivity and stability of PEDOT:PSS films was achieved using a combination of thermal annealing followed by ethylene glycol treatment and subsequent thermal annealing.

- The performance of prepared printed OECTs arrays were successfully proved by determination of response of living 3T3 fibroblasts.

- OECT sensors with gold printed electrodes were constructed. A transconductance up to 7 mS and a time constant of 20 milliseconds were achieved, which is sufficient for the sensing of beating cardiomyocytes. The

fabrication process is straightforward and compatible with the methods for the preparation of sensitive organic semiconducting devices. It allows to modify the transistor channel length, width and easy modification of the printed pattern. This approach is also suitable for preparation of large-scale, fast and easily prototyped devices, such as sensors, OFETs, OLEDs, OPVs and other applications.

8 OVERVIEW AND CONTRIBUTION OF PAPERS

[S1] Solution processable diketopyrrolopyrrole semiconductor: towards bio-electronic applications

Stanislav Stříteský, Martin Vala, Jan David, Eva Šafaříková, Jan Víteček, Martin Weiter

In this paper, the possibility to use diketopyrrolopyrrole (DPP) for the construction of electrical devices designed to interact with animal cells was studied. For this purpose, the biocompatibility and electrical properties of the selected DPP derivative (3,6-bis(5-(benzofuran-2-yl)thiophen-2-yl)-2,5-bis(2-ethyl-hexyl)pyrrolo[3,4-c]pyrrole-1,4-dione) [referred as DPP$(TBFu)_2$] were researched. The electrical properties were studied using model organic field-effect transistors. Mainly investigated was under what conditions maximum charge carrier mobility can be achieved. Using the cumulative effect of self-assembled monolayers on dielectrics and electrodes and detailed thermal analysis of the DPP, a higher charge carrier mobility was achieved than has been previously reported (5.5×10^{-3} $cm^2V^{-1}s^{-1}$). The biocompatibility was studied based on a culture of 3T3 fibroblasts. This research revealed that DPP$(TBFu)_2$ can be used in applications involving direct contact with living animal cells. The conclusions found with these model devices can be applied to components suitable for biosensing applications, e.g., water- or electrolyte-gated organic field-effect transistors.

Contributions: This paper is the authors' research. The author prepared and set all research experiments. The author prepared all samples, built up probe station, performed electrical measurements and data analysis of all measurements. The author cooperates on biocompatibility test with institute of biophysics ASCR. Author co-wrote the introduction, experimental, results and discussion chapters of the paper.

[S2] Thiophene-free diphenyl-amino-stilbene-diketo-pyrrolo-pyrrole derivatives as donors for organic bulk heterojunction solar cells

Jana Honová, Stanislav Luňák, Martin Vala, **Stanislav Stříteský,** Ladislav Fekete, Martin Weiter, Alexander Kovalenko

An extended study on a group of four soluble diphenyl-amino-stilbene based diphenyl-diketopyrrolo-pyrrole molecules has been carried out. Using the materials in thin-film transistors it was shown that the above-mentioned compounds can be successfully used as donors in organic photovoltaic devices. Influence of the molecular symmetry and solubilizing chain on the morphology and solar cell performance are described. It was shown that a shorter and non-branched ethyl acetate chain leads to higher charge carrier mobility, short circuit current, and better fill factor. After the basic optimization, a power

conversion efficiency of about 1.5 % was reached. This, to the best of our knowledge, is the highest reported efficiency of thiophene-free small-molecule diketo-pyrrolopyrroles.

Contributions: The author participated in the design of experiments and the preparation of samples of organic solar cells. The author prepared samples of OFETs, thin layers for optical measurements and AFM measurements. The author performed electrical characterisation of OFETs, optical measurements of thin layers and solutions. The author contributed to the introduction, experimental and results and discussion chapters of paper.

[S3] The influence of diketopyrrolopyrrole chemical structure on organic field-effect transistors performance

Stanislav Stříteský, Jozef Krajčovič, Martin Vala and Martin Weiter

Organic semiconductors are suitable for application in biosensors and sensors based on transistors. The influence of position solubilisation group on diketopyrrolopyrrole core bonded throught oxygen (O) or nitrogen (N) on the performance of diketopyrrolopyrrole-based organic field-effect transistors (OFETs) is studied. The lowest mobility $1 \cdot 10^{-9}$ cm^2/Vs was observed for nonsymmetric substitution *O*,*N* of "EthylAdamantyl" solubilization group. Measurable charge carrier mobility was observed due to reduction of the density of charge trapping states after application of organosilane self-assembled monolayers (SAMs) on thinner gate-dielectrics (90 nm). We report similar drift mobility $1 \cdot 10^{-7}$ cm^2/Vs for smallest solubilization group "butyl" as for the biggest group "EthylAdamantyl" in *N*,*N* and *O*,*O* substitution prepared by spin-coating.

Contributions: This paper is the authors' research. Author designed experiments, prepare samples, conduced measurements, and co-wrote the paper.

[S4] Adamantane substitutions: a path to high-performing, soluble, versatile and sustainable organic semiconducting materials

Alexander Kovalenko, Cigdem Yumusak, Patricie Heinrichova, **Stanislav Stritesky**, Ladislav Fekete, Martin Vala, Martin Weiter, Niyazi Serdar Sariciftci and Jozef Krajcovic

Novel ethyladamantyl solubilization side groups were found to induce p–p interactions between the conjugated cores through adamantyl–adamantyl stacking in soluble diketopyrrolopyrrole (DPP) derivatives. The closeness of the DPP cores amplifies charge transfer in the material, as far as the p–p interaction is a dominant charge-hopping pathway. As a result, tenfold enhancement of hole mobilities exceeding those obtained for insoluble derivatives was reached. Moreover, due to high crystallinity and co-planarity

of the conjugated cores, electron transfer was preserved with a mobility of 0.2 $cm^2V^{-1}s^{-1}$ for dithiophene-DPP. At the same time, the material remained soluble, which is a significant advantage for purification and processing. This approach can be universally applied for many types of semiconducting organic materials containing the imide motif, where solubilization is achieved by side-group substitution.

Contributions: Author participated in the design of experiments. The author prepared samples of OFETs, thin layers for optical measurements, AFM and cyclic voltammetry measurements. Author performed electrical characterisation of OFETs, optical measurements of thin layers and solutions. Author contributed to the introduction, experimental and results part of paper.

[S5] Effect of the ethynylene linker on the properties and carrier mobility of naphthalene derivatives with hexylbithienyl arms

Róbert Mišicák, **Stanislav Stříteský**, Martin Vala, Martin Weiter, Marek Cigáň, Katarína Gmucová, Karol Végsö, Martin Weis, Jozef Kožíšek, Milan Pavúk, Martin Putala

A series of new naphthalene derivatives with (50-hexyl-2,20-bithiophene-5-yl)ethynyl side arms attached to the central naphthalene core at positions 1 and 4 (H2TA14N), 1 and 5 (H2TA15N), and 2 and 6 (H2TA26N) were synthesized by a sequencing of alkynylations performed according to a Negishi cross-coupling protocol. This synthetic approach provides higher yields compared to Sonogashira-based alkynylations, particularly when aryl bromides are used as starting materials. Compared to the analogous derivatives with hexylbithienyl arms directly attached to the naphthalene core (H2T14N,H2T15N, and H2T26N), an ethynylene linker ensures the planarity of the molecules, causing a change in the order of derivatives by intramolecular conjugation from H2T15N < H2T14N < H2T26N to H2TA15N ≈ H2TA26N < H2TA14N, as can be seen from the solution, and thin film optical and electrochemical properties as well. However, the order of derivatives by the hole mobility in a field effect transistor remains unaltered by an ethynylene linker (H2TA14N < H2TA15N < H2TA26N). The tendency in charge mobility can be explained by different packing motifs affected by molecular symmetry and was revealed by single crystal X-ray analysis and 2D X-ray GIWAXS and AFM characterization of the thin films.

Contributions: Author prepared, characterised and evaluate parameters of OFETs. Author prepared thin layers and solutions for optical measurements and AFM measurements. Author performed UV-VIS measurement of thin layers and solutions. Author contributed to the experimental and results chapters of paper.

[S6] Evaluation and improvement of organic semiconductors'biocompatibility towards fibroblasts and cardiomyocytes

Eva Šafaříková, Lenka Švihálková Šindlerová, **Stanislav Stříteský**, Lukáš Kubala, Martin Vala, Martin Weiter, Jan Víteček

The use of organic semiconductors in bioelectronic devices has received considerable attention over the past decade, since they have the potential to form an excellent biointerface for living cells and tissues.The aim was to determine multiple aspects of the biocompatibility of selected organic semiconductors with high conductivity and to further improve their potential for cell cultivation. Two representatives oflow-molecular weight organic semiconductors triisopropylsilyethynyl pentacene (TIPS-pentacene) anddiketopyrrolopyrrole ($DPP(TBFu)_2$) were selected together with two semiconducting organic polymerspoly(3-hexylthiophene-2,5-diyl) (P3HT) and poly(3,4-ethylenedioxythiophene):poly(styrenesulfonate)(PEDOT:PSS). The stability of these materials in physiological environment and their wetting proper-ties, which are preconditions for biocompatibility, were determined. TIPS-Pentacene, $DPP(TBFu)_2$ and P3HT were stable but PEDOT:PPS produced some leachates. Native TIPS-Pentacene, $DPP(TBFu)_2$ and P3HT exhibited lowered wettability. Their biocompatibility was studied by means of fibroblasts and differentiated cardiomyocytes. It was limited compared to standard cell culture plastics, thus coating of surfaceby proteins was applied. Among others collagen IV coating was shown to significantly improve biocom-patibility of all tested organic semiconductors. Finally, cultures of spontaneously beating cardiomyocyteswere established on TIPS-Pentacene, $DPP(TBFu)_2$, P3HT and PEDOT:PSS.

Contributions: Author cooperates in the set up of experiments. Autor prepared samples, conduced optical measurements, measured contact angle a cooperate on biocompatibility tests. Author contributed to the introduction, experimental and results and discussion part of paper.

[S7] Printing inks of electroactive polymer PEDOT:PSS: The study of biocompatibility, stability, and electrical properties

Stanislav Stříteský, Aneta Marková, Jan Víteček, Eva Šafaříková, Michal Hrabal, Lubomír Kubáč, Lukáš Kubala, Martin Weiter, Martin Vala

Biocompatibility tests and a study of the electrical properties of thin films prepared from six electroactive polymer ink formulations based on poly(3,4-ethylenedioxythiophene): poly(styrene sulfonate) (PEDOT:PSS) were performed. The aim was to find a suitable formulation of PEDOT:PSS and conditions for preparing thin films in order to construct printed bioelectronic

devices for biomedical applications. The stability and electrical properties of such films were tested on organic electrochemical transistor (OECT)-based sensor platforms and their biocompatibility was evaluated in assays with 3T3 fibroblasts and murine cardiomyocytes. It was found that the thin films prepared from inks without an additive or any thin film post-treatment provide limited conductivity and stability for use in biomedical applications. These properties were greatly improved by using ethylene glycol and thermal annealing. Addition or post-treatment by ethylene glycol in combination with thermal annealing provided thin films with electrical resistance and a stability sufficient to be used in sensing of animal cell physiology. These films coated with collagen IV showed good biocompatibility in the assay with 3T3 fibroblasts when compared to standard cell culture plastics. Selected films were then used in assays with murine cardiomyocytes. We observed that these cells were able to attach to the PEDOT:PSS films and form an active sensor element. Spontaneously beating clusters were formed, indicating a good physiological status for the cardiomyocyte cells. These results open the door to construction of cheap printed electronic devices for biointerfacing in biomedical applications.

Contributions: This paper is the authors' research. Author designed all experiments, co-prepared samples, conduced measurements and analysed data. Autor co-wrote the paper.

[S8] Organic Electrochemical Transistor Microplate for Real-Time Cell Culture Monitoring

Ota Salyk, Jan Víteček, Lukáš Omasta, Eva Šafaříková, **Stanislav Stříteský**, Martin Vala and MartinWeiter

Human cell cultures provide a potentially powerful means for pharmacological and toxicological research. A microplate with a multielectrode array of 96 organic electrochemical transistors (OECTs) based on the semiconductive polymer poly(3,4-ethylenedioxythio-phene):poly (styrene sulfonic acid) PEDOT:PSS was developed and fabricated by the screen printing method. It consists of a microplate of a 12 x 8 chimney–well array with transistors on the bottom. The OECT is circular with a channel of 1.5 mm2 in the centre surrounded by the circular gate electrode. The device is designed for electrogenic cell monitoring. Simulations with the electrolyte revealed good electrical characteristics and indicated the setup information of the experimental conditions. A transconductance of g = 1.4 mS was achieved in the wide range of gate voltages Vgs = ±0.4 V when the drain potential Vds = -0.735 V was set and the long term relaxation was compensated for. The time constant 0.15 s limited by the channel-electrolyte charge electrical double layer (EDL)

capacitance was measured. The device was tested on a 3T3 fibroblast cell culture and the sudden environmental changes were recorded. The living cells can be observed on the channel of the OECT and during electrical stimulation by gate voltage, as well as during the source current response.

Contributions: Autor participate on the design of experiments. Autor performed electrical measurement of prepared OECTs with living 3T3 fibroblast cells. Autor contributes to the experimental and result and discussion part of paper.

9 ABBREVIATIONS

(Ph)	Phenyl
(Th)	Thiophene
3T3 fibroblast	"3-day transfer, inoculum 3×10^5 cells"
A	Thermal annealing
AFM	Atomic force microscopy
$A_{G,C}$	Electron affinity of gas and crystal states
ATP	adenosin triphosphate
BG, TG, BC, TC	Bottom/Top Gate, Bottom/Top Contact
C60	Fulleren with 60 carbon atoms
CB, VB, Δ	Conduction band, valence band, interface dipole
CMOS	Complementary Metal–Oxide–Semiconductor
COC Ltd.	Centre for Organic Chemistry Ltd.
DMF	Dimethyl formamide
DMSO	Dimethyl Sulfoxide
DOS	Density of states
dpi	dots per inch
DPP	Diketo-pyrrolo-pyrroles
$DPP(TBFu)_2$	(3,6-bis(5-(benzofuran-2-yl)thiophen-2-yl)-2,5-bis(2-ethyl-hexyl)pyrrolo[3,4-c]pyrrole-1,4-dione)
DSC	Differential scanning calorimetry
EA	Electron affinity
E_G	Energy gap
EG	Ethylenglycol annealing
EGO-FET	Electrolyte gated organic field-effect transistor
$E_{th,te}$	Energy of trap states for holes and electrones
eV	electronvolt
g_m	Transconductance
H2TxyN	(5-hexyl-2,2-bithiophene-5-yl)ethynyl, xy = position of substitution
HH	Head to head
HMDS	Hexamethyldisilazan
HOMO	Highest occupied molecular orbital
HT	Head to tail
I_{DS}	Current going through channel between source and drain
IEEE	Institute of Electrical and Electronics Engineers
$I_{G,C}$	ionization potential of gas and crystal state
ISO	International Organization for Standardization
KFM	Kelvin probe force microscopy
LUMO	Lowest unoccupied molecular orbital
MTR	Multiple trapping and thermal release model

MTT	3-(4,5-dimethylthiazol-2-yl)-2,5-diphenyltetrazolium bromide
OECT	Organic electrochemical transistor
OFET	Organic field-effect transistor
OLED	Organic light-emitting diod
OS	Organic semiconductor
OTS	Octadecyl trichlorsilan
p, n	Hole and electron
P3HT	poly(3-hexylthiophene)
PBS	fosfate buffer saline
PEDOT	Poly(3,4-ethylenedioxythiophene)
PFBT	Penta(per)fluorbenzothiol
pH	Potential of hydrogen
$P_{h,e}$	polarization energy of holes and electrons
PSS	Poly(styrene sulfonate)
PTFE	polytetrafluor ethylene
PWM	pulse width modulation
R_C	Contact resistance
RFID	Radio Frequency Identification
$R_{Channel}$	Channel resistance
R_{TOT}	Total resistance
S, D, G	Source, drain, gait
S_0, S_1, S_2	singlet states
SAM	Self-assembled monolayer
SQC	Quartz crystal monitor and deposition controller
T_1	triplet states
TGA	thermogravimetric analysis
TLM	Transfer or transmission line method
UV-VIS	Ultraviolet–visible spectroscopy
V_{DS}	Voltage between source and drain electrode
V_{GS}	Voltage between source and gait electrode
VRH	Variable range hopping model
XTT	(2,3-bis-(2-methoxy-4-nitro-5-sulfophenyl)-2H-tetrazolium-5-carboxanilide)
ΔE_G	wide of band gap
σ, π, σ^*, π^*	sigma and pi bonds and antibonds
φ_M	Schotky barrier
Φ_m, W_f	Work function

10 REFERENCES

[1] GAO, Xike a Zheng ZHAO. High mobility organic semiconductors for field-effect transistors. *Science China Chemistry* [online]. 2015, **58**(6), 947-968 [cit. 2019-05-05]. DOI: 10.1007/s11426-015-5399-5. ISSN 1674-7291. Dostupné z: http://link.springer.com/10.1007/s11426-015-5399-5

[2] KLAUK, Hagen. Organic thin-film transistors. *Chemical Society Reviews* [online]. 2010, **39**(7) [cit. 2019-05-05]. DOI: 10.1039/b909902f. ISSN 0306-0012. Dostupné z: http://xlink.rsc.org/?DOI=b909902f

[3] ZHOU, Ke, Huanli DONG, Hao-li ZHANG a Wenping HU. High performance n-type and ambipolar small organic semiconductors for organic thin film transistors. *Phys. Chem. Chem. Phys* [online]. 2014, **16**(41), 22448-22457 [cit. 2019-05-05]. DOI: 10.1039/C4CP01700E. ISSN 1463-9076. Dostupné z: http://xlink.rsc.org/?DOI=C4CP01700E

[4] KYMISSIS, Ioannis. *Organic field effect transistors: theory, fabrication and characterization*. New York: Springer, 2009, xii, 148 s. Series on Integrated Circuits and Systems. ISBN 978-0-387-92133-4.

[5] HOUK, K. N., Patrick S. LEE a Maja NENDEL. Polyacene and Cyclacene Geometries and Electronic Structures: Bond Equalization, Vanishing Band Gaps, and Triplet Ground States Contrast with Polyacetylene. *The Journal of Organic Chemistry*. 2001, **66**(16), 5517-5521. DOI: 10.1021/jo010391f. ISSN 0022-3263. Dostupné také z: https://pubs.acs.org/doi/10.1021/jo010391f

[6] MCGARRY, Kathryn A., Wei XIE, Christopher SUTTON et al. Rubrene-Based Single-Crystal Organic Semiconductors: Synthesis, Electronic Structure, and Charge-Transport Properties. *Chemistry of Materials* [online]. 2013, **25**(11), 2254-2263 [cit. 2019-05-05]. DOI: 10.1021/cm400736s. ISSN 0897-4756. Dostupné z: http://pubs.acs.org/doi/10.1021/cm400736s

[7] KAGAN, Jacques. *Organic photochemistry: principles and applications*. San Diego: Academic Press, 1993. ISBN 01-239-4320-5.

[8] SO, Franky. *Organic electronics: materials, processing, devices and applications*. Boca Raton, FL: CRC Press, 2010, xiii, 567 p. ISBN 14-200-7290-0.

[9] ROUNDHILL, D. M. *Photochemistry and photophysics of metal complexes*. New York: Plenum Press, 1994. ISBN 03-064-4694-4.

[10] ZHUIYKOV, Serge. Electrons and holes in a semiconductor. *Nanostructured Semiconductor Oxides for the Next Generation of Electronics and Functional Devices*. Elsevier, 2014, , 1-49. DOI: 10.1533/9781782422242.1. ISBN 9781782422204. Dostupné také z: https://linkinghub.elsevier.com/retrieve/pii/B9781782422204500019

[11] ZHAO, Yan, Yunlong GUO a Yunqi LIU. 25th Anniversary Article: Recent Advances in n-Type and Ambipolar Organic Field-Effect Transistors.

Advanced Materials. 2013, **25**(38), 5372-5391. DOI: 10.1002/adma.201302315. ISSN 09359648. Dostupné také z: http://doi.wiley.com/10.1002/adma.201302315

[12] BAO, Zhenan a Jason John LOCKLIN. *Organic field-effect transistors*. Boca Raton: CRC Press, 2007, 616 p., [2] p. of plates. Optical science and engineering (Boca Raton, Fla.), 128. ISBN 08-493-8080-4.

[13] STALLINGA, P. Electronic Transport in Organic Materials: Comparison of Band Theory with Percolation/(Variable Range) Hopping Theory. *Advanced Materials* [online]. 2011, **23**(30), 3356-3362 [cit. 2019-05-05]. DOI: 10.1002/adma.201101129. ISSN 09359648. Dostupné z: http://doi.wiley.com/10.1002/adma.201101129

[14] ASHCROFT, Neil W. *Solid state physics*. New York: Saunders College Publishers, 1976, 826 s. ISBN 00-304-9346-3.

[15] KARL, Norbert, Jörg MARKTANNER, Roland STEHLE a Wilhelm WARTA. High-field saturation of charge carrier drift velocities in ultrapurified organic photoconductors. *Synthetic Metals*. 1991, **42**(3), 2473-2481. DOI: 10.1016/0379-6779(91)91407-2. ISSN 03796779. Dostupné také z: http://linkinghub.elsevier.com/retrieve/pii/0379677991914072

[16] WANG, Chengliang, Huanli DONG, Lang JIANG a Wenping HU. Organic semiconductor crystals. *Chemical Society Reviews* [online]. 2018, **47**(2), 422-500 [cit. 2019-05-05]. DOI: 10.1039/C7CS00490G. ISSN 0306-0012. Dostupné z: http://xlink.rsc.org/?DOI=C7CS00490G

[17] LE COMBER, P. a W. SPEAR. Electronic Transport in Amorphous Silicon Films. *Physical Review Letters*. 1970, **25**(8), 509-511. DOI: 10.1103/PhysRevLett.25.509. ISSN 0031-9007. Dostupné také z: http://link.aps.org/doi/10.1103/PhysRevLett.25.509

[18] BRÜTTING, Wolfgang, Chihaya ADACHI a Russell James Delmar HOLMES. *Physics of organic semiconductors*. 2nd completely new rev. ed. Weinheim, Germany: Wiley-VCH, 2012. ISBN 978-3-527-41053-8.

[19] GILL, W. D. Drift mobilities in amorphous charge-transfer complexes of trinitrofluorenone and poly-n-vinylcarbazole. *Journal of Applied Physics*. 1972, **43**(12), 5033-. DOI: 10.1063/1.1661065. ISSN 00218979. Dostupné také z: http://scitation.aip.org/content/aip/journal/jap/43/12/10.1063/1.1661065

[20] BÄSSLER, H. Charge Transport in Disordered Organic Photoconductors a Monte Carlo Simulation Study. *Physica status solidi (b)*. 1993, **175**(1), 15-56. DOI: 10.1002/pssb.2221750102. ISSN 03701972. Dostupné také z: http://doi.wiley.com/10.1002/pssb.2221750102

[21] SILIŅŠ, E a Vladislav CÁPEK. *Organic molecular crystals: interaction, localization, and transport phenomena*. New York: American Institute of Physics, 1994, xxiv, 402 p. ISBN 15-639-6069-9.

[22] DONG, Huanli, Chengliang WANG a Wenping HU. High performance organic semiconductors for field-effect transistors. *Chemical Communications* [online]. 2010, **46**(29) [cit. 2019-05-05]. DOI: 10.1039/c0cc00947d. ISSN 1359-7345. Dostupné z: http://xlink.rsc.org/?DOI=c0cc00947d

[23] ALESHIN, A. N., J. Y. LEE, S. W. CHU, J. S. KIM a Y. W. PARK. Mobility studies of field-effect transistor structures basedon anthracene single crystals. *Applied Physics Letters* [online]. 2004, **84**(26), 5383-5385 [cit. 2019-05-05]. DOI: 10.1063/1.1767282. ISSN 0003-6951. Dostupné z: http://aip.scitation.org/doi/10.1063/1.1767282

[24] GOLDMANN, C., S. HAAS, C. KRELLNER, K. P. PERNSTICH, D. J. GUNDLACH a B. BATLOGG. Hole mobility in organic single crystals measured by a "flip-crystal" field-effect technique. *Journal of Applied Physics* [online]. 2004, **96**(4), 2080-2086 [cit. 2019-05-05]. DOI: 10.1063/1.1767292. ISSN 0021-8979. Dostupné z: http://aip.scitation.org/doi/10.1063/1.1767292

[25] HASEGAWA, Tatsuo a Jun TAKEYA. Organic field-effect transistors using single crystals. *Science and Technology of Advanced Materials* [online]. 2016, **10**(2), 024314- [cit. 2016-06-14]. DOI: 10.1088/1468-6996/10/2/024314. ISSN 14686996. Dostupné z: http://www.tandfonline.com/doi/full/10.1088/1468-6996/10/2/024314

[26] WATANABE, Motonori, Yuan Jay CHANG, Shun-Wei LIU et al. The synthesis, crystal structure and charge-transport properties of hexacene. *Nature Chemistry* [online]. 2012, **4**(7), 574-578 [cit. 2019-05-05]. DOI: 10.1038/nchem.1381. ISSN 1755-4330. Dostupné z: http://www.nature.com/articles/nchem.1381

[27] DHAR, J., D. P. KAROTHU a S. PATIL. Herringbone to cofacial solid state packing via H-bonding in diketopyrrolopyrrole (DPP) based molecular crystals: influence on charge transport: influence on charge transport. *Chemical Communications*. 2015, **51**(1), 97-100. DOI: 10.1039/c4cc06063f. ISSN 13597345. Dostupné také z: Go to ISI://WOS:000345909400016

[28] HAO, Zhimin a Abul IQBAL. Some aspects of organic pigments. *Chemical Society Reviews* [online]. 1997, **26**(3) [cit. 2019-05-05]. DOI: 10.1039/cs9972600203. ISSN 0306-0012. Dostupné z: http://xlink.rsc.org/?DOI=cs9972600203

[29] DHAR, Joydeep, Durga Prasad KAROTHU a Satish PATIL. Herringbone to cofacial solid state packing via H-bonding in diketopyrrolopyrrole (DPP) based molecular crystals: influence on charge transport. *Chemical Communications* [online]. 2015, **51**(1), 97-100 [cit. 2019-05-05]. DOI: 10.1039/C4CC06063F. ISSN 1359-7345. Dostupné z: http://xlink.rsc.org/?DOI=C4CC06063F

[30] MIZUGUCHI, Jin a Gary WOODEN. A Large Bathochromic Shift from the Solution to the Solid State in 1,4-Diketo-3,6-Diphenyl-Pyrrolo-[3,4-c]-Pyrrole. *Berichte der Bunsengesellschaft für physikalische Chemie* [online]. 1991, **95**(10), 1264-1274 [cit. 2019-05-05]. DOI: 10.1002/bbpc.19910951016. ISSN 00059021. Dostupné z: http://doi.wiley.com/10.1002/bbpc.19910951016

[31] VALA, Martin, Martin WEITER, Jan VYŇUCHAL, Petr TOMAN a Stanislav LUŇÁK. Comparative Studies of Diphenyl-Diketo-Pyrrolopyrrole Derivatives for Electroluminescence Applications. *Journal of Fluorescence* [online]. 2008, **18**(6), 1181-1186 [cit. 2019-05-05]. DOI: 10.1007/s10895-008-0370-x. ISSN 1053-0509. Dostupné z: http://link.springer.com/10.1007/s10895-008-0370-x

[32] MIZUGUCHI, J., A. GRUBENMANN, G. WOODEN a G. RIHS. Structures of 3,6-diphenylpyrrolo[3,4-c]pyrrole-1,4-dione and 2,5-dimethyl-3,6-diphenylpyrrolo[3,4-c]pyrrole-1,4-dione. *Acta Crystallographica Section B Structural Science* [online]. **48**(5), 696-700 [cit. 2019-05-05]. DOI: 10.1107/S0108768192003033. ISSN 01087681. Dostupné z: http://scripts.iucr.org/cgi-bin/paper?S0108768192003033

[33] DAVID, Jan, Martin WEITER, Martin VALA, Jan VYŇUCHAL, Jiří KUČERÍK, Suresh S. TATE a Alton MEISTER. Stability and structural aspects of diketopyrrolopyrrole pigment and its N-alkyl derivatives: catalytic, structural and functional aspects. *Dyes and Pigments*. 2011, **89**(2), 357-368. DOI: 10.1007/978-94-009-8027-3_23.

[34] NAIK, Mallari A., N. VENKATRAMAIAH, Catherine KANIMOZHI a Satish PATIL. Influence of Side-Chain on Structural Order and Photophysical Properties in Thiophene Based Diketopyrrolopyrroles: A Systematic Study. *The Journal of Physical Chemistry C* [online]. 2012, **116**(50), 26128-26137 [cit. 2019-05-05]. DOI: 10.1021/jp306365q. ISSN 1932-7447. Dostupné z: http://pubs.acs.org/doi/10.1021/jp306365q

[35] DHAR, J., N. VENKATRAMAIAH, A. ANITHA a S. PATIL. Photophysical, electrochemical and solid state properties of diketopyrrolopyrrole based molecular materials: importance of the donor group: importance of the donor group. *Journal of Materials Chemistry C*. 2014, **2**(17), 3457-3466. ISSN 20507526. Dostupné také z: Go to ISI://WOS:000334124800043

[36] WEITER, Martin, Ota SALYK, Pavel BEDNÁŘ, Martin VALA, Jiří NAVRÁTIL, Odlřich ZMEŠKAL, Jan VYŇUCHAL a Stanislav LUŇÁK. Morphology and properties of thin films of diketopyrrolopyrrole derivatives. *Materials Science and Engineering: B* [online]. 2009, **165**(3), 148-152 [cit. 2019-05-05]. DOI: 10.1016/j.mseb.2009.09.017. ISSN 09215107. Dostupné z: https://linkinghub.elsevier.com/retrieve/pii/S092151070900395X

[37] MIZUGUCHI, J., A. GRUBENMANN, G. WOODEN a G. RIHS. STRUCTURES OF 3,6-DIPHENYLPYRROLO 3,4-C PYRROLE-1,4-DIONE AND 2,5-DIMETHYL-3,6-DIPHENYLPYRROLO 3,4-C PYRROLE-1,4-DIONE. *Acta Crystallographica Section B-Structural Science*. Oct, **48**, 696-700. DOI: 10.1107/s0108768192003033. ISSN 01087681. Dostupné také z: Go to ISI://WOS:A1992JU40800020

[38] SILVER, M., G. WINBORNE, D. ADLER a V. CANNELLA. Electron mobility in hydrogenated amorphous silicon under single and double injection. *Applied Physics Letters* [online]. 1987, **50**(15), 983-985 [cit. 2019-05-05]. DOI: 10.1063/1.98005. ISSN 0003-6951. Dostupné z: http://aip.scitation.org/doi/10.1063/1.98005

[39] YANAGISAWA, H., J. MIZUGUCHI, S. ARAMAKI a Y. SAKAI. Organic field-effect transistor devices based on latent pigments of unsubstituted diketopyrrolopyrrole or quinacridone. *Japanese Journal of Applied Physics*. Jun, **47**(6), 4728-4731. DOI: 10.1143/jjap.47.4728. ISSN 00214922. Dostupné také z: Go to ISI://WOS:000257260600074

[40] KOJIMA, H. a T. MORI. Estimated Mobility of Ambipolar Organic Semiconductors, Indigo and Diketopyrrolopyrrole. *Chemistry Letters*. Jan, **42**(1), 68-70. DOI: 10.1246/cl.2013.68. ISSN 03667022. Dostupné také z: Go to ISI://WOS:000315542200025

[41] GLOWACKI, E. D., H. COSKUN, M. A. BLOOD-FORSYTHE et al. Hydrogen-bonded diketopyrrolopyrrole (DPP) pigments as organic semiconductors. *Organic Electronics*. Dec, **15**(12), 3521-3528. DOI: 10.1016/j.orgel.2014.09.038. ISSN 15661199. Dostupné také z: Go to ISI://WOS:000345649200016

[42] KWON, Jaehyuk, Hanah NA, Akshaya K. PALAI, Amit KUMAR, Uijin JEONG, Sungwoo CHO a Seungmoon PYO. Utilization of simply alkylated diketopyrrolopyrrole derivative as a p-channel semiconductor for organic devices. *Synthetic Metals* [online]. 2015, **209**, 240-246 [cit. 2019-05-05]. DOI: 10.1016/j.synthmet.2015.07.015. ISSN 03796779. Dostupné z: https://linkinghub.elsevier.com/retrieve/pii/S0379677915300230

[43] PALAI, Akshaya K., Hyejin CHO, Sungwoo CHO, Tae Joo SHIN, Soonmin JANG, Seung-Un PARK a Seungmoon PYO. Non-functionalized soluble diketopyrrolopyrrole: Simplest p-channel core for organic field-effect transistors. *Organic Electronics* [online]. 2013, **14**(5), 1396-1406 [cit. 2019-05-05]. DOI: 10.1016/j.orgel.2013.03.002. ISSN 15661199. Dostupné z: https://linkinghub.elsevier.com/retrieve/pii/S156611991300102X

[44] STOLTE, Matthias, Sabin-Lucian SURARU, Patricia DIEMER, Tao HE, Christian BURSCHKA, Ute ZSCHIESCHANG, Hagen KLAUK a Frank WÜRTHNER. Diketopyrrolopyrrole Organic Thin-Film Transistors: Impact of Alkyl Substituents and Tolerance of Ethylhexyl Stereoisomers. *Advanced Functional Materials* [online]. 2016, **26**(41), 7415-7422 [cit. 2019-05-05].

DOI: 10.1002/adfm.201602994. ISSN 1616301X. Dostupné z: http://doi.wiley.com/10.1002/adfm.201602994

[45] QIAO, Yali, Yunlong GUO, Chunmeng YU, Fengjiao ZHANG, Wei XU, Yunqi LIU a Daoben ZHU. Diketopyrrolopyrrole-Containing Quinoidal Small Molecules for High-Performance, Air-Stable, and Solution-Processable n-Channel Organic Field-Effect Transistors. *Journal of the American Chemical Society* [online]. 2012, **134**(9), 4084-4087 [cit. 2019-05-05]. DOI: 10.1021/ja3003183. ISSN 0002-7863. Dostupné z: http://pubs.acs.org/doi/10.1021/ja3003183

[46] YOON, Won Sik, Sang Kyu PARK, Illhun CHO, Jeong-A OH, Jong H. KIM a Soo Young PARK. High-Mobility n-Type Organic Transistors Based on a Crystallized Diketopyrrolopyrrole Derivative. *Advanced Functional Materials* [online]. 2013, **23**(28), 3519-3524 [cit. 2019-05-05]. DOI: 10.1002/adfm.201203065. ISSN 1616301X. Dostupné z: http://doi.wiley.com/10.1002/adfm.201203065

[47] LILIENFELD, Julius Edgar. *Method and apparatus for controlling electric currents*. 1926. US 1745175 A Grant. Uděleno Jan 28, 1930. Zapsáno Oct 8, 1926. Dostupné také z: http://www.google.com/patents/US1745175

[48] CHODOS, Alan. American Physical Society Sites: This Month in Physics History November 17 - December 23, 1947: Invention of the First Transistor. *APS Physics* [online]. 1995 [cit. 2014-07-29]. Dostupné z: http://www.aps.org/publications/apsnews/200011/history.cfm

[49] KOEZUKA, H., A. TSUMURA a T. ANDO. Field-effect transistor with polythiophene thin film. *Synthetic Metals*. 1987, **18**(1-3), 699-704. DOI: 10.1016/0379-6779(87)90964-7. ISSN 03796779. Dostupné také z: http://linkinghub.elsevier.com/retrieve/pii/0379677987909647

[50] SEO, Hoon-Seok, Jeong-Do OH, Dae-Kyu KIM, Eun-Sol SHIN a Jong-Ho CHOI. π -Conjugated organic-based devices with different layered structures produced by the neutral cluster beam deposition method and operating conduction mechanism. *Journal of Physics D: Applied Physics*. 2012, **45**(50), 505108-. DOI: 10.1088/0022-3727/45/50/505108. ISSN 0022-3727. Dostupné také z: http://stacks.iop.org/0022-3727/45/i=50/a=505108?key=crossref.154e7c611b1129a16bbc362046b8bd62

[51] KIGUCHI, Manabu, Manabu NAKAYAMA, Toshihiro SHIMADA a Koichiro SAIKI. Electric-field-induced charge injection or exhaustion in organic thin film transistor. *Physical Review B*. 2005, **71**(3), -. DOI: 10.1103/PhysRevB.71.035332. ISSN 1098-0121. Dostupné také z: http://link.aps.org/doi/10.1103/PhysRevB.71.035332

[52] IEEE 1620. *IEEE Standard for Test Methods for the Characterization of Organic Transistors and Materials*. 2008.

[53] TIWARI, Sanjay a N. C. GREENHAM. Charge mobility measurement techniques in organic semiconductors. *Optical and Quantum Electronics*. 2009, **41**(2), 69-89. DOI: 10.1007/s11082-009-9323-0. ISSN 0306-8919. Dostupné také z: http://link.springer.com/10.1007/s11082-009-9323-0

[54] ORTIZ-CONDE, Adelmo, Francisco J. GARCÍA-SÁNCHEZ, Juan MUCI, Andrea SUCRE-GONZÁLEZ, João Antonio MARTINO, Paula Ghedini Der AGOPIAN a Cor CLAEYS. Threshold voltage extraction in Tunnel FETs. *Solid-State Electronics*. 2014, **93**, 49-55. DOI: 10.1016/j.sse.2013.12.010. ISSN 00381101. Dostupné také z: http://linkinghub.elsevier.com/retrieve/pii/S0038110113003675

[55] KERGOAT, Loïg, Benoît PIRO, Magnus BERGGREN, Gilles HOROWITZ a Minh-Chau PHAM. Advances in organic transistor-based biosensors: from organic electrochemical transistors to electrolyte-gated organic field-effect transistors. *Analytical and Bioanalytical Chemistry* [online]. 2012, **402**(5), 1813-1826 [cit. 2019-06-28]. DOI: 10.1007/s00216-011-5363-y. ISSN 1618-2642. Dostupné z: http://link.springer.com/10.1007/s00216-011-5363-y

[56] TORSI, Luisa, Maria MAGLIULO, Kyriaki MANOLI a Gerardo PALAZZO. Organic field-effect transistor sensors: a tutorial review. *Chemical Society Reviews* [online]. 2013, **42**(22) [cit. 2019-06-28]. DOI: 10.1039/c3cs60127g. ISSN 0306-0012. Dostupné z: http://xlink.rsc.org/?DOI=c3cs60127g

[57] BERGGREN, M. a A. RICHTER-DAHLFORS. Organic Bioelectronics. *Advanced Materials* [online]. 2007, **19**(20), 3201-3213 [cit. 2019-06-28]. DOI: 10.1002/adma.200700419. ISSN 09359648. Dostupné z: http://doi.wiley.com/10.1002/adma.200700419

[58] RIVNAY, Jonathan, Sahika INAL, Alberto SALLEO, Róisín M. OWENS, Magnus BERGGREN a George G. MALLIARAS. Organic electrochemical transistors. *Nature Reviews Materials* [online]. 2018, **3**(2) [cit. 2019-06-28]. DOI: 10.1038/natrevmats.2017.86. ISSN 2058-8437. Dostupné z: http://www.nature.com/articles/natrevmats201786

[59] FRIEDLEIN, Jacob T., Robert R. MCLEOD a Jonathan RIVNAY. Device physics of organic electrochemical transistors. *Organic Electronics* [online]. 2018, **63**, 398-414 [cit. 2019-06-28]. DOI: 10.1016/j.orgel.2018.09.010. ISSN 15661199. Dostupné z: https://linkinghub.elsevier.com/retrieve/pii/S1566119918304683

[60] BERNARDS, D. A. a G. G. MALLIARAS. Steady-State and Transient Behavior of Organic Electrochemical Transistors. *Advanced Functional Materials* [online]. 2007, **17**(17), 3538-3544 [cit. 2019-06-28]. DOI: 10.1002/adfm.200601239. ISSN 1616301X. Dostupné z: http://doi.wiley.com/10.1002/adfm.200601239

[61] RIVNAY, Jonathan, Pierre LELEUX, Michele SESSOLO, Dion KHODAGHOLY, Thierry HERVÉ, Michel FIOCCHI a George G. MALLIARAS. Organic Electrochemical Transistors with Maximum Transconductance at Zero Gate Bias. *Advanced Materials* [online]. 2013, **25**(48), 7010-7014 [cit. 2019-06-28]. DOI: 10.1002/adma.201303080. ISSN 09359648. Dostupné z: http://doi.wiley.com/10.1002/adma.201303080

[62] KHODAGHOLY, Dion, Jonathan RIVNAY, Michele SESSOLO et al. High transconductance organic electrochemical transistors. *Nature Communications* [online]. 2013, **4**(1) [cit. 2019-06-28]. DOI: 10.1038/ncomms3133. ISSN 2041-1723. Dostupné z: http://www.nature.com/articles/ncomms3133

[63] STRAKOSAS, Xenofon, Manuelle BONGO a Róisín M. OWENS. The organic electrochemical transistor for biological applications. *Journal of Applied Polymer Science* [online]. 2015, **132**(15), - [cit. 2019-06-28]. DOI: 10.1002/app.41735. ISSN 00218995. Dostupné z: http://doi.wiley.com/10.1002/app.41735

[64] GU, Xi, Chunlei YAO, Ying LIU a I-Ming HSING. 16-Channel Organic Electrochemical Transistor Array for In Vitro Conduction Mapping of Cardiac Action Potential. *Advanced Healthcare Materials* [online]. 2016, **5**(18), 2345-2351 [cit. 2019-06-28]. DOI: 10.1002/adhm.201600189. ISSN 21922640. Dostupné z: http://doi.wiley.com/10.1002/adhm.201600189

[65] YAO, Chunlei, Qianqian LI, Jing GUO, Feng YAN a I-Ming HSING. Rigid and Flexible Organic Electrochemical Transistor Arrays for Monitoring Action Potentials from Electrogenic Cells. *Advanced Healthcare Materials* [online]. 2015, **4**(4), 528-533 [cit. 2019-06-28]. DOI: 10.1002/adhm.201400406. ISSN 21922640. Dostupné z: http://doi.wiley.com/10.1002/adhm.201400406

[66] OUYANG, Jianyong. "Secondary doping" methods to significantly enhance the conductivity of PEDOT: PSS for its application as transparent electrode of optoelectronic devices. *Displays* [online]. 2013, **34**(5), 423-436 [cit. 2019-06-28]. DOI: 10.1016/j.displa.2013.08.007. ISSN 01419382. Dostupné z: https://linkinghub.elsevier.com/retrieve/pii/S0141938213000668

[67] WHITE, Henry S., Gregg P. KITTLESEN a Mark S. WRIGHTON. Chemical derivatization of an array of three gold microelectrodes with polypyrrole: fabrication of a molecule-based transistor. *Journal of the American Chemical Society*. 1984, **106**(18), 5375-5377. DOI: 10.1021/ja00330a070. ISSN 0002-7863. Dostupné také z: http://pubs.acs.org/doi/abs/10.1021/ja00330a070

[68] RIVNAY, Jonathan, Pierre LELEUX, Marc FERRO et al. High-performance transistors for bioelectronics through tuning of channel thickness. *Science Advances* [online]. 2015, **1**(4) [cit. 2019-06-28]. DOI:

10.1126/sciadv.1400251. ISSN 2375-2548. Dostupné z: http://advances.sciencemag.org/lookup/doi/10.1126/sciadv.1400251

[69] FERON, Krishna, Rebecca LIM, Connor SHERWOOD, Angela KEYNES, Alan BRICHTA a Paul DASTOOR. Organic Bioelectronics: Materials and Biocompatibility. *International Journal of Molecular Sciences* [online]. 2018, **19**(8) [cit. 2019-06-13]. DOI: 10.3390/ijms19082382. ISSN 1422-0067. Dostupné z: http://www.mdpi.com/1422-0067/19/8/2382

[70] ASPLUND, Maria, Tobias NYBERG a Olle INGANÄS. Electroactive polymers for neural interfaces. *Polymer Chemistry* [online]. 2010, **1**(9) [cit. 2019-06-28]. DOI: 10.1039/c0py00077a. ISSN 1759-9954. Dostupné z: http://xlink.rsc.org/?DOI=c0py00077a

[71] RIVNAY, Jonathan, Sahika INAL, Brian A. COLLINS et al. Structural control of mixed ionic and electronic transport in conducting polymers. *Nature Communications* [online]. 2016, **7**(1) [cit. 2019-06-28]. DOI: 10.1038/ncomms11287. ISSN 2041-1723. Dostupné z: http://www.nature.com/articles/ncomms11287

[72] AGRAWAL, C. Mauli. *Introduction to biomaterials: basic theory with engineering applications*. New York: Cambridge University Press, 2014. Cambridge texts in biomedical engineering. ISBN 978-0521116909.

[73] GAD, Shayne C. *Safety evaluation of pharmaceuticals and medical devices: international regulatory guidelines*. New York: Springer, 2011. ISBN 978-1-44-197448-8.

[74] GAUTAM, Vini, David RAND, Yael HANEIN a K. S. NARAYAN. A Polymer Optoelectronic Interface Provides Visual Cues to a Blind Retina. *Advanced Materials* [online]. 2014, **26**(11), 1751-1756 [cit. 2019-06-28]. DOI: 10.1002/adma.201304368. ISSN 09359648. Dostupné z: http://doi.wiley.com/10.1002/adma.201304368

[75] ISO 10993-5:2009. *Biological evaluation of medical devices: Part 5: Tests for in vitro cytotoxicity*. Third edition. Istanbul: International Organization for Standardization, 2009.

[76] LIU, Jianhua, Bright WALKER, Arnold TAMAYO, Yuan ZHANG a Thuc-Quyen NGUYEN. Effects of Heteroatom Substitutions on the Crystal Structure, Film Formation, and Optoelectronic Properties of Diketopyrrolopyrrole-Based Materials. *Advanced Functional Materials* [online]. 2013, **23**(1), 47-56 [cit. 2019-06-13]. DOI: 10.1002/adfm.201201599. ISSN 1616301X. Dostupné z: http://doi.wiley.com/10.1002/adfm.201201599

[77] LIU, Jianhua, Yuan ZHANG, Hung PHAN, Alexander SHARENKO, Preecha MOONSIN, Bright WALKER, Vinich PROMARAK a Thuc-Quyen NGUYEN. Effects of Stereoisomerism on the Crystallization Behavior and Optoelectrical Properties of Conjugated Molecules. *Advanced Materials*

[online]. 2013, **25**(27), 3645-3650 [cit. 2019-06-13]. DOI: 10.1002/adma.201300255. ISSN 09359648. Dostupné z: http://doi.wiley.com/10.1002/adma.201300255

[78] LI, Zi, Xu ZHANG, Yuan ZHANG, Cristiano F. WOELLNER, Martijn KUIK, Jianhua LIU, Thuc-Quyen NGUYEN a Gang LU. Hole Transport in Diketopyrrolopyrrole (DPP) Small Molecules: A Joint Theoretical and Experimental Study. *The Journal of Physical Chemistry C* [online]. 2013, **117**(13), 6730-6740 [cit. 2019-06-13]. DOI: 10.1021/jp310475d. ISSN 1932-7447. Dostupné z: http://pubs.acs.org/doi/10.1021/jp310475d

[79] FILO, Juraj, Róbert MIŠICÁK, Marek CIGÁŇ et al. Oligothiophenes with the naphthalene core for organic thin-film transistors: variation in positions of bithiophenyl attachment to the naphthalene. *Synthetic Metals*. 2015, **202**, 73-81. DOI: 10.1016/j.synthmet.2015.01.020. ISSN 03796779. Dostupné také z: https://linkinghub.elsevier.com/retrieve/pii/S0379677915000223

[80] MIŠICÁK, Róbert, Stanislav STŘÍTESKÝ, Martin VALA a WEITER. Effect of the ethynylene linker on the properties and carrier mobility of naphthalene derivatives with hexylbithienyl arms. *Synthetic Metals*. 2016, **2016**(217), 156-171. DOI: 10.1016/j.synthmet.2016.03.034. ISSN 03796779.

[81] DZIK, Petr, Michal VESELÝ a Michael NEUMANN-SPALLART. Inkjet Printed Interdigitated Conductivity Cells with Low Cell Constant. *ECS Journal of Solid State Science and Technology*. 2016, **5**(7), 412-418. DOI: 10.1149/2.0171607jss. ISSN 2162-8769. Dostupné také z: http://jss.ecsdl.org/lookup/doi/10.1149/2.0171607jss

[82] CARABINEIRO, Sónia A. C. a Bernard E. NIEUWENHUYS. *Adsorption of small molecules on gold single crystal surfaces*. DOI: 10.1007/BF03214951. Dostupné také z: http://link.springer.com/10.1007/BF03214951

[83] DEVYNCK, Mélanie, Pascal TARDY, Guillaume WANTZ, Yohann NICOLAS, Luc VELLUTINI, Christine LABRUGÈRE a Lionel HIRSCH. Cumulative effects of electrode and dielectric surface modifications on pentacene-based transistors. *Applied Physics Letters*. 2012, **100**(5), 053308-. DOI: 10.1063/1.3681791. ISSN 00036951. Dostupné také z: http://scitation.aip.org/content/aip/journal/apl/100/5/10.1063/1.3681791

[84] DEVYNCK, Mélanie, Pascal TARDY, Guillaume WANTZ, Yohann NICOLAS, Luc VELLUTINI, Christine LABRUGÈRE a Lionel HIRSCH. Cumulative effects of electrode and dielectric surface modifications on pentacene-based transistors. *Applied Physics Letters*. 2012, **100**(5), 053308-. DOI: 10.1063/1.3681791. ISSN 00036951. Dostupné také z: http://link.aip.org/link/APPLAB/v100/i5/p053308/s1

[85] KUZUMOTO, Yasutaka a Masatoshi KITAMURA. Work function of gold surfaces modified using substituted benzenethiols: Reaction time dependence

and thermal stability. *Applied Physics Express* [online]. 2014, **7**(3) [cit. 2020-05-28]. DOI: 10.7567/APEX.7.035701. ISSN 1882-0778. Dostupné z: https://iopscience.iop.org/article/10.7567/APEX.7.035701

[86] KOVALENKO, Alexander, Darina STOYANOVA, Jan POSPISIL et al. Morphology versus Vertical Phase Segregation in Solvent Annealed Small Molecule Bulk Heterojunction Organic Solar Cells. *International Journal of Photoenergy* [online]. 2015, **2015**, 1-8 [cit. 2020-05-29]. DOI: 10.1155/2015/238981. ISSN 1110-662X. Dostupné z: http://www.hindawi.com/journals/ijp/2015/238981/

[87] HONOVÁ, Jana, Stanislav LUŇÁK, Martin VALA, Stanislav STŘÍTESKÝ, Ladislav FEKETE, Martin WEITER a Alexander KOVALENKO. Thiophene-free diphenyl-amino-stilbene-diketo-pyrrolo-pyrrole derivatives as donors for organic bulk heterojunction solar cells. *Chemical Papers* [online]. 2016, **70**(10) [cit. 2020-05-28]. DOI: 10.1515/chempap-2016-0068. ISSN 1336-9075. Dostupné z: http://www.degruyter.com/view/j/chempap.2016.70.issue-10/chempap-2016-0068/chempap-2016-0068.xml

[88] EBENHOCH, Bernd, Stuart A.J. THOMSON, Kristijonas GENEVIČIUS, Gytis JUŠKA a Ifor D.W. SAMUEL. Charge carrier mobility of the organic photovoltaic materials PTB7 and PC71BM and its influence on device performance. *Organic Electronics* [online]. 2015, **22**, 62-68 [cit. 2020-05-28]. DOI: 10.1016/j.orgel.2015.03.013. ISSN 15661199. Dostupné z: https://linkinghub.elsevier.com/retrieve/pii/S1566119915001044

[89] LUŇÁK, Stanislav, Martin VALA, Jan VYŇUCHAL, Imad OUZZANE, Petra HORÁKOVÁ, Petra MOŽÍŠKOVÁ, Zdeněk ELIÁŠ a Martin WEITER. Absorption and fluorescence of soluble polar diketo-pyrrolo-pyrroles. *Dyes and Pigments*. 2011, **91**(3), 269-278. DOI: 10.1016/j.dyepig.2011.05.004.

[90] KRAJČOVIČ, Jozef, Alexander KOVALENKO, Patricie HEINRICHOVÁ, Martin VALA a Martin WEITER. Adamantyl side groups boosting the efficiency and thermal stability of organic solid-state fluorescent dyes. *Journal of Luminescence* [online]. 2016, **175**, 94-99 [cit. 2020-05-28]. DOI: 10.1016/j.jlumin.2016.02.019. ISSN 00222313. Dostupné z: https://linkinghub.elsevier.com/retrieve/pii/S0022231315305457

[91] STŘÍTESKÝ, Stanislav, Jozef KRAJČOVIČ, Martin VALA a Martin WEITER. The Influence of Diketopyrrolopyrrole Chemical Structure on Organic Field-Effect Transistors Performance. *Materials Science Forum* [online]. 2016, **851**, 189-193 [cit. 2020-05-28]. DOI: 10.4028/www.scientific.net/MSF.851.189. ISSN 1662-9752. Dostupné z: https://www.scientific.net/MSF.851.189

[92] CALMETTES, Bastien, Nicolas ESTRAMPES, Christophe COUDRET, Thomas J. ROUSSEL, Jordi FARAUDO a Roland CORATGER. Observation

and modeling of conformational molecular structures driving the self-assembly of tri-adamantyl benzene on Ag(111). *Physical Chemistry Chemical Physics* [online]. 2016, **18**(30), 20281-20289 [cit. 2020-05-28]. DOI: 10.1039/C5CP06733B. ISSN 1463-9076. Dostupné z: http://xlink.rsc.org/?DOI=C5CP06733B

[93] KOVALENKO, Alexander, Cigdem YUMUSAK, Patricie HEINRICHOVA et al. Adamantane substitutions: a path to high-performing, soluble, versatile and sustainable organic semiconducting materials. *Journal of Materials Chemistry C* [online]. 2017, **5**(19), 4716-4723 [cit. 2020-05-28]. DOI: 10.1039/C6TC05076J. ISSN 2050-7526. Dostupné z: http://xlink.rsc.org/?DOI=C6TC05076J

[94] LIU, Qian, Steven E. BOTTLE a Prashant SONAR. Developments of Diketopyrrolopyrrole-Dye-Based Organic Semiconductors for a Wide Range of Applications in Electronics. *Advanced Materials* [online]. 2019, **32**(4) [cit. 2020-05-28]. DOI: 10.1002/adma.201903882. ISSN 0935-9648. Dostupné z: https://onlinelibrary.wiley.com/doi/abs/10.1002/adma.201903882

[95] CALVO-CASTRO, J., C. J. MCHUGH a A. J. MCLEAN. Torsional angle dependence and switching of inner sphere reorganisation energies for electron and hole transfer processes involving phenyl substituted diketopyrrolopyrroles; a density functional study. *Dyes and Pigments*. Feb, **113**, 609-617. DOI: 10.1016/j.dyepig.2014.09.031. ISSN 01437208. Dostupné také z: Go to ISI://WOS:000346543200077

[96] TAKAYOSHI, Kobayashi. *J-aggregates*. Volume 2. Singapore: Worl scientific publishing Co. Pte. Ltd., 2012. ISBN 978-981-4365-74-1.

[97] HIRAMOTO, Masahiro. Small-Molecular-Type Organic Thin-Film Solar Cells. *Journal of The Society of Photographic Science and Technology of Japan*. 2009, **2009**(72), 337-343. DOI: 10.11454/photogrst.72.337. ISSN 1884-5932.

[98] OKADA, Shinsuke a Hiroshi SEGAWA. Substituent-Control Exciton in J-Aggregates of Protonated Water-Insoluble Porphyrins. *Journal of the American Chemical Society* [online]. 2003, **125**(9), 2792-2796 [cit. 2020-05-29]. DOI: 10.1021/ja017768j. ISSN 0002-7863. Dostupné z: https://pubs.acs.org/doi/10.1021/ja017768j

[99] TANI, Tadaaki. *Photographic Science: Advances in Nanoparticles, J-Aggregates, Dye Sensitization, and Organic Devices*. First. New York: Oxford university press, 2011. ISBN 978-0-19-957295-3.

[100] MENZIES, Kara L. a Lyndon JONES. The Impact of Contact Angle on the Biocompatibility of Biomaterials. *Optometry and Vision Science* [online]. 2010 [cit. 2020-05-29]. DOI: 10.1097/OPX.0b013e3181da863e. ISSN 1040-5488. Dostupné z: http://journals.lww.com/00006324-900000000-99741

[101] ŠAFAŘÍKOVÁ, Eva, Lenka ŠVIHÁLKOVÁ ŠINDLEROVÁ, Stanislav STŘÍTESKÝ, Lukáš KUBALA, Martin VALA, Martin WEITER a Jan VÍTEČEK. Evaluation and improvement of organic semiconductors' biocompatibility towards fibroblasts and cardiomyocytes. *Sensors and Actuators B: Chemical* [online]. 2018, **260**, 418-425 [cit. 2020-05-31]. DOI: 10.1016/j.snb.2017.12.108. ISSN 09254005. Dostupné z: https://linkinghub.elsevier.com/retrieve/pii/S0925400517324401

[102] STŘÍTESKÝ, Stanislav, Aneta MARKOVÁ, Jan VÍTEČEK et al. Printing inks of electroactive polymer PEDOT: PSS. *Journal of Biomedical Materials Research Part A* [online]. 2018, **106**(4), 1121-1128 [cit. 2020-05-31]. DOI: 10.1002/jbm.a.36314. ISSN 15493296. Dostupné z: http://doi.wiley.com/10.1002/jbm.a.36314

[103] SHI, Hui, Congcong LIU, Qinglin JIANG a Jingkun XU. Effective Approaches to Improve the Electrical Conductivity of PEDOT: PSS. *Advanced Electronic Materials* [online]. 2015, **1**(4) [cit. 2020-05-29]. DOI: 10.1002/aelm.201500017. ISSN 2199160X. Dostupné z: http://doi.wiley.com/10.1002/aelm.201500017

[104] SALYK, Ota, Jan VÍTEČEK, Lukáš OMASTA, Eva ŠAFAŘÍKOVÁ, Stanislav STŘÍTESKÝ, Martin VALA a Martin WEITER. Organic Electrochemical Transistor Microplate for Real-Time Cell Culture Monitoring. *Applied Sciences* [online]. 2017, **7**(10) [cit. 2020-05-31]. DOI: 10.3390/app7100998. ISSN 2076-3417. Dostupné z: http://www.mdpi.com/2076-3417/7/10/998

[105] DONAHUE, Mary J., Adam WILLIAMSON, Xenofon STRAKOSAS, Jacob T. FRIEDLEIN, Robert R. MCLEOD, Helena GLESKOVA a George G. MALLIARAS. High-Performance Vertical Organic Electrochemical Transistors. *Advanced Materials* [online]. 2018, **30**(5) [cit. 2020-05-31]. DOI: 10.1002/adma.201705031. ISSN 09359648. Dostupné z: http://doi.wiley.com/10.1002/adma.201705031

11 CURRICULUM VITAE

Ing. Stanislav Stříteský

PRACOVNÍ ZKUŠENOSTI:

2020 – současnost	**Siemens Electric Machines s.r.o., Drásov** Technolog – materiálový specialista
2017 - 2019	**Centrum Materiálového Výzkumu, Brno** Výzkumný pracovník - Junior
2012 - 2016	**Centrum Materiálového Výzkumu, Brno** Výzkumný pracovník - Ph.D. student
7-9/2011	**IFE-CR a.s., Brno** Asistent technologa
7-8/2010	**Sporten a.s., Nové Město na Moravě** Asistent technologa
7-9/2009	**Solartec a.s., Rožnov pod Radhoštěm** Pomocný technik

VZDĚLÁNÍ:

2012 - současnost	**VUT, Fakulta chemická** Purkyňova 118, Brno, Doktorské studium
2010 - 2012	**VUT, Fakulta chemická** Purkyňova 118, Brno, obor Chemie, technologie a vlastnosti materiálů Diplomová práce: Elektrické transportní vlastnosti materiálů pro organickou elektroniku.
2007 - 2010	**VUT, Fakulta chemická** Purkyňova 118, Brno, obor Chemie, technologie a vlastnosti materiálů Bakalářská práce: Automatizace systému měření charakteristik senzorů plynu
2003 - 2007	**SPŠ a SOU Hranice** obor Aplikovaná chemie – Analytická chemie

Zahraniční stáže:

6-11/2018	**Linz Institute for Organic Solar Cells, Linz, AT** Pracovní stáž - výzkumný pracovník Výzkumná pracovní stáž ve společnosti LIOS pod vedení o. Univ. Prof. Mag. Dr.DDr. h.c. Niyazi Serdar Sariciftci.
4/2016	**Linz Institute for Organic Solar Cells, Linz, AT** Týdení pracovní stáž - výzkumný pracovník
10/2013	**Ossila Ltd, Sheffield, UK** Měsíční pracovní stáž - výzkumný pracovník

PROJEKTOVÁ ČINNOST:

2017 - 2019	Spoluřešitel projektu GA17-24707S Nové přírodou inspirované organické polovodiče pro bioelektroniku
2013 - 2016	Spoluřešitel projektu GA13-29358S Materiály pro integraci živočišných buněk a organické elektroniky pro budoucí biolektronické zařízení
2015	Řešitel projektu Specifického výzkumu VUT Multifunkční obvodové prvky na bázi hybridní organické elektroniky
2011	Spoluřešitel projektu FRVŠ 2745/2011 Inovace obsahu předmětu Měřící technika
2011	Spoluřešitel projektu ChemLearning Tvorba databáze chemických rovnic
2009	Spoluřešitel projektu FRVŠ IS2198/2009 Inovace cvičení Elektrotechnika a měřicí technika

KURZY A CERTIFIKÁTY:

Omnic Specta	Course for analysis of FTIR spectra – Nicoletcz s.r.o.
Ossila Ltd	Practical training course for OFETs
CLAD National Instruments	National Instruments Certified LabVIEW Associate Developers

DALŠÍ SCHOPNOSTI A DOVEDNOSTI:

Jazykové znalosti:	Anglicky: Pokročilý (B2)
Řidičské oprávnění:	skupina B (aktivní řidič)
Další schopnosti:	Logické a analytické myšlení, MS office, Autocad, LabVIEW, EsaComp, OriginLab, psaní „všemi deseti", Práce v čistých prostorech, práce s Gloveboxem, PVD, 3D tisk FDM.

12 LIST OF PUBLICATIONS

12.1 IMPACTED PUBLICATIONS

[1] HEINRICHOVÁ, Patricie, Jan POSPÍŠIL, Stanislav STŘÍTESKÝ et al. Diketopyrrolopyrrole-Based Organic Solar Cells Functionality: The Role of Orbital Energy and Crystallinity. *The Journal of Physical Chemistry C* [online]. 2019, **123**(18), 11447-11463 [cit. 2020-06-20]. DOI: 10.1021/acs.jpcc.9b01328. ISSN 1932-7447.

[2] STŘÍTESKÝ, Stanislav, Martin VALA, Jan DAVID, Eva ŠAFAŘÍKOVÁ, Jan VÍTEČEK a Martin WEITER. Solution processable diketopyrrolopyrrole semiconductor: towards bio-electronic applications. *Chemical Papers* [online]. 2018, **72**(7), 1635-1643 [cit. 2020-05-28]. DOI: 10.1007/s11696-018-0479-6. ISSN 2585-7290.

[3] ŠAFAŘÍKOVÁ, Eva, Lenka ŠVIHÁLKOVÁ ŠINDLEROVÁ, Stanislav STŘÍTESKÝ, Lukáš KUBALA, Martin VALA, Martin WEITER a Jan VÍTEČEK. Evaluation and improvement of organic semiconductors' biocompatibility towards fibroblasts and cardiomyocytes. *Sensors and Actuators B: Chemical* [online]. 2018, **260**, 418-425 [cit. 2020-05-31]. DOI: 10.1016/j.snb.2017.12.108. ISSN 09254005.

[4] STŘÍTESKÝ, Stanislav, Aneta MARKOVÁ, Jan VÍTEČEK et al. Printing inks of electroactive polymer PEDOT: PSS. *Journal of Biomedical Materials Research Part A* [online]. 2018, **106**(4), 1121-1128 [cit. 2020-05-31]. DOI: 10.1002/jbm.a.36314. ISSN 15493296.

[5] SALYK, Ota, Jan VÍTEČEK, Lukáš OMASTA, Eva ŠAFAŘÍKOVÁ, Stanislav STŘÍTESKÝ, Martin VALA a Martin WEITER. Organic Electrochemical Transistor Microplate for Real-Time Cell Culture Monitoring. *Applied Sciences* [online]. 2017, **7**(10) [cit. 2020-05-31]. DOI: 10.3390/app7100998. ISSN 2076-3417.

[6] KOVALENKO, Alexander, YUMUSAK Cigdem, HEINRICHOVA Patricie, STŘÍTESKÝ Stanislav, et al. Adamantane substitutions: a path to high-performing, soluble, versatile and sustainable organic semiconducting materials. *Journal of Materials Chemistry C* [online]. 2017, **5**(19), 4716-4723 [cit. 2020-05-28]. DOI: 10.1039/C6TC05076J. ISSN 2050-7526.

[7] HONOVÁ, Jana, Stanislav LUŇÁK, Martin VALA, Stanislav STŘÍTESKÝ, Ladislav FEKETE, Martin WEITER a KOVALENKO. *Chemical Papers*. 2016, **70**(10). DOI: 10.1515/chempap-2016-0068. ISSN 1336-9075.

[8] MIŠICÁK, Róbert, Stanislav STŘÍTESKÝ, Martin VALA et al. Effect of the ethynylene linker on the properties and carrier mobility of naphthalene derivatives with hexylbithienyl arms. *Synthetic Metals* [online]. 2016, **217**,

12.2 OTHER PUBLICATIONS AND CONFERENCE CONTRIBUTIONS

[1] TUMOVÁ, Šárka, Romana MALEČKOVÁ, Vojtěch ENEV, Stanislav STŘÍTESKÝ, Jan VÍTEČEK, Martin VALA a Martin WEITER. Modification of PEDOT: PSS Surface by RGD Peptide. *Materials Science Forum* [online]. 2019, **955**, 68-73 [cit. 2020-06-20]. DOI: 10.4028/www.scientific.net/MSF.955.68. ISSN 1662-9752.

[2] SIMEK, Vaclav, Stanislav STRITESKY, Michal REZNICEK, Adam CRHA a Richard RUZICKA. Towards implementation of logic circuits based on intrinsically reconfigurable organic transistors. In: *2016 6th Electronic System-Integration Technology Conference (ESTC)* [online]. IEEE, 2016, s. 1-6 [cit. 2020-06-20]. DOI: 10.1109/ESTC.2016.7764738. ISBN 978-1-5090-1402-6.

[3] STŘÍTESKÝ, Stanislav, Jozef KRAJČOVIČ, Martin VALA a Martin WEITER. The Influence of Diketopyrrolopyrrole Chemical Structure on Organic Field-Effect Transistors Performance. *Materials Science Forum* [online]. 2016, **851**, 189-193 [cit. 2020-05-28]. DOI: 10.4028/www.scientific.net/MSF.851.189. ISSN 1662-9752

[4] GEORGIEV, Y, I ZHIVKOV, T TAKOV, G ANGELOV, R PRIKRYL, S STRITESKY, J HONOVA a M WEITER. Vacuum-deposited diphenyl-diketo-pyrrolopyrroles structures with photoelectrical applications. Journal of Physics: Conference Series [online]. 2014, 514 [cit. 2020-06-20]. DOI: 10.1088/1742-6596/514/1/012005. ISSN 1742-6596.

13 APPENDIX